Nuclear Reactor Process Monitoring in Time-Domain using Stochastic Signals

Nuclear Reactor Process Monitoring in Time-Domain using Stochastic Signals

Hielke Schoonewelle

Interfacultair Reactor Instituut
Technische Universiteit Delft
Nederland

Februari 1997

CIP-GEGEVENS KONINKLIJKE BIBLIOTHEEK, DEN HAAG

Schoonewelle, Hielke

Nuclear Reactor Process Monitoring in Time-Domain using Stochastic Signals /
Hielke Schoonewelle. - Delft: Interfaculty Reactor Institute,
Delft University of Technology.
With summary in Dutch. - With references.
ISBN 90-73861-46-2
NUGI 812
Subject Headings: Nuclear Reactors, Process Monitoring

Printed in the Netherlands

Nuclear Reactor Process Monitoring in Time-Domain using Stochastic Signals

PROEFSCHRIFT

ter verkrijging van de graad van doctor
aan de Technische Universiteit Delft,
op gezag van de Rector Magnificus Prof. dr. ir. J. Blaauwendraad
in het openbaar te verdedigen ten overstaan van een commissie,
door het College van Dekanen aangewezen,
op maandag 17 februari 1997 te 13:30
door

Hielke SCHOONEWELLE

natuurkundig ingenieur
geboren te Zwijndrecht

Dit proefschrift is goedgekeurd door de promotor:
Prof. dr. ir. H. van Dam

Toegevoegd promotor: Dr. ir. T.H.J.J. van der Hagen

Samenstelling promotiecommissie:

Rector Magnificus, voorzitter	
Prof. dr. ir. H. van Dam,	TU Delft, promotor
Dr. ir. T.H.J.J. van der Hagen,	TU Delft, promotor
Prof. dr. ir. H.E.A. van den Akker,	TU Delft
Prof. dr. ir. A. van den Bos,	TU Delft
Prof. dr. ir. C.W.E. van Eijk,	TU Delft
Prof. dr. ir. A.H.M. Verkooijen,	TU Delft
Dr. H. Arnold,	GKN, Dodewaard

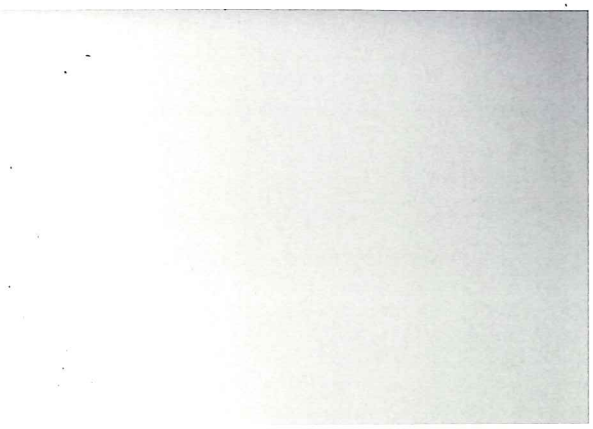

The research described in this thesis has been performed at the group of Nuclear Reactors of the Reactor Physics Department, Interfaculty Reactor Institute (IRI), Delft University of Technology, Mekelweg 15, 2629 JB Delft, The Netherlands.
This research was financially supported by GKN Nuclear Power Plant, P.O. Box 40, 6669 ZG Dodewaard, The Netherlands.

Contents

chapter 1

GENERAL INTRODUCTION

For safety reasons it is very important to guard the operation of a nuclear power plant continuously. To this end, all nuclear power plants, like the Dodewaard plant, are equipped with an operating- and safety-system. This system controls the process of power production and guards the process from exceeding its limitations. If, for example, the power of the reactor increases too much, the safety-system will induce a safety shutdown of the reactor. In this way dangerous situations can be prevented.

For performing its task, the operating- and safety-system collects a lot of physical information about the nuclear power plant, like the temperature of the primary coolant, the pressure of the primary circuit, the neutron flux etc. The collecting of information is also called "process-monitoring" and must be performed in a non-intrusive way without interrupting the normal operation of a nuclear power plant. The information is used for determining whether the nuclear power plant is still operating under normal conditions. If this is not the case, then the system can take action itself or can help the operators, through supply of information, to take the correct actions. Unintended deviations from normal reactor operation are called "process anomalies".

In order to obtain process information, physical quantities have to be measured. Figure 1-1 gives the general setup for obtaining information about a process. For measuring a physical quantity a sensor is needed, like a pressure sensor, a thermocouple or a neutron detector. The measurement data are made available for further processing with the use of electronic equipment. As part of the electronic

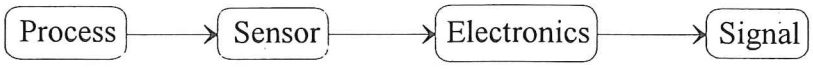

Figure 1-1. Obtaining information about a process

equipment there is usually a device which samples the sensor output thus obtaining a discrete signal. Filters are also a good example of electronic equipment.

For detecting large process anomalies, like a 20 % decrease in nominal power or a turbine trip, the average value of a signal usually suffices. However, for studying small process changes, like the onset of boiling of the coolant in a PWR, the fluctuating component of a signal is usually needed. These process changes are very important since they can be the forerunner of large changes. The fluctuating component of an incore neutron detector can, for example, indicate the presence of coolant boiling (Kozma, 1992). This fluctuating component, which contains information about the higher frequencies of a signal, will be called the noise component of a signal and will be referred to as the noise or noise signal. This noise component is usually obtained by high-pass filtering the signal using a low cut-off frequency. Studying the noise component of nuclear reactor signals is called "reactor noise analysis". It must be noticed that reactor noise analysis is an indirect way of obtaining process information and requires expert knowledge for interpreting the analysis results.

When a certain feature of the (noise) signal changes, it may have been caused by a process anomaly, malfunctioning of one or more sensors, malfunctioning of the electronic equipment or a combination of two or all of them. In order to be sure that the (noise) signal change was caused by anomalous behaviour of the process, one must be certain that the sensor(s) and electronics are working properly. Checking the reliability of the sensor(s) and electronics and identifying faulty ones can be done using sensor validation techniques (Upadhyaya *et al.*, 1992; Holbert *et al.*, 1994). Concerning the cause of signal change no distinction is made between the process and the sensors/ equipment. Moreover, in this work, signal changes are taken as a fact and no study is made of the causal relation between the anomaly and the signal change.

There are several possible causes of anomalous behaviour in a nuclear power plant, like: leakage of primary or secondary coolant, vibrations of mechanical parts (vessel, control rods, fuel assemblies, detector tubes, primary pumps, steam generator internals, etc.), water column vibrations, coolant boiling in PWRs, loose parts etc. (Bernard *et al.*, 1986 ; Kiss *et al.*, 1995). In order to measure the various physical parameters of the power plant, different sensors, located throughout the power plant, are used, like: accelerometers, acoustic detectors, self-powered neutron detectors, thermocouples and pressure sensors (Bernard *et al.*, 1986). The signals obtained from measurements with these sensors are used to learn more about the physical behaviour of the power plant.

The appropriate methods for performing noise analysis depend, among others, on

the frequency range of interest which, again, depends on the anomaly that occurs. The noise caused by sodium coolant leakage, sodium boiling, steam generator internal vibrations and loose parts is usually found in the high frequency range ($>10^3$ Hz) whereas the noise produced by coolant boiling in PWRs and primary circuit mechanical vibrations is usually relatively low frequent ($<10^2$ Hz) (Kiss *et al.*, 1995). In the high frequency range spectral and distribution methods are commonly used. In the low frequency range spectral methods are less favourable, since they usually require a lot of data points and thus, usually, a long time for analysis. This makes those methods relatively slow compared to time-domain methods.

The first applications of reactor noise analysis can be found at the end of the 50s, beginning of the 60s (Thie, 1963; Uhrig, 1964). These applications mainly focussed on studying the statistical properties and spectral features of the reactor noise. At the end of 60s (1969) the first European reactor noise meeting took place. Later these meetings were given the name *Informal Meeting on Reactor Noise* (IMORN). In 1974 the first *Specialists' Meeting on Reactor Noise* (SMORN) was held in Rome, Italy (SMORN-1, 1975). Until now (1996) 26 IMORNs and 7 SMORNs were held. These meetings greatly stimulated the research and applications in the field of reactor noise analysis.

Many different methods for reactor noise analysis and anomaly detection were developed and applied to different noise signals. Methods for extracting certain features of the power spectral density and the probability density function of a signal obtained from an acoustic sensor were applied to detect sodium coolant boiling and leakage in a liquid metal fast breeder reactor (Singh *et al.*, 1988; Srinivasan *et al.*, 1990; Black *et al.*, 1993). Pattern-recognition and cluster methods were applied successfully to neutron noise signals (Dzwinel *et al.*, 1995). Also Neural network models are widely used in the field of anomaly detection (Kim *et al.*, 1993; Kozma *et al.*, 1995).

Scope of this work

Present-day operating-, safety- and monitoring systems usually mainly pay attention to the large process changes or anomalies. As was mentioned before, small process changes can be a forerunner of large changes. Thus by focussing on small changes it may be possible to detect certain process disturbances or malfunctioning of the nuclear power plant in an early stage. In this manner unwanted disturbances can be dealt with before they cause any serious problems. In this work techniques and methods are presented that are designed to detect and analyse these small process changes.

This work proceeds from the research that was done to detect boiling in a research reactor (Kozma, 1992). In the framework of this research, a facility, called NIOBE (Noise Investigations On Boiling Effects), was designed to study the effect of boiling on the neutron flux in the research reactor of the Interfaculty Reactor Institute (IRI) in Delft, the Netherlands. The NIOBE facility consists of a simulated fuel assembly having 3 electrically heated plates. Between the fuel plates there are cooling channels. The thermocouples are positioned inside the plates and the facility is equipped with several neutron detector strings. The facility is placed next to the core of the research reactor. Signals from measurements performed with this facility are also used in this work (see chapter 2 and chapter 5). Due to malfunctioning and shortcomings of this facility a new facility, called SIMBOL (SIMulation of BOiLing by blowing nitrogen bubbles) was designed and build. Further details of this facility are given in chapter 6 of this thesis. Since the effect of coolant boiling on neutron noise signals is found in the range of low frequencies ($\leq$ 10 Hz) (Kozma, 1992), it was decided to focus on time-domain methods for noise analysis and anomaly detection.

In chapter 2, several signal processing techniques (sometimes also called signal analysis techniques) are discussed. Signal processing techniques are techniques that are applied to a (noise) signal in order to extract certain features from the signal. Three techniques are presented, namely autoregressive, wavelet and fractal analysis. Autoregressive analysis has already quite some applications in the field of reactor noise analysis (Çiftçioglu *et al.*, 1988) but wavelet and fractal analysis are relatively young techniques in this field. The result of a signal processing technique is called a "time series". In general, a sequence of data values is called a "data series". This means that a "(noise) signal" and a "time series" are all considered "data series".

Chapter 3 deals with anomaly detection methods of which three are discussed, namely the extremes method, the distribution method and the sequential probability ratio test. An anomaly detection method is a method that detects changes of one or more specific statistical parameters of a data series. In this chapter the three methods are designed to detect a change of the standard deviation. The methods distinguish only two states, namely the normal and the anomalous state.

There are three quantities associated with anomaly detection, namely the false alarm probability (*FAP*), the alarm failure probability (*AFP*) and the average time to alarm (*ATA*). These quantities can be explained using figure 1-2 which shows the detection of an anomaly. This anomaly could, for example, be coolant boiling which causes an increase of the standard deviation of the neutron noise (see section 2.2.2). This

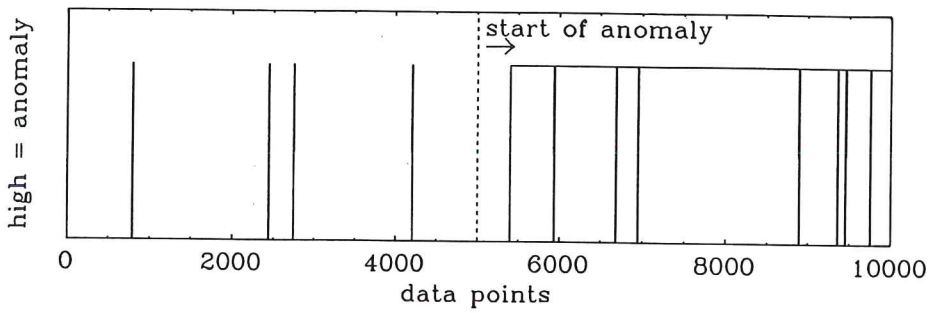

Figure 1-2. Example of the detection of an anomaly

increase can be detected by an anomaly detection method (see chapter 3). The anomaly starts at data point 5001.

The *FAP* is the probability that a normal situation is present but an anomaly is detected. In figure 1-2 there are 4 false alarms meaning that the *FAP* equals $4/5000 = 8 \cdot 10^{-4}$. The *AFP* is the probability that an anomaly is present but none is detected. Figure 1-2 shows 7 alarm failures so that the *AFP* equals $7/4600 = 1.52 \cdot 10^{-3}$. The *FAP* and *AFP* determined here, are in fact estimators of the *FAP* and *AFP*, respectively. Exact values of these probabilities can only be determined in case of an infinite number of data points. The number of alarm failures is divided by 4600 since there is always a delay in the detection of an anomaly. This delay is called "time to alarm" (*TA*). In this case it takes the method 400 data points to detect the anomaly. For calculating the *TA* the sampling frequency f_s must be known. Suppose $f_s = 100$ Hz then $TA = 4$ s. In the same manner, the false alarm rate (*FAR*) and alarm failure rate (*AFR*) can be calculated: $FAR = FAP \times f_s = 8 \cdot 10^{-2}$ s^{-1} and $AFR = AFP \times f_s = 0.152$ s^{-1} . The *ATA* is defined as the average time interval between the occurrence of an anomaly and its detection. It can be calculated by averaging over a large number of *TA*s. All these *TA*s must be determined using signals having the same characteristics and showing the same change in characteristics.

In practical situations, it is usually demanded that the *FAR* is very small (< once a year), since it is very costly to have an unnecessary reactor safety shutdown. It is also very important to know the presence of an anomaly as soon as possible in order to be able to take countermeasures and avoid worse situations (thus: *ATA* as small as possible). This means that the *AFR* is usually less important in practical situations. The *AFR* is of interest when the duration of the anomaly must be known and whether it is

still present or not some time after its first detection.

In chapter 4 each anomaly detection method is optimized and the three methods are compared using results from theory and simulation. Optimization means that the method parameters are chosen in such a way that the method is able to detect an anomaly as soon as possible for a given *FAR*. The best method is the method which gives on the average the smallest *ATA* for a set of *FAR* values.

The signal processing techniques presented in chapter 2 can be applied simultaneously to one signal. A method for combining the outcomes of several techniques, which were applied to a synthetic neutron noise signal, is presented in chapter 5. This is done using an approach based on fuzzy logic.

In chapter 6 the new experimental setup SIMBOL and the measurements that were performed with this facility are presented. This facility simulates coolant boiling by blowing nitrogen bubbles in the streaming coolant. The signal processing techniques, anomaly detection methods and the fuzzy-logic approach are applied to the measurement results.

In chapter 7 the first step towards an application of a process-monitoring system is done and presented. The setup of a system installed at the Dodewaard nuclear power plant is described and some results obtained with it are discussed. Finally, some ideas for an expert surveillance and diagnosis system are suggested.

The techniques and methods presented in this thesis have a broader area of application than just reactor noise signals. In fact they can be applied to any (noise) signal obtained through measurement or simulation. Therefore, this thesis can also be of interest to anyone working in the field of signal processing, data analysis or fault detection.

Chapter 2

SIGNAL PROCESSING AND FEATURE EXTRACTION

2.1 Introduction

When monitoring a process, it is desirable to acquire as many statistical features of the measured signals as possible. This can be obtained by applying several signal processing techniques to the signals. In this manner, it may be possible to distinguish different modes of the process or to illuminate different signal characteristics. It can happen, for example, that only the high-frequency components of the signal change due to a certain anomaly. This might not be detected by merely looking at the signal itself. If, for example, a high-pass filter would be applied to the signal, a much better picture of the anomaly could be obtained.

In this chapter three signal processing techniques will be presented, namely autoregressive analysis, wavelet analysis and fractal analysis. Each technique is applied directly to the signal itself and returns, after some initialisation time, an output data value for each input signal value. For the autoregressive, wavelet and fractal analysis techniques the output data are called the residual noise, the wavelet coefficient time series and the fractal dimension time series, respectively. These time series can be used as input for the anomaly detection methods which are presented in the next chapter.

The first analysis technique that will be discussed is autoregressive analysis. With this technique a parametric model is obtained with which the momentary signal value can be predicted using former ones. The difference between the predicted and the actual signal value is called the residue, being the output of this analysis technique. The second technique is wavelet analysis. By applying wavelet analysis, the signal is convoluted with a so-called wavelet function resulting in a wavelet coefficient value.

The last technique, fractal analysis, focuses on discovering self-similarity of the signal by calculating the partial length for different time intervals.

Each technique requires a certain initialisation time. In case of autoregressive analysis a number of successive signal data points are needed for establishing the autoregressive model. The other two analysis techniques do not require a model determination but do need former signal data points for determining the momentary output value.

The theory of each technique will be presented here briefly. A practical application of each technique will show the usefulness of the technique in illuminating specific anomalous behaviour.

2.2 Autoregressive analysis

2.2.1 Basic theory of autoregressive analysis

Autoregressive (AR) analysis is a widely employed approach for performing noise or signal analysis in time domain. Using AR analysis, a parametric model of the signal data is made in which each signal data point is assumed to be linearly related to a limited number of previously signal data. Once an AR model has been fitted to a record of signal data the model can be used to predict future data values from its predecessors.

In AR analysis a discrete signal y_i at time instant i is represented as a linear contribution from successive signal values at earlier time instances plus a random contribution e_i independent of the signal values at earlier times. In formula:

$$y_i = \sum_{n=1}^{p} A_n y_{i-n} + e_i = \tilde{y}_i + e_i . \qquad (2\text{-}1)$$

y_i is thus represented by a univariate AR model with model order p (Ljung, 1987). A_i $\{i=1, ...,p\}$ are the AR-coefficients. $\tilde{y}_i$ is the prediction of the signal value. There are several methods for determining the coefficients of the AR model, for example Yule-Walker, least-squares, least-squares forward-backward, Burg etc.. Detailed information about these methods can be found in several textbooks (Box *et al.*, 1970; Ljung, 1987; Priestley, 1994). They will not be discussed here.

The difference between the actual signal values and the predictions is called the

residual noise:

$$e_i = y_i - \tilde{y}_i . \tag{2-2}$$

If the AR model is correct the residual noise is white, meaning that the actual signal and the predicted signal have the same characteristics.

There are several approaches for determining the optimum model order. Probably the best known technique is Akaike's final prediction error (*FPE*) or his closely related information criterion (*AIC*) (Ljung, 1991). Here the *FPE* will be used, which is formed as:

$$FPE \equiv \frac{1 + p/N}{1 - p/N} \cdot \sum_{i=1}^{N} e_i^2 , \tag{2-3}$$

where N is the number of data points for which the AR model was established. The *FPE* compensates for the automatic decrease of the sum of the squared residues due to an increase of the model structure (increase of p). According to Akaike's theory, in a collection of different models, the one with the smallest *FPE* (or *AIC*) has to be chosen.

It is also possible to define a multivariate AR model in which y_i is a column vector containing the values of a number signals and A_i is a row vector. A multivariate AR model also accounts for the cross-correlation between the different signals. It will not be used here.

2.2.2 AR analysis applied to a signal from a benchmark test

In this paragraph an example will be shown of applying autoregressive modelling to a signal from a benchmark test. The benchmark test used here is a well defined problem with a known solution. The known solution is used as a standard of comparison for other estimations. The data in this example were taken from the 1994 International Atomic Energy Agency (IAEA) benchmark test on leak detection in a steam generator of a liquid metal fast breeder reactor (Journeau, 1994). The test data were artificially synthesized of background noise as well as leak noise at different signal to noise ratios. The background noise was measured at the superheater no. 2 of the Dounreay Fast Breeder Reactor and the leak noise was recorded at the ASB loop

at Bensberg, Germany, when injecting 3.8 g/s water. The data were sampled at a frequency of 131072 Hz. Here the setup of AR-analysis will be presented, using a signal with a 'leak noise to background noise' ratio of -6 dB.

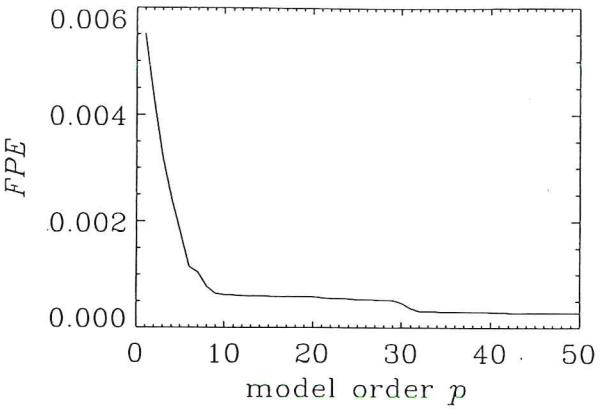

Figure 2-1. The *FPE* for the Yule-Walker method

The autoregressive model was estimated from the first 2048 data points of the background noise signal using the Yule-Walker method (Hoogenboom *et al.*, 1994a). This was done for increasing model orders using the System Identification Toolbox of the MATLAB computation software (Ljung, 1991). The *FPE* was calculated for every model order and is shown in figure 2-1.

From figure 2-1 it can be seen that the *FPE* decreases quickly until model order 10 after which it shows only minor decrease until model order 30. At model order 31 there is a sudden decrease of the *FPE* and beyond model order 32 the decrease of the *FPE* is very small.

For determining the best model order the residual noise is studied first. For model orders 30 and 32 the autocorrelation functions of the residual noise are shown in figure 2-2. The horizontal dotted lines are the boundaries of the 99 % confidence interval assuming the residual noise to be white. For model order 30 the residual noise is less white than for model order 32. The same is true for model

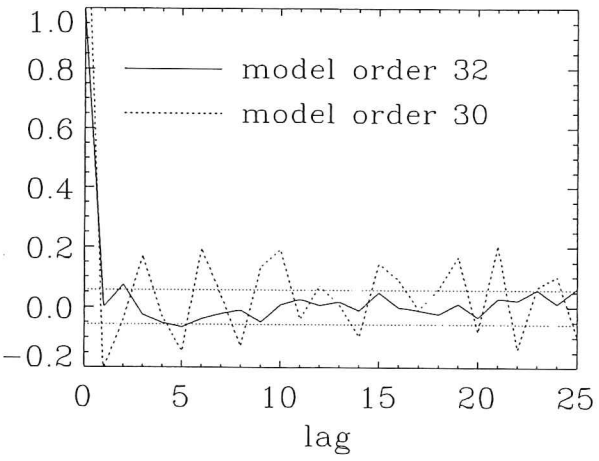

Figure 2-2. Autocorrelation functions of the residual noise for two model orders

orders smaller than 30 (not shown here). Since the *FPE* shows only a very small decrease beyond model order 32, this model order was chosen as the most suitable one.

A method for checking the correctness of the model is to study the position of its poles. Although Yule-Walker guarantees a stable model (all poles lie within the unit circle (Box *et al.*, 1970)), it should not be used if the poles are near to the unit circle, since it might result in a large residual and prediction error variance and consequently in an invalid model (De Hoon *et al.*, 1996). Figure 2-3 presents the poles of the AR model. It can be seen that the poles lie close to the unit circle, meaning that the usage of Yule Walker is not recommended.

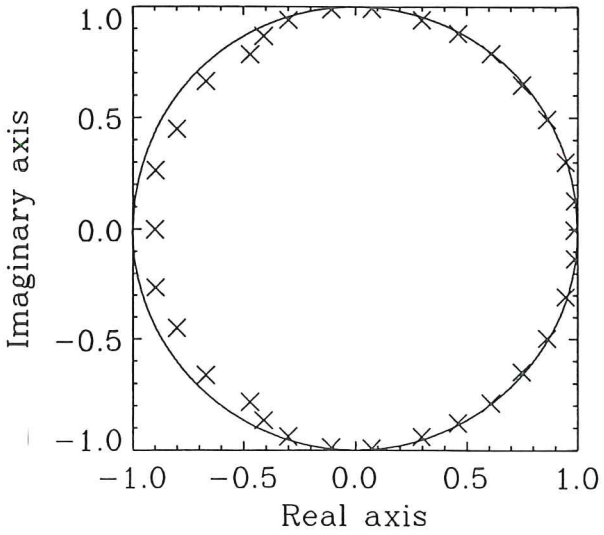

Figure 2-3. Poles of the AR model (Yule-Walker)

Instead of Yule-Walker the least-squares or the least-squares forward-backward approach can be used. The problem with these approaches is that they do not guarantee a stable model and should therefore be used with caution. Burg's method is actually the most reliable technique, since it does not suffer from the drawbacks of the beforementioned approaches (De Hoon *et al.*, 1996).

Applying Burg's method also led to an optimum model order of 32. The *FPE* for this model order is 44 % less than the *FPE* obtained with Yule-Walker.

The AR model was estimated using a background noise signal from the benchmark test. The model is now used for prediction purposes by applying it to the leak noise signal from the same benchmark. It is expected that a change of the characteristics of this signal, caused by anomalous behaviour (leakage), will cause a change in the prediction capacity of the model and will therefore affect the characteristics of the residual noise.

Figure 2-4 shows the results of applying both models (derived using the Yule-Walker and Burg's method) to the leak noise. It shows clearly that the anomaly in the

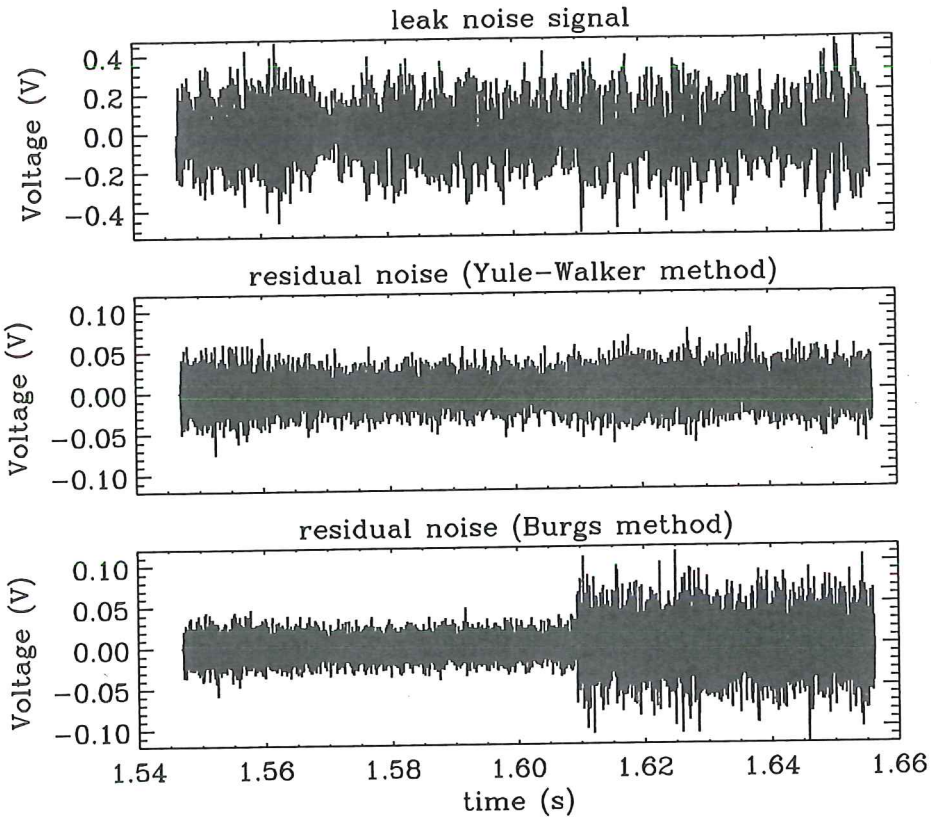

Figure 2-4. Results of applying the AR-models to a leak noise signal

leak noise cannot be detected when the AR model is used, which was estimated using the Yule-Walker method. In the third graph (Burg's method) the start of the anomaly can be appointed at approximately 1.609 s (Hoogenboom *et al.*, 1994b). The residual noise in the second graph has a larger standard deviation in the normal situation (no anomaly) ($\sigma = 0.0171$ V) than the residual noise in the third graph ($\sigma = 0.0126$ V). This endorses the statement that Yule-Walker leads to a large prediction error if the poles are located near the unit circle.

In order to determine the start of the anomaly more precisely, anomaly detection methods can be used. One could for example calculate the standard deviation of a subset of the points of the residual noise signal and compare it with a reference value determined in a learning period (i.e. the period during which no anomaly is present).

When the calculated standard deviation deviates too much from the reference value an anomaly could be declared. This is a rather simple method; more sophisticated anomaly detection methods will be presented in the next chapter.

2.3 Wavelet analysis

The wavelet transform is a relatively new topic in signal processing and was initially proposed by Morlet and Grossmann (Grossmann *et al.*, 1984). Together with Meyer (Meyer, 1987) they developed the mathematical foundations of wavelets. Daubechies and Mallat where the first to make the connection between wavelets and digital signal processing (Daubechies, 1988). Recently, wavelet analysis was applied to reactor noise signals (Sakuma *et al.*, 1995).

The wavelet transform (WT) shows its strength when analyzing non-stationary signals. If those kind of signals would be analysed using the Fourier transform (FT), all local information of the signal would be lost since the FT is applied over the entire time domain. Another option would be to use the short time Fourier transform (STFT) being merely a time-windowed FT (Bentley *et al.*, 1994). The STFT allows the generation of a time-frequency description of the signal. The disadvantage of the STFT is that it uses a constant window size independent of the frequency, which has a detrimental effect upon frequency resolution.

For the WT, however, there is a direct coupling between the resolution in time and the resolution in frequency domain giving it a constant optimum time-frequency resolution for the entire time and frequency domain. Analogous to Heisenberg's uncertainty principle the best time-frequency resolution is reached when $\Delta t \cdot \Delta\omega = 1$ and can never be smaller than this value (Hunt *et al.*, 1990). Notice that the Fourier transform corresponds to the limit where $\Delta t \to \infty$ and $\Delta\omega \to 0$.

Figure 2-5 shows the Gabor 'mother' wavelet which is used in the WT (the meaning of input order will be explained later on). The WT is obtained by dilating and translating the 'mother' wavelet and then convoluting it with the signal. The coupling between time and frequency domain is obvious: when the central frequency of the wavelet function is reduced (input order 10), the window size is enlarged causing the number of oscillations within the window to remain constant. It is also clear that at the same time the range in frequency domain becomes smaller. Thus when analyzing a signal which is characterized by short and high-frequent disturbances a low input order

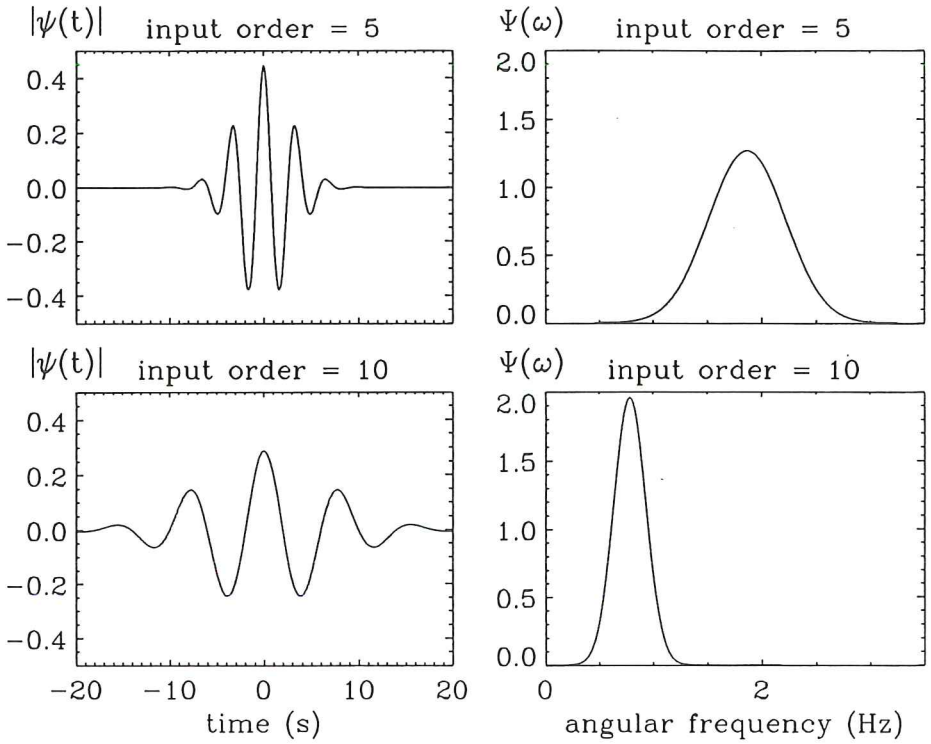

Figure 2-5. Gabor 'mother' wavelet and its Fourier transform

must be chosen whereas in case of slow disturbances a high input order must be used.

The parameters in the wavelet transform are a location τ for the translation and a scale a for the dilation of the 'mother' wavelet. The wavelet is thus defined by:

$$\Psi_{(a,\tau)}(t) = \frac{1}{\sqrt{|a|}}\Psi\left(\frac{t-\tau}{a}\right). \tag{2-4}$$

The continuous wavelet transform $CWT(a,\tau)$ is a convolution of the signal $y(t)$ with the wavelet $\Psi_{(a,\tau)}(t)$:

$$CWT(a,\tau) = \langle y, \Psi_{(a,\tau)} \rangle = \frac{1}{\sqrt{|a|}} \int y(t)\Psi\left(\frac{t-\tau}{a}\right) dt. \tag{2-5}$$

The result of the WT is called the wavelet coefficient. For $\psi(t)$ to be a 'mother' wavelet it should be well localised in both time and frequency domain. A function which satisfies this criterium is the Gabor function (Gabor, 1946):

$$\psi(t) = \pi^{-\frac{1}{4}}(\omega_p/\gamma)^{\frac{1}{2}} \exp[-(t\omega_p/\gamma)^2/2 - i\omega_p t], \qquad (2\text{-}6)$$

where $\gamma=\pi(2/\ln 2)^{1/2}=5.336$. With this γ value the necessary precision of the results of the wavelet transform is satisfied for this application (Goupillaud *et al.*, 1984).

It must be noted here that future signal values must be known in order to determine the momentary wavelet coefficient using the wavelet function given in equation (2-6). After Fourier transforming the above equation the following equation is obtained:

$$\hat{\Psi}(\omega) = \pi^{-\frac{1}{4}}(\omega_p/\gamma)^{-\frac{1}{2}} \exp\left(-\frac{(\omega-\omega_p)^2}{2(\omega_p/\gamma)^2}\right). \qquad (2\text{-}7)$$

The standard deviation of $\psi(t)$ and its Fourier transform equal γ/ω_p and ω_p/γ respectively. This means that $\Delta t \cdot \Delta\omega=1$ which is equal to the lower limit as was mentioned earlier.

Before continuing, the following should be noted. In general, the term wavelet analysis is reserved for situations for which the set of wavelet functions $\{\psi_{(a,\tau)}\}$ has sufficient members to allow any function g to be reconstructed from its wavelet coefficients $\langle g,\psi_{(a,\tau)}\rangle$ (Ruskai, 1992). This does actually not hold for the Gabor wavelet. In the present application, the WT is used for multi-resolution analysis meaning that the properties needed for reconstructing functions are not required here. Nevertheless, it was decided to use the names "wavelet analysis" and "wavelet coefficient" here.

For the discrete wavelet transform (DWT) the wavelet function must be discretised and the integration in equation (2-5) must be written as a summation. Only N values of the discretised wavelet function are used in the summation. The parameters a, τ and ω are chosen properly depending on the sampling period ΔT and the frequency range of interest: $a = 2^{j/4}$, $\tau = (n-(N-1)/2)\Delta T$ and $\omega_p = 2^{1/2}\,\pi/\Delta T$ (Morlet *et al.* 1982). The integer j is the so-called input order of the *DWT*. The *DWT* can be written as:

$$DWT(n\Delta T,j) = \frac{1}{2^{j/8}} \sum_{i=n-N+1}^{n} y(i\Delta T)\psi\left(\frac{(i-n+(N-1)/2)\Delta T}{2^{j/4}}\right), \qquad (2\text{-}8)$$

where

$$N = 3\left(\left[\frac{2^{j/4+1}\gamma}{\omega_p \Delta T}\right] + 1\right) \qquad (2\text{-}9)$$

(Morlet *et al.*, 1982). N covers approximately 5 periods of the Gabor function. The discretised wavelet function ψ is shifted by an extra $-((N-1)/2)\Delta T$ which stems from the fact that in practical situations only former signal values are known and can be used to calculate the 'momentary' wavelet coefficient.

Equation (2-8) shows that by changing the input order, the central frequency and the frequency range of the wavelet can be changed. The central frequency of the wavelet can be determined from the input order using the equation: $f_c = 2^{-(2+j)/4}\Delta T^{-1}$.

When wavelet analysis is applied to a measured signal in which an anomaly might occur, it is recommendable to use a set of input orders. One could, for example, perform the analysis for input orders j = 2-20 in parallel. These input orders correspond to $f_c = 0.5f_s - 0.022f_s$, where f_s is the sampling frequency. It is necessary to use a set of input orders since it is not known beforehand for which input order(s) the wavelet analysis will respond to a certain anomaly.

Wavelet analysis was applied to a neutron noise signal measured with the NIOBE facility (see chapter 1). Figure 2-6.b shows this neutron noise signal. Figure 2-6.a represents the temperature inside the middle plate of the NIOBE facility measured with a thermocouple. It must be noted here that the thermocouple does certainly not measure the temperature of the coolant since there is a considerable temperature gradient between the inside of the fuel plate and the coolant. Moreover, the coolant will not respond as quickly to a change of heating power as the thermocouple inside the plate (Kozma, 1992). The horizontal dashed line shown in the first graph represents the estimated saturation temperature.

Figure 2-7 shows the result of the analysis for a range of input orders: j=5-16 (f_c=9.9 Hz - 1.5 Hz). The wavelet coefficient increases considerably in the range from approximately 2.5 until 5 Hz due to the boiling. The 'intermediate boiling' and 'full boiling' part of the neutron noise signal can also be distinguished in this figure. These

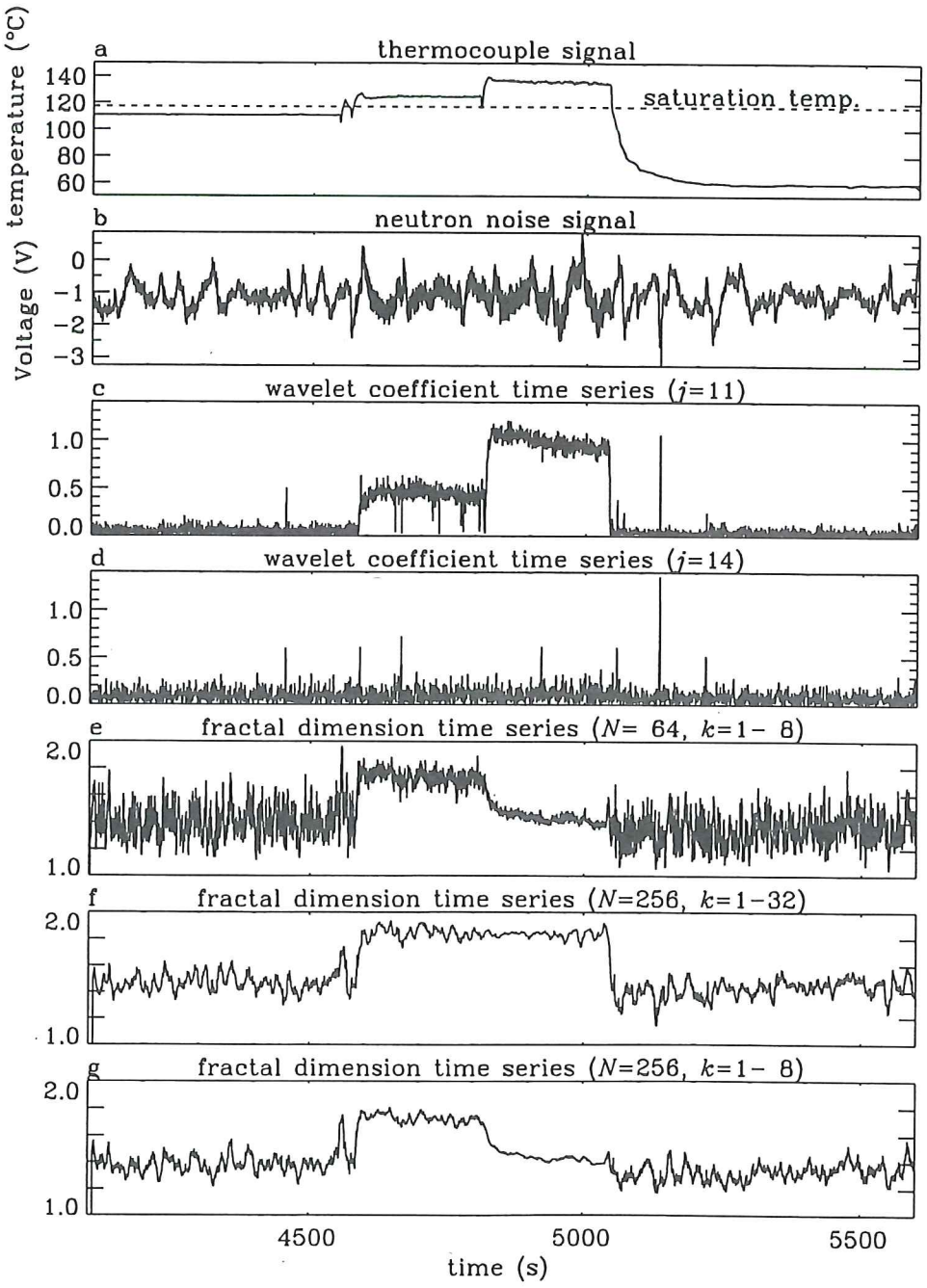

Figure 2-6. Results of applying wavelet and fractal analysis to neutron noise signal

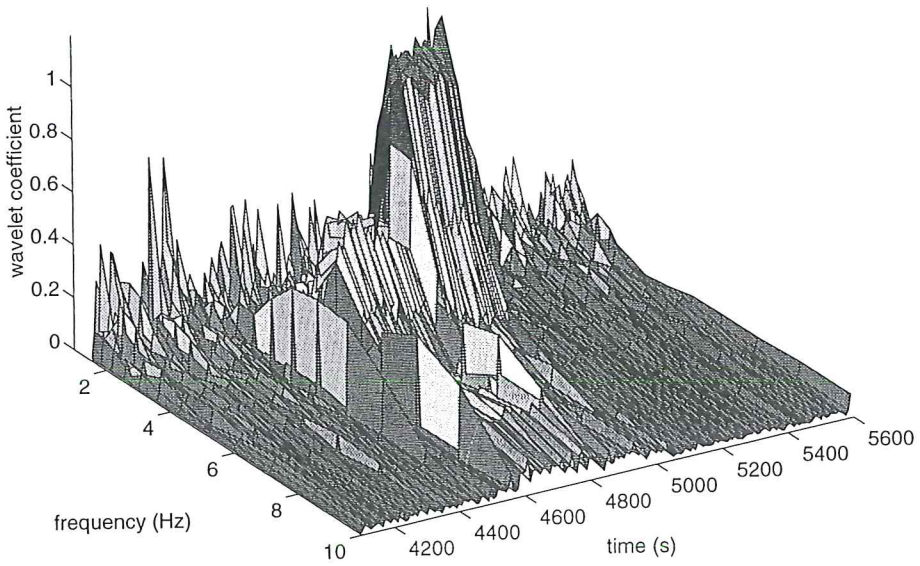

Figure 2-7. The wavelet coefficient as a function of time and frequency (obtained from analyzing the neutron noise signal shown in figure 2-6.b)

parts correspond to the time intervals t=4600-4800 s and t=4850-5050 s, respectively, of the neutron noise signal (see fig. 2-6.b). It can be seen that the second part results in much higher wavelet coefficient values then the first part. Two input orders were picked out from figure 2-7 and are shown in figure 2-6.c and 2-6.d. Input order 11 corresponds to f_c=3.5 Hz and 14 to f_c=2.1 Hz. These results illustrate the importance of applying a set of input orders when analyzing a signal.

2.4 Fractal analysis

Fractal analysis was originally introduced to describe the self-similarity of 2- and 3-dimensional complex shapes observed in natural phenomena. Mandelbrot was one of the first to propose the idea of fractal theory (Mandelbrot, 1982). The number of applications of fractal theory has been increasing since then. Applications are found in many different fields like mathematics, image processing, computer graphics, signal

analysis, etc.. Recently, fractal analysis was used to monitor two-phase flows (Djainal *et al.*, 1995). In this paragraph, fractal analysis is presented as a general method for describing the self-similarity of data series. Data series that show self-similarity can be represented by a parameter called the fractal dimension.

In order to calculate the fractal dimension of an irregular data series, the partial length of this series has to be determined first. The partial length of a data series is defined as follows (Mandelbrot, 1977):

$$L(k) = \frac{1}{N-k}\left(\sum_{i=1}^{N-k} |y(i+k)-y(i)|\right) \qquad (2\text{-}10)$$

where k denotes the time interval.

If $\langle L(k)\rangle \propto k^{\eta}$, then the data series reveals fractal characteristics (self-similarity) which can be denoted by the fractal dimension $D = 2\text{-}\eta$. For a data series D should lie between 1 and 2. The fractal dimension of a straight line equals one and the fractal dimension of white noise equals two (Mandelbrot, 1977).

The fractal dimension can be estimated by fitting a straight line to the log-log plot of $\langle L(k)\rangle$ versus k and estimating the slope of the line. The fitting can be done using the least-squares procedure. The variable η is then equal to the slope of the line. Since the fractal dimension of a data series can come very close to 2, η and thus the slope of the fitted line can approach 0. In order to increase the accuracy of the fit it is therefore better to fit a line to the log-log plot of $\langle L(k)\rangle/k^2$ versus k. The slope of the fitted line is then equal to $-D$.

The χ^2 value of the fit is a measure of the degree of fractalness of the data series. The smaller this value, the more the data series resembles the fractal model. It must be noted that the fractal dimension may depend on the range of k and on the value of N. It is therefore recommendable to first study the graph of $\langle L(k)\rangle/k^2$ versus k before N and the range of k are chosen.

When applying fractal analysis N is usually chosen as a power of 2 (32, 64, ... , 1024, 2048 etc.) and k is not taken larger than $N/8$. The following values are used for the time interval k; k=1,2,3,4 and $k=[2^{(j-1)/4}]$ (j=11,12,13,...) for k larger than 4 (Higuchi, 1988). It is also possible to take an k-range which doesn't start at k=1 and/or ends with $k=N/8$.

Fractal analysis was applied to a neutron detector signal measured with the NIOBE facility. Figure 2-8 shows the log-log plot of $\langle L(k)\rangle/k^2$ versus k for the 'full boiling',

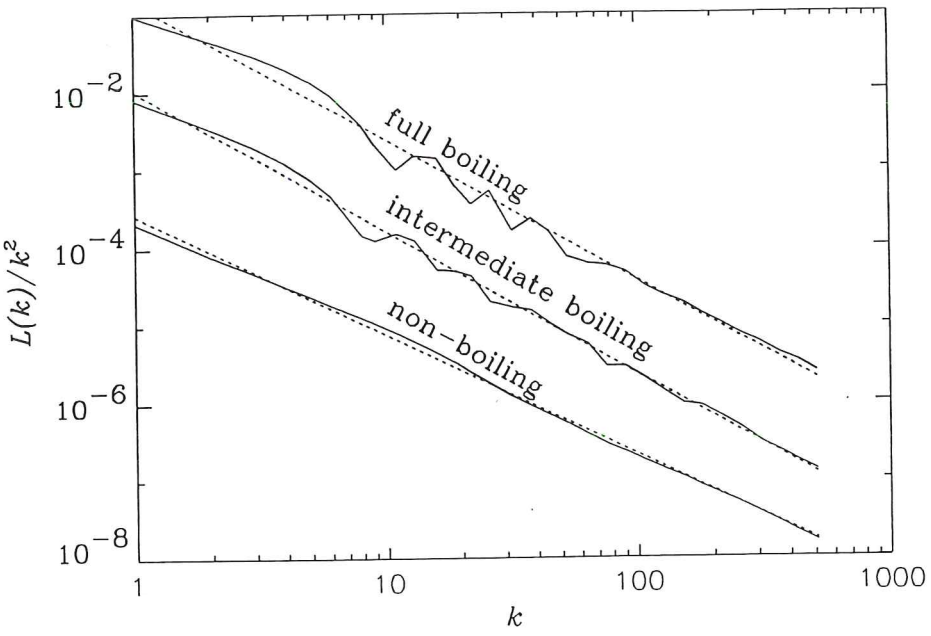

Figure 2-8. Determining the fractal dimension of the neutron detector signal

'intermediate boiling' and 'non-boiling' part of the neutron noise signal. It must be noted here that the 'intermediate boiling' curve and 'non-boiling' curve were shifted down one decade and two decades, respectively, in order to be able to distinguish the three curves.

For N the value of 4096 was taken and k ranges from 1 to 512. Each curve was fitted with a straight line. According to the fit, the fractal dimensions of the 'non-boiling', 'intermediate boiling' and 'full boiling' signal are equal to 1.55, 1.83 and 1.80, respectively. The fact that the neutron noise signal of the two 'boiling' parts shows stronger fluctuating behaviour (see fig. 2-6.b) could explain the higher fractal dimension values for these two parts.

Figure 2-6 shows three results of applying fractal analysis to the neutron noise signal shown in the second graph from the top of this figure. Figure 2-6.e and f give the fractal dimension for {N=64, k=1-8} and {N=256, k=1-32}, respectively. For N=64 there is a difference between the fractal dimensions of the two boiling states which is not the case for N=256. Moreover, the fractal dimensions of the two boiling states are smaller for N=64 than for N=256. These differences can be understood by looking at figure 2-8. When the two boiling curves are fitted over the interval k=1-8 (N=64) a

different slope is obtained then when they are fitted over the interval k=1-32 (N=256). For k=1-8 (N=64), a fit to the 'intermediate boiling' curve results in a steeper slope than a fit to the 'full boiling' curve, which explains the difference between the fractal dimensions of the two boiling states.

For {N=256, k=1-32} the fractal dimensions of the full and intermediate boiling states are equal to 1.84 and 1.83 which come very close to the results obtained with N=4096. For N values ranging from 256 to 4096 (k-range from 1 to N/8) the fractal dimensions of the three states differ only slightly from the corresponding fractal dimensions obtained with N=4096.

The fluctuation of the fractal dimension time series becomes smaller when N is increased. Thus when N is large and the k-interval is kept small, the difference between the two boiling states is maintained and the fluctuation is reduced. This is shown in figure 2-6.g, where N=256 and k=1-8. For these N and k values it is possible to distinguish the three states.

2.5 Conclusions

The practical applications of the three analysis techniques show that each one is able to detect the presence of certain anomalous behaviour in a signal. Without applying these techniques it would be much more difficult to 'see' the anomalies.

It is not yet known to which anomalies the analysis techniques will respond and to which not. As long as this is not known it is advisable to use all of the three techniques and to use a set of parameters in case of wavelet and fractal analysis. More applications of these methods will be shown in chapter 4.

When comparing the three analysis techniques fractal analysis shows a disadvantage in this case, namely that it usually requires more former data points then the other two techniques. In case of the applications shown in this chapter, AR required p+1=33 and wavelet required 51 former data points for calculating an output data value in contrast with fractal analysis which needed 256 former data points.

The analysis techniques indicate the presence of an anomaly; they do not give a definite answer about the state of the process. In the next chapter methods will be presented which do take a decision about the state of the process and deliver an output saying 'anomaly present' or 'no anomaly present'.

Chapter 3

ANOMALY DETECTION METHODS[1]

3.1 Introduction

Anomaly detection methods can make a decision about the state of the process under investigation by applying them to noise signals obtained through measurements. They can be applied to the noise signal itself or to any result from signal processing as presented in the previous chapter. At every time step, an anomaly detection method determines whether the process is in normal or anomalous state. As was mentioned in chapter 1 time-domain methods will be presented here.

Simple methods for anomaly detection are based on calculation of the average value or the standard deviation of a subset of points of the noise signal or time series. These methods will in general be slow and able to detect only relatively large changes. For obtaining a fast anomaly detection, able to detect small changes, it is necessary to use more sophisticated methods of detection.

In this chapter, three anomaly detection methods will be presented, namely the extremes method, the distribution method and the sequential probability ratio test (Wald, 1947). These methods have been used before for the detection of anomalies in reactor noise signals (Hoogenboom *et al.*, 1988; Glöckler, 1991). They will be studied using an artificially generated Gaussian distributed white noise signal in which a

---

[1] This chapter is an adapted version of the papers:
H. Schoonewelle, T.H.J.J. van der Hagen and J.E. Hoogenboom, "Theoretical and Numerical Investigations into the SPRT Method for Anomaly Detection", *Annals of Nuclear Energy*, **22**, 731 (1995)
H. Schoonewelle, T.H.J.J. van der Hagen and J.E. Hoogenboom, "A Comparison of Three Time-Domain Anomaly Detection Methods", *Annals of Nuclear Energy*, **23-2**, 159 (1996)

change of the standard deviation occurs. The goal of this study is to compare the methods (see chapter 4) in order to determine which method gives the fastest detection for a given false alarm rate.

The choice to focus on the detection of a change of the standard deviation of a Gaussian distributed white noise signal originated from studying the behaviour of neutron noise and thermocouple noise signals during boiling of the coolant using autoregressive modelling. Figure 3-1 shows the distribution of the residual noise from a thermocouple noise signal in case of boiling and in case of a normal situation (non-boiling). The distribution functions were determined using the measurements performed with the DeSiRe-facility (see section 4.4). It can be seen that the standard deviation of the residual noise increases due to boiling. The other moments of the two distributions are almost identical. The curtosis of both the distributions is near to 3 (3.3 for non-boiling and 3.2 for boiling) and the skewness is relatively small (<0.30 in both cases). This means that they can very well be approximated by a Gaussian distribution. Figure 3-2 shows the autocorrelation function of the residual noise in both cases. It can be seen that the residual noise is white in the non-boiling case (which is to be expected since the AR-model was determined using the non-boiling thermocouple noise signal) as well as in the boiling case.

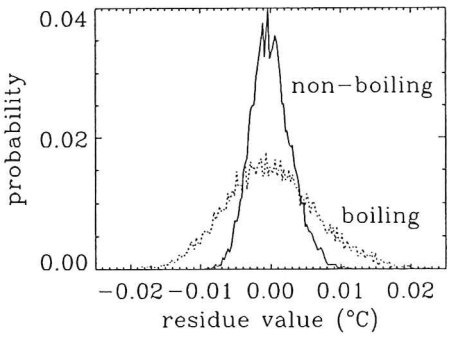

Figure 3-1. Distribution of the residual noise

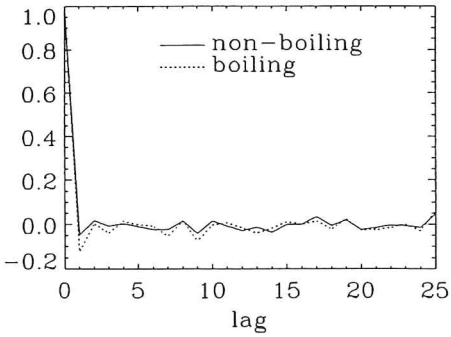

Figure 3-2. Autocorrelation function of the residual noise

For each of the three anomaly detection methods the *FAP*, *AFP* (and corresponding rates) and the *ATA* will be derived. For the extremes and distribution method the *FAP* and *AFP* can be determined theoretically, whereas for the SPRT they can only be approximated theoretically and have to be determined using numerical simulations. The

ATA has to be determined by numerical simulation for each of the three methods. These detection parameters will be used in the comparison presented in chapter 4.

As was mentioned at the beginning of this section, the detection methods can also be applied directly to the noise signal or to any other result from signal processing (wavelet, fractal). It should be noticed, however, that in this case the detection parameters can not be determined, since the probability distribution of the input noise signal or time series is not known and the noise signal or time series will most probably not be white. It is also possible that the average value or both the standard deviation and average value will change due to an anomaly. For the distribution and the SPRT method both an equation to detect a change in the average value and an equation to detect a change in the standard deviation will be given. The detection parameters will not be derived for the case of a change in average value. Some results of applying the detection methods to the outcomes of wavelet and fractal analysis will be shown at the end of chapter 4.

This chapter continues with the introduction and treatment of each anomaly detection method separately. The SPRT method will be dealt with more thoroughly, since all the detection parameters have to be determined by numerical simulation. For this method a comparison will be given between the theoretical approximations and numerical results.

3.2 Extremes method

For this method a record of N successive data values is considered and the number of values whose absolute value exceeds a certain predetermined threshold is counted. This threshold has been set equal to k (k>1) times the standard deviation of the data series under normal conditions (σ_0):

$$|x_i| > k \cdot \sigma_0 . \qquad (3\text{-}1)$$

An anomaly is declared whenever the number of values for which equation (3-1) holds, exceeds m ($1 \le m \le N$), assuming that the standard deviation increases due to the anomaly. k, m and N will be called the method parameters.

The extremes method can also be used for detecting a decrease of the standard deviation. In this case the number of absolute data values that are smaller than the

threshold $k\cdot\sigma_0$ ($k<1$) must be counted. Another possibility is to maintain equation (3-1) and to declare an anomaly whenever the number of values for which this equation holds, becomes smaller than m ($1\le m\le N$). If it is not known whether the standard deviation will increase or decrease, two thresholds or two values of m can be defined. The method is also able to detect an increase or decrease of the average value if an upper or a lower threshold, respectively, is used. Both the detection of a decrease in standard deviation and a change in average value will not be treated any further. For the remaining of this section it is assumed that the standard deviation increases.

The *FAP* and *AFP* can be calculated exactly assuming the data series to be white:

$$FAP = \sum_{i=m}^{N} \binom{N}{i} (1-p_0)^{N-i} \cdot p_0^{\,i}, \tag{3-2}$$

$$AFP = \sum_{i=0}^{m-1} \binom{N}{i} (1-p_1)^{i} \cdot p_1^{\,N-i}, \tag{3-3}$$

where p_0 and p_1 are the false alarm and the alarm failure probability, respectively, for a single data value. They can be calculated as follows, assuming the data series to be Gaussian distributed and having an average value equal to zero:

$$p_0 = 1 - \frac{2}{\sigma_0\sqrt{2\pi}} \int_0^{k\sigma_0} \exp\left(-\frac{x^2}{2\sigma_0^2}\right) dx = 1 - \mathrm{erf}\left(\frac{1}{2}\sqrt{2}\cdot k\right), \tag{3-4}$$

$$p_1 = \frac{2}{\sigma_1\sqrt{2\pi}} \int_0^{k\sigma_0} \exp\left(-\frac{x^2}{2\sigma_1^2}\right) dx = 1 - \mathrm{erf}\left(\frac{1}{2}\sqrt{2}\cdot\frac{k}{q}\right), \tag{3-5}$$

where $q\equiv\sigma_1/\sigma_0$ and $\mathrm{erf}(x)$ is the error function:

$$\mathrm{erf}(x) \equiv \frac{2}{\sqrt{\pi}} \int_0^{x} \exp(-t^2) dt. \tag{3-6}$$

In applying this method the record of length N is shifted one time step at a time so that successive records overlap each other. This means that a record contains the last N-1 data values of the previous record, plus the momentary value. In this way it is possible to make a decision about the state of the process every time step. It must be noted here that successive records are correlated.

The *FAR* and the *AFR* can be calculated from the *FAP* and the *AFP*, respectively, by multiplying the probabilities with the sampling frequency. The *ATA* can be determined by simulation using an artificially generated white noise signal in which a step in standard deviation from σ_0 to σ_1 occurs. The *ATA* can never be smaller than one sampling period since it takes at least one time step for the detection method to recognize the anomaly.

Table 3-1 presents the *FAR*, the *AFR* and the *ATA* for several values of k, m and N. In the table q is equal to 1.5 and the sampling frequency is taken to be 100 Hz. The table shows that increasing N for constant m and k increases the *FAR* but decreases the *AFR*, since more data values will pass the threshold due to the fact that more values are considered. The opposite is true when m is increased and N and k are kept constant, since in this case the number of data values that exceed the threshold remains the same, whereas the minimum number of values required (m) is increased. Large values of N are needed to achieve small values for both the *FAR* and the *AFR*. In order to have, for example, both rates smaller than 10^{-5} s^{-1} N must be at least 535 and m must be chosen properly, as is shown in row 5 of Table 3-1. Reducing both the *FAR* and the *AFR* leads to an increase of the *ATA*. The last two rows of the table show that the factor k also has

Table 3-1. The *FAR*, the *AFR* and the *ATA* for several combinations of the parameters of the extremes method (f_s = 100 Hz)

k	m	N	*FAR* (s^{-1})	*AFR* (s^{-1})	*ATA* (ms)
1.5	1	1	13.4	68.3	32.0 (±0.26)
1.5	1	10	76.2	2.20	15.9 (±0.17)
1.5	3	10	13.9	33.8	74.5 (±0.67)
1.5	3	100	99.9	$3.0 \cdot 10^{-11}$	10.0 (±0.005)
1.5	22	100	1.20	1.22	448 (±2.1)
1.5	116	535	$8.9 \cdot 10^{-6}$	$9.3 \cdot 10^{-6}$	2386 (±5)
1.75	22	100	0.0012	25.8	888 (±3.9)
1.25	22	100	45.5	0.0029	92.5 (±1.2)

a substantial influence on each of the three detection parameters. The table clearly shows that it is not possible to minimize the three detection parameters simultaneously.

3.3 Distribution method

The distribution method is based on the Neyman-Pearson Lemma (Hoel, 1984). This lemma provides a method for determining the test that minimizes the *AFP* for a given *FAP*. The basis of this lemma is the following inequality:

$$\frac{\prod_{i=1}^{N} F(x_i|a)}{\prod_{i=1}^{N} F(x_i|0)} \geq K, \tag{3-7}$$

where K is related to the *FAP* as will be shown later. $F(x_i|a)$ denotes the distribution function of the data series under anomalous conditions and $F(x_i|0)$ the distribution function of the data series under normal conditions. By substituting the distribution functions into inequality (3-7) the correct test is obtained. Suppose

$$F(x_i|a) = \frac{1}{\sigma_1\sqrt{2\pi}} \exp\left(-\frac{(x_i-\bar{x})^2}{2\sigma_1^2}\right) \tag{3-8}$$

and $F(x_i|0)$ is the normal distribution function with zero average value. Both distribution functions can now be substituted into inequality (3-7). It is assumed that the data series are white. Taking the logarithm of both sides of the inequality results in a test for the detection of a combined change of the average value and the standard deviation of a Gaussian distributed white noise signal:

$$\sum_{i=1}^{N}\left(\frac{1}{2}\left(\frac{1}{\sigma_0^2}-\frac{1}{\sigma_1^2}\right)x_i^2+\frac{\bar{x}}{\sigma_1^2}x_i\right) \geq \ln K + N\ln\left(\frac{\sigma_1}{\sigma_0}\right) + \frac{\bar{x}^2 N}{2\sigma_1^2}. \tag{3-9}$$

In case $\sigma_0=\sigma_1$, equation (3-9) results in a test for the detection of a change of the average value:

$$\sum_{i=1}^{N} \frac{x_i}{\sigma_0} \geq \frac{\sigma_0}{\bar{x}} \ln K + \frac{\bar{x} N}{2\sigma_0} . \qquad (3\text{-}10)$$

For the comparison in chapter 4 the main interest is in a change of the standard deviation. If $\bar{x}$ is set equal to zero in equation (3-9), a test for the detection of a change of the standard deviation is obtained:

$$S = \sum_{i=1}^{N} \frac{x_i^2}{\sigma_0^2} \geq 2 \frac{\ln K + N \ln(\sigma_1/\sigma_0)}{1 - (\sigma_0/\sigma_1)^2} \equiv B , \qquad (3\text{-}11)$$

where B is the threshold of the test. K is directly related to B which in turn is determined by the desired FAP (see eq. (3-13)). S will have a χ^2 distribution if the white noise has a Gaussian distribution and is in normal mode. From here on this method will be called the χ^2 method to distinguish it from the method which detects a change of the average value. An anomaly is declared when S exceeds B. In practice, the record of N successive data values is shifted one time step at a time (as in the extremes method), so that a decision about the state of the process is given every sampling period.

The distribution function of S is

$$F(S,\sigma) = \frac{S^{N/2-1} \sigma_0^N}{2^{N/2} \sigma^N \Gamma(N/2)} \exp\left(-\frac{S\sigma_0^2}{2\sigma^2} \right) \qquad (3\text{-}12)$$

and can be derived from the χ^2 distribution function. Γ denotes the gamma function. $F(S,\sigma)$ equals the χ^2-distribution function for $\sigma=\sigma_0$. Using equation (3-12), the FAP:

$$FAP = \int_B^{\infty} F(S,\sigma_0)\, dS \qquad (3\text{-}13)$$

and the AFP:

$$AFP = \int_0^B F(S,\sigma_1)\, dS = \int_0^{B/q^2} F(S,\sigma_0)\, dS . \qquad (3\text{-}14)$$

can be calculated. The *FAR* and *AFR* can be calculated from the corresponding probabilities by multiplying the probabilities with the sampling frequency.

This method can also be used when the standard deviation decreases. In this case, an anomaly is declared when the variable S becomes less than a certain lower threshold A. The χ^2 method requires less parameters than the extremes method: only two parameters (N and B) instead of three (k, m and N).

Table 3-2 presents the *FAR*, *AFR* and *ATA* for several combinations of N and B. The *ATA* was determined by simulation in the same way as with the extremes method. Again q was chosen equal to 1.5 and the sampling frequency was set at 100 Hz.

Table 3-2 shows that increasing N for constant B increases the *FAR* but decreases the *AFR*. The opposite is true when B is increased and N is kept constant. Comparing the 6th row of Table 3-2 with the 5th row of Table 3-1 it can be seen that the χ^2 method gives a smaller *AFR* than the extremes method for the same values of the *FAR* and N. It can also be seen that reducing both the *FAR* and *AFR* causes the *ATA* to increase. Again the results show that the *FAR*, the *AFR* and the *ATA* cannot be minimized simultaneously.

Table 3-2. The *FAR*, the *AFR* and the *ATA* for several combinations of the parameters of the χ^2 method

N	B	*FAR* (s^{-1})	*AFR* (s^{-1})	*ATA* (ms)
1	2.0	15.7	65.4	28.7 (±0.23)
10	2.0	99.6	0.010	10.05 (±0.01)
10	15.0	13.2	24.4	60.7 (±0.54)
30	15.0	99.0	$2.39 \cdot 10^{-4}$	10.23 (±0.03)
100	150.0	0.0904	0.418	416 (±2)
100	134.6	1.20	0.0488	290 (±1.6)
335	488.0	$9.0 \cdot 10^{-6}$	$8.94 \cdot 10^{-6}$	1237 (±3)

3.4 Sequential probability ratio test

The sequential probability ratio test was originally developed for testing a binary decision of one mode (normal) against an alternative mode (degradation). According

to Wald, who developed the method, it is an optimal method for testing a hypothesis against an alternative one in the sense that it requires, on the average, the minimum number of samples necessary to identify either mode for specified error probabilities (Wald, 1947).

The approach presented here differs in two respects from Wald's approach. First, the SPRT is applied continuously and the analysis is not stopped after the first decision. Second, it is assumed that a transition takes place from one state to the other at a random point in time during the analysis. The same approach has been used before (Chien *et al.*, 1976) for detecting an anomaly in a Gaussian noise signal and even for detecting a change in the standard deviation of a Gaussian noise signal (Glöckler, 1991), showing that SPRT is a method well suited for anomaly detection.

3.4.1 Basic theory of the SPRT-method

The SPRT is performed on a data series sample by sample. If the sample data set $X=\{x_1,x_2,...,x_i\}$ has an i-dimensional distribution $F_i(X|H_0)$ then hypothesis H_0 is true and if X has an i-dimensional distribution $F_i(X|H_1)$ then the alternative hypothesis H_1 is true. By definition, the basis of the SPRT method is the logarithm of the likelihood ratio function of the normal mode and an alternate degraded mode based on i samples (Wald, 1947):

$$\lambda(i) \equiv \ln \frac{F_i(x_1,x_2,....,x_i|H_1)}{F_i(x_1,x_2,....,x_i|H_0)} \qquad (3\text{-}15)$$

where $\lambda(i)$ is the decision parameter of the SPRT method.

In order to test hypothesis H_0 against H_1 two thresholds A and B are defined. At every sample $\lambda(i)$ is compared with these two thresholds. If

$$\lambda(i) = \ln \frac{F_i(X|H_1)}{F_i(X|H_0)} \geq B \qquad (3\text{-}16)$$

H_1 is accepted to be true. B is the upper decision threshold and is a positive constant. The inequality (3-16) implies that the probability that X belongs to hypothesis H_1 is at least $\exp(B)$ times larger than the probability that X belongs to hypothesis H_0. Since H_1 is accepted when inequality (3-16) holds, the sentence above can be rewritten in: $1-AFP$ is at least $\exp(B)$ times larger than FAP. Thus from equation (3-16) the following inequality is obtained:

$$1-AFP \geq FAP \cdot \exp(B) . \tag{3-17}$$

This can be rewritten in:

$$B \leq \ln \frac{1-AFP}{FAP} . \tag{3-18}$$

In the same way, it is defined that hypothesis H_0 is accepted when

$$\lambda(i) = \ln \frac{F_i(X|H_1)}{F_i(X|H_0)} \leq A . \tag{3-19}$$

A is the lower decision threshold and is a negative constant. Here the probability that X belongs to H_1 is at least $\exp(A)$ times smaller than the probability that X belongs to H_0. Since H_0 is accepted, inequality (3-19) can be rewritten in:

$$AFP \leq (1-FAP) \cdot \exp(A) . \tag{3-20}$$

This can be rewritten in:

$$A \geq \ln \frac{AFP}{1-FAP} . \tag{3-21}$$

Suppose the thresholds are chosen to be:

$$A = \ln \frac{AFP_{des}}{1-FAP_{des}}, \qquad B = \ln \frac{1-AFP_{des}}{FAP_{des}}, \tag{3-22}$$

where the desired probabilities are denoted by the subscript *des*. In this case, it is possible that the actual FAP and AFP deviate from the desired FAP and AFP. Combining equations (3-21) and (3-22) results in:

$$\ln \frac{AFP_{act}}{1-FAP_{act}} \leq A = \ln \frac{AFP_{des}}{1-FAP_{des}} \tag{3-23}$$

and

$$\ln \frac{1-AFP_{act}}{FAP_{act}} \geq B = \ln \frac{1-AFP_{des}}{FAP_{des}}, \tag{3-24}$$

where the subscript *act* denotes the actual probabilities. Rewriting and combining the two inequalities gives:

$$FAP_{act} \leq \frac{FAP_{des}}{1-AFP_{des}} \tag{3-25}$$

and

$$AFP_{act} \leq \frac{AFP_{des}}{1-FAP_{des}} . \tag{3-26}$$

In most practical cases FAP_{des} and AFP_{des} will be small meaning that $FAP_{des}/(1-AFP_{des})$ and $AFP_{des}/(1-FAP_{des})$ will be nearly equal to FAP_{des} and AFP_{des}, respectively. So by choosing A equal to $\ln(FAP_{des}/(1-AFP_{des}))$ and B equal to $\ln((1-AFP_{des})/FAP_{des})$ the FAP_{act} and the AFP_{act} will be smaller than or equal to the FAP_{des} and AFP_{des}, respectively, in most practical cases.

The difference between the actual and the desired probabilities is caused by the fact that $\lambda(i)$ can pass the thresholds A and B which is caused by the discontinuity of the test. The number of observations can only take integer values. The nearer $F_i(X|H_1)$ is to $F_i(X|H_0)$, the smaller will be the expected excess of $\lambda(i)$ over the thresholds and the smaller will be the discrepancy between the actual and the desired probabilities.

3.4.2 Testing of the standard deviation of a normal distribution

In this section, the definition of the SPRT method will be applied to the case that the expected anomaly is a combined change of the standard deviation and of the average value of a normal distribution function. Two equations to approximate the ATA will be derived.

If the data series x is assumed to be white, the data points x_i are mutually independent and the distribution function $F_i(X|H)$ in equation (3-15) can be rewritten in:

$$F_i(x_1,x_2,\ldots,x_i|H) = \prod_{j=1}^{i} F_1(x_j|H) . \tag{3-27}$$

Combining equations (3-15) and (3-27) and putting the resulting equation in a recursive form, results in:

$$\lambda(i) = \lambda(i-1) + \ln\frac{F_1(x_i|H_1)}{F_1(x_i|H_0)} . \tag{3-28}$$

When $F_1(x_i|H_0)$ is taken to be the normal distribution function with standard deviation

σ_0 and $F_1(x_i|H_1)$ is chosen equal to:

$$F_1(x_i|H_1) = \frac{1}{\sqrt{2\pi}\sigma_1}\exp\left(-\frac{(x_i-\bar{x})^2}{2\sigma_1^2}\right), \tag{3-29}$$

the following is obtained after some rewriting:

$$\lambda(i) = \lambda(i-1) + \frac{\sigma_1^2-\sigma_0^2}{2\sigma_1^2\sigma_0^2}x_i^2 + \left(x_i-\frac{\bar{x}}{2}\right)\frac{\bar{x}}{\sigma_1^2} - \ln\left(\frac{\sigma_1}{\sigma_0}\right). \tag{3-30}$$

If $\sigma_1=\sigma_0$, a SPRT for the detection of a change in the average value of the white noise is obtained:

$$\lambda(i) = \lambda(i-1) + \left(x_i-\frac{\bar{x}}{2}\right)\frac{\bar{x}}{\sigma_0^2}. \tag{3-31}$$

For the detection of a change in the standard deviation ($\bar{x} = 0$) equation (3-30) can be rewritten in:

$$\lambda(i) = \lambda(i-1) + \frac{\sigma_1^2-\sigma_0^2}{2\sigma_1^2\sigma_0^2}x_i^2 - \ln\left(\frac{\sigma_1}{\sigma_0}\right). \tag{3-32}$$

The rest of this section is focussed on the detection of a change in the standard deviation. Notice that equation (3-32) can also be used in case $\sigma_1<\sigma_0$.

At each time step i the parameter λ is compared with the two thresholds A and B (eq. (3-22)). When parameter λ passes threshold A data series x is concluded to be in normal mode. When λ passes threshold B x is said to be anomalous and in case λ lies in between the two thresholds no decision is made. After a decision λ is reset to zero.

From equation (3-32) $\Delta\lambda(i)$ can be determined:

$$\Delta\lambda(i) = \lambda(i) - \lambda(i-1) = \frac{\sigma_1^2-\sigma_0^2}{2\sigma_1^2\sigma_0^2}x_i^2 - \ln\left(\frac{\sigma_1}{\sigma_0}\right). \tag{3-33}$$

Since data series x is assumed to be a Gaussian distributed and white with standard deviation σ the expectation value of x_i^2 is equal to σ^2. In case x is in normal mode equation (3-33) can be rewritten to:

$$\langle\Delta\lambda\rangle_{norm} = \frac{q^2-1}{2q^2} - \ln(q) \tag{3-34}$$

and for x anomalous to:

$$\langle \Delta\lambda \rangle_{anom} = \frac{q^2 - 1}{2} - \ln(q), \qquad (3\text{-}35)$$

where $q=\sigma_1/\sigma_0$.

These equations show that the expected value of λ will decrease at each time step when x is in normal mode and it will increase at each time step when x is anomalous, irrespective of whether $\sigma_0>\sigma_1$ or $\sigma_0<\sigma_1$.

Figure 3-3 gives an example of the behaviour of λ. This behaviour was simulated using a Gaussian distributed white noise signal in which an anomaly occurred at time step 501. A decision about the state of the process is taken every time λ passes a threshold. The figure shows that the time interval between two decisions is not constant.

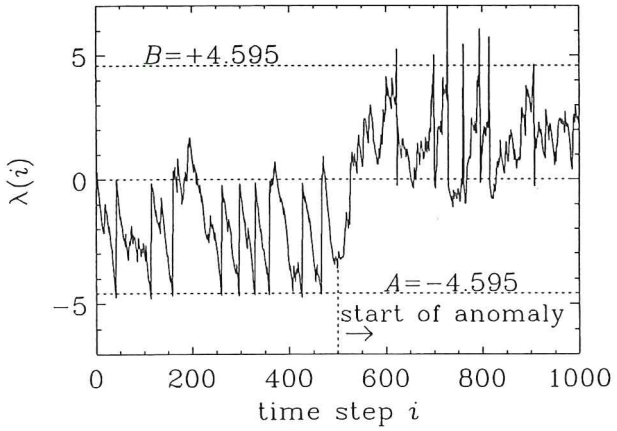

Figure 3-3. Example of behaviour of λ in case of anomaly ($\sigma_1=1.3\cdot\sigma_0$; $FAP_{des}=AFP_{des}=0.01$)

In order to determine the average time to alarm (ATA), the expectation value of λ at the start of the anomaly must be known as well as the average number of time steps it takes for λ to reach the upper threshold B. Figure 3-4 shows the expectation value of λ for FAP_{des} and AFP_{des} both equal to 0.01 and q=1.5 for a noise signal in normal mode.

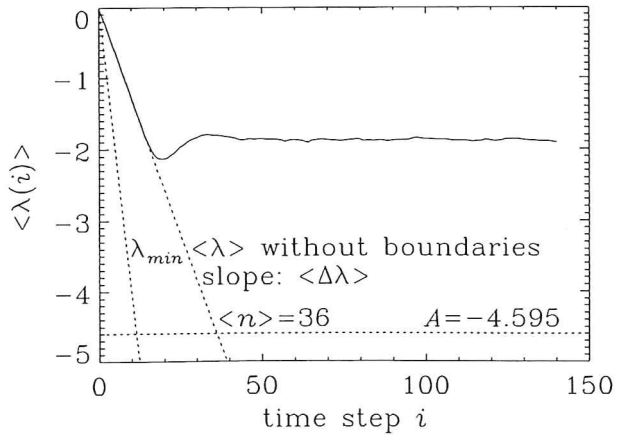

Figure 3-4. Expectation value of λ in normal situation ($FAP_{des}=AFP_{des}=0.01$)

This graph was determined by making 10000 independent calculations of $\lambda(i)$ $\{i=1..142\}$, using a normal distributed white noise signal and averaging over all these sets of $\lambda(i)$. For every calculation λ started at zero. The signal was generated by routine G05FDF from the NAG-library (NAG, 1991).

We can see in figure 3-4 that $\langle\lambda\rangle$ starts to deviate from the line $\langle\lambda\rangle=\langle\Delta\lambda\rangle \cdot i$ for approximately $i=15$. This can be understood by looking at equation (3-35). From this equation it follows that $\Delta\lambda_{min}=-\ln(q)$; in this case $A/\Delta\lambda_{min}=11.3$. So it is possible for λ to reach the lower threshold A in 12 time steps. Beyond this value of i the resetting of λ has such a major effect on its expectation value that $\langle\lambda\rangle$ quickly stabilises at a value of -1.87 after approximately 40 time steps. This means that for the entire duration of the SPRT analysis, with exception of the first 40 time steps, $\langle\lambda\rangle$ is equal to -1.87 in this case.

When the presence of the lower threshold A and the fact that the ATA can only take integer values in actual situations are neglected, the ATA can be calculated using the expectation value of λ:

$$ATA = \frac{(B-\langle\lambda\rangle)}{\langle\Delta\lambda\rangle_{anom}}. \qquad (3\text{-}36)$$

Here it is assumed that $\langle\lambda\rangle$ has stabilised, meaning that the anomaly does not occur before the 40th time step (counted from the start of the analysis) in case of the example in figure 3-4. $\langle\Delta\lambda\rangle_{anom}$ can be calculated using equation (3-35).

Before the ATA can be calculated with this equation $\langle\lambda\rangle$ must be known. The latter has to be determined by simulation for all possible combinations of FAP_{des}, AFP_{des} and q. Therefore, it would be better to have an approximation of equation (3-36) by approximating the distribution of λ.

Figure 3-5 shows the distribution of λ for FAP_{des} and AFP_{des} equal to 0.01. The peak for $\lambda=-0.405$ can be ascribed to the distribu-

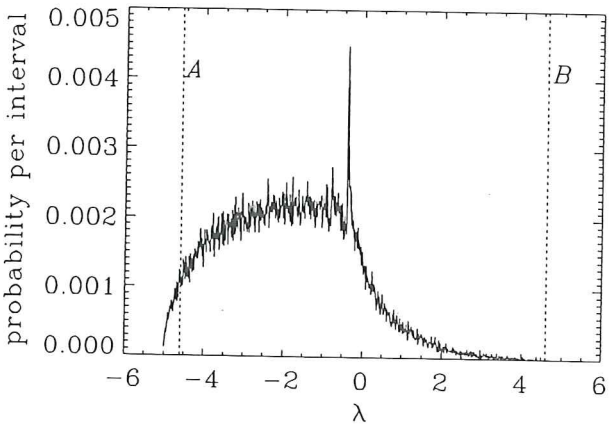

Figure 3-5. PDF of λ for 1000 intervals ($FAP_{des} = AFP_{des} = 0.01$)

tion of λ after one time step. Looking at equation (3-32), it can be seen that $\lambda(1)$ is χ^2-distributed with one degree of freedom. Equation (3-37) gives the distribution function of $\lambda(1)$. This function is limited to the left by an asymptote for $x=-\ln(q) = -0.405$ ($=\Delta\lambda_{min}$) where $g(x)$ goes to plus infinity. This explains the peak in the distribution of λ. The distribution function of $\lambda(1)$ equals:

$$g(x) = \frac{\sqrt{q^2-1}}{2\sqrt{\pi}\sigma_0^2 q}(x+\ln(q))^{-\frac{1}{2}} \cdot \exp\left(-\frac{1}{2}(x+\ln(q))\frac{2q^2}{q^2-1}\right). \qquad (3\text{-}37)$$

If the distribution of λ is approximated by a distribution that is uniform between 0 and A and zero elsewhere, $\langle\lambda\rangle$ will be equal to $\frac{1}{2}A$ in case of a noise signal in normal mode. This approximation will be better the lower the values of FAP_{des} and AFP_{des}. Comparing this with $\langle\lambda\rangle = -1.87$ obtained from figure 3-4, it can be seen that the approximation gives a smaller value for $\langle\lambda\rangle$, namely $\frac{1}{2}A = -2.298$. For values of q higher than 1.5 but smaller than 2.3, the approximation becomes better and for $q > 2.3$ the approximation gives higher values for $\langle\lambda\rangle$ (FAP_{des} and AFP_{des} equal to 0.01).

Starting with the approximation that $\langle\lambda\rangle=\frac{1}{2}A$, the ATA can be determined using the definition of the thresholds A and B (eq. (3-22)) and equation (3-35) for $\langle\Delta\lambda\rangle_{anom}$:

$$ATA = \frac{\ln[(1-FAP_{des})\cdot(1-AFP_{des})^2/(AFP_{des}FAP_{des}^2)]}{q^2 - 1 - 2\cdot\ln(q)}. \qquad (3\text{-}38)$$

In the equation it is neglected that λ can pass the thresholds and that the number of observations is in fact a discrete variable. When the anomaly is detected one time step later than its occurrence the ATA is equal to 1 by definition.

In the next section, the results from determining the ATA by simulation will be compared with the results from the two equations (3-36) and (3-38).

3.4.3 Comparison of theoretical and calculational results

As was mentioned before, FAP_{des} and AFP_{des} give an upper limit for the FAP_{act} and the AFP_{act}, respectively, in most practical cases. By using an artificially generated white noise signal with Gaussian distribution, approximations of the FAP_{act} and the AFP_{act} can be determined. For these approximations the same notations will be used. The ATA will also be determined for different cases by simulation and a comparison will be made with the theoretical prediction given in the previous section.

Routines from the NAG-Library (NAG,1991) for generating the white noise signal have been used. The number of data points used for simulation was always less than the square root of the cycle length of the random generator, in order to have reliable statistical properties of the signal.

For calculating the FAP_{act} and AFP_{act} the following two equations were used:

$$FAP_{act} = \frac{number\ of\ crossings\ of\ B}{total\ number\ of\ crossings} \tag{3-39}$$

in case of a normal noise signal ($\sigma=\sigma_0$) and

$$AFP_{act} = \frac{number\ of\ crossings\ of\ A}{total\ number\ of\ crossings} \tag{3-40}$$

in case of an anomalous noise signal ($\sigma=\sigma_1$). The total number of crossings is equal to the number of crossings of A plus the number of crossings of B.

The uncertainty in the FAP_{act} and AFP_{act} is mainly determined by the uncertainty in the numerator of equation (3-39) and (3-40), respectively. The standard deviation of the number of crossings is approximately equal to the square root of the number of crossings. This approximation is better the fewer the number of crossings and will give an overestimation in case of a large number of crossings.

Determining the FAP_{act}

The FAP_{act} was determined using a white noise signal with standard deviation σ_0. In order to get statistically reliable results 10 million sample points were used. Figure 3-6 shows the calculated FAP_{act} as a function of q ($FAP_{des}=AFP_{des}=10^{-2}$). The graph also shows a fit with the empirical function:

$$FAP_{act}(q) = c_1 \cdot q^{-c_2} \tag{3-41}$$

with c_1 having the value of $0.950 \cdot 10^{-2}$ and c_2 having the value of 1.628. The FAP_{act} is

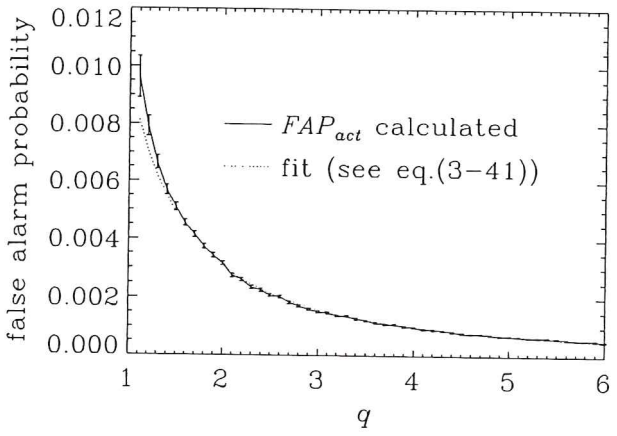

Figure 3-6. FAP_{act} as a function of q ($FAP_{des} = AFP_{des} = 0.01$)

indeed smaller than the FAP_{des} (eq. (3-25)) and decreases for increasing values of q. This can be understood by considering the fact that the excess of λ over the thresholds becomes greater when q increases, since $\langle\Delta\lambda\rangle_{norm}$ (eq. (3-34)) increases. The former causes the FAP_{act} to decrease. The statistical error becomes smaller with increasing q because $\langle\Delta\lambda\rangle_{norm}$ and thus the number of crossings increases.

The calculation of the FAP_{act} has been performed for 74 different combinations of FAP_{des} and AFP_{des} and values of q ranging from 1.1 to 6. The values of FAP_{des} ranged from 10^{-1} to $3\cdot10^{-4}$ and the values of AFP_{des} ranged from 10^{-1} to 10^{-9}. For each combination of FAP_{des} and AFP_{des} the graph was fitted with function (3-41) which resulted in the following average value for c_2:

$$c_2 = 1.616 \quad (\sigma = 0.056)\,. \tag{3-42}$$

Hence the decrease of FAP_{act} with q is nearly independent of FAP_{des} and AFP_{des}. In two of the 74 different combinations c_1 was larger than FAP_{des} but in both cases the difference was only minor. The relative difference between c_1 and FAP_{des} was never larger than 17.7 %.

So in order to have a reasonable approximation of FAP_{act} one can replace q by FAP_{des} in equation (3-41). The calculations show that for all the values of q ($1.1 \le q \le 6.0$) the FAP_{act} is indeed smaller than FAP_{des}. For q between 1 and 1.1 it may be possible that the FAP_{act} is slightly larger than the FAP_{des}. This, however, can be neglected when the AFP_{des} is small (see eq. (3-25)). From equation (3-22) it can be seen that for $AFP_{des} \le 0.1$ threshold B is practically independent of AFP_{des}. Apparently, the FAP_{act} is especially determined by the upper threshold B.

In case $q<1$ the graph of FAP_{act} can not be fitted with a simple function like eq. (3-42). It can still be seen, however, that for $q \le 0.9$, the FAP_{act} is smaller than the FAP_{des} and decreases for decreasing values of q.

Determining the AFP_{act}

The alarm failure probability can be determined using a white noise signal with standard deviation σ_1. Starting with the same value of AFP_{des} ($= 10^{-2}$) gives figure 3-7 for the AFP_{act} as a function of q for four different values of FAP_{des}. Again 10 million sample points per value of q were used for determining the AFP_{act}.

In this case, it was not possible to fit a function to the graph of AFP_{act}. Again, however, the calculations showed that for all values of q ranging from 1.1 to 6, AFP_{des} is indeed an upper limit for the alarm failure probability. This is also true for $q<1$ (not

shown here). For q between 1 and 1.1 it may be possible that the AFP_{act} is slightly larger than the AFP_{des}. This, however, can be neglected when the FAP_{des} is small (see eq. (3-26)). Calculations showed that for small values of FAP_{des} (≤ 0.01) the AFP_{act} shows no demonstrable dependence on FAP_{des} as can be seen in figure 3-7. In the case that FAP_{des} is small, threshold A is almost independent of FAP_{des} (see eq. (3-22)). Thus the AFP_{act} is apparently mostly determined by the lower threshold A.

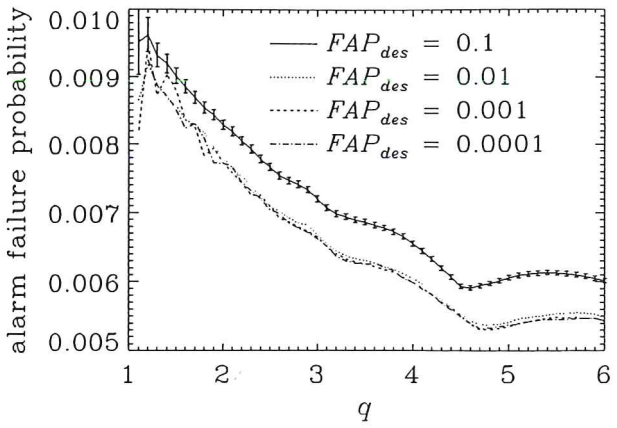

Figure 3-7. Alarm failure probability as a function of q ($AFP_{des} = 0.01$)

The graph also shows that the AFP_{act} decreases more slowly than the FAP_{act} with increasing q. Here, again, the decrease of AFP_{act} can be explained by the fact that the excess of λ over the thresholds becomes greater when q increases. For q=6 the AFP_{act} is still larger than half the value of AFP_{des}.

Figure 3-7 shows that the AFP_{act} is not monotonic in q since there is a (local) minimum for $q \approx 4.5$. The graph also shows a dip for q=3.1. When the graph is extended to higher values of q it can be seen that the AFP_{act} has also local minima for $q \approx 9.5$ and $q \approx 90$. For these values of q $A/\Delta\lambda_{min} = -A/\ln(q)$ is approximately equal to 3, 4 (for q=3.1), 2 and 1, respectively. This means that for q between 4.5 and 9.5 λ can reach the lower threshold A from zero in 3 time steps and for q higher than 9.5 this is possible in 2 time steps. This decrease in number of steps will at first cause the number of crossings of A to increase with increasing q (q just above 4.5). Since the number of crossings of B increases only slightly and is much higher than the number of crossings of A, the AFP_{act} will increase too.

Determining the ATA

The ATA can be determined using an artificially generated Gaussian distributed white noise signal in which a step in standard deviation from σ_0 to σ_1 occurs. The number of sample points before the step was always enough to get a correct

expectation value of λ at the instant of the step (see fig. 3-4). By averaging over a great number of white noise signals an average value for the *ATA* depending on FAP_{des}, AFP_{des} and q can be determined.

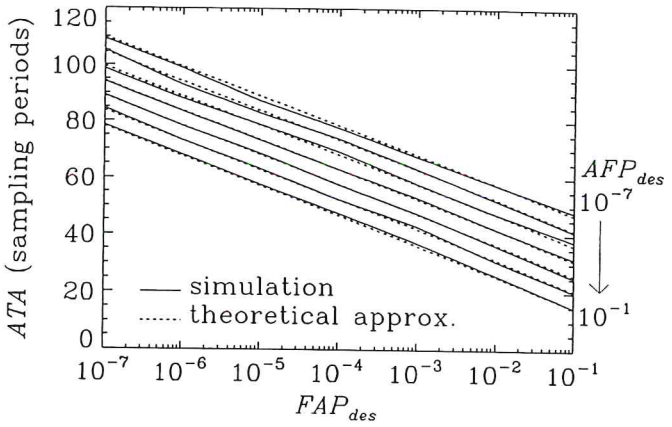

Figure 3-8. *ATA* as a function of FAP_{des} and AFP_{des}

Figure 3-8 shows the *ATA* as a function of FAP_{des} and AFP_{des} for q=1.5. The *ATA* is linearly dependent on ln(FAP_{des}) and on ln(AFP_{des}) as was deter mined theoretically. Figure 3-8 shows the theoretical result (eq. (3-38)) which comes very close to the result obtained by simulation. The relative difference between the calculated and theoretical *ATA* is never larger than 3.5 %. The graph also shows that the *ATA* decreases for increasing values of FAP_{des} and AFP_{des} which means that in practical cases one always has to make a compromise between a small value for the *ATA* and small values for the probabilities.

Figure 3-9 shows the *ATA* as a function of q for $FAP_{des}=AFP_{des}=10^{-2}$. It can be seen that the *ATA* decreases for increasing values of q. If $q<1$, it can be found that the *ATA* decreases with decreasing values of q. This case will not be presented here. The error margins are shown too, but are very small. For larger values of q the two theoretical predictions using equations (3-36) and (3-38) give comparable values for the *ATA* which are smaller than those determined by simulation. This difference between the predicted and simulated values is mainly caused by

i. the fact that the number of observations is a discrete variable;
ii. the fact that the *ATA* can never be smaller than one sampling period by definition.

For small values of q the theoretical prediction using the simulated expectation value of λ is substantially better than the prediction using $\langle\lambda\rangle = \frac{1}{2}A$. This difference becomes smaller, however, for smaller values of FAP_{des} and AFP_{des}. For FAP_{des} and AFP_{des} equal to 10^{-7} the relative difference between the *ATA* determined by simulation and the *ATA* determined with equation (3-36) is only 2.0 %. For the prediction with equation (3-38) the difference with the simulated *ATA* is 5.2 %. The theoretical predictions of the *ATA*

are larger than the one determined by simulation, for these values of q. This difference is mainly caused by:

i. the fact that the average value of λ is larger than $\frac{1}{2}A$ in case of a signal in normal mode for this value of q (this only applies to the second theoretical prediction);
ii. the fact that the presence of a lower threshold can cause λ to jump to zero after passing the lower threshold.

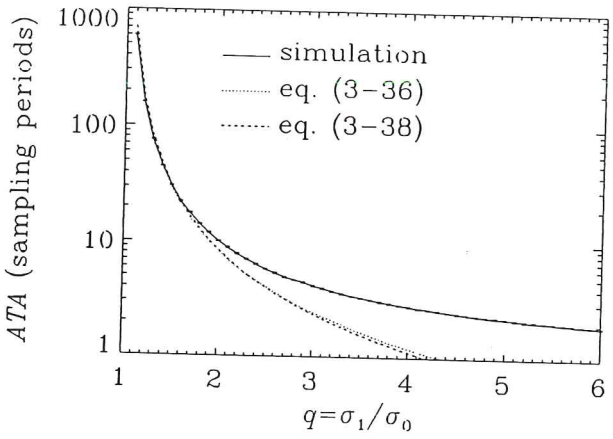

Figure 3-9. ATA as a function of q ($FAP_{des} = AFP_{des} = 0.01$)

The simulated curve and the curve from the first theoretical prediction (eq. (3-36)) cross each other at approximately q=1.35. The simulated curve and the third curve cross each other at approximately q=1.59.

For determining the actual ATA for an arbitrary value of q the graph in figure 3-9 and eq. 3-38 are needed. The actual ATA is determined by summing the ATA obtained with eq. 3-38 and the difference between the simulated curve and the curve from eq. 3-38 (fig. 3-9) for the given value of q. It should be noted here, that it is assumed that the beforementioned difference is independent of FAP_{des} and AFP_{des}.

Determining the ATA with eq. 3-36 is only significant when q is small (q<1.5) and FAP_{des} and AFP_{des} are relatively large (FAP_{des}, $AFP_{des} > 10^{-5}$). In other cases, the little extra accuracy is not worth the effort of determining $\langle\lambda\rangle$ by simulation.

Determining the FAR, AFR and the ATA (seconds)

In practical situations, the alarm rates are more important than the alarm probabilities, since they give an idea about the number of alarms per period of time. Also, it is better to know the ATA in seconds instead of sampling periods. The rates can be calculated as follows:

$$Rate = \frac{number\ of\ crossings\ of\ A\ or\ B}{total\ number\ of\ samples} \cdot f_s, \qquad (3\text{-}43)$$

where f_s stands for the sampling frequency.

In order to derive the false alarm or alarm failure rate from the corresponding probabilities, these probabilities have to be multiplied with the sampling frequency and divided by the average number of samples per decision. The *ATA* in seconds can simply be determined by dividing the *ATA* in sampling periods by the sampling frequency.

Figure 3-10 gives the *ATA* as a function of the $^{10}\log(FAR)$ and $^{10}\log(AFR)$. All three variables were determined by simulation. From the figure it can be concluded that the *ATA* is approximately linearly dependent on $^{10}\log(FAR)$ and on $^{10}\log(AFR)$ and depends more on the *FAR* than on the *AFR*.

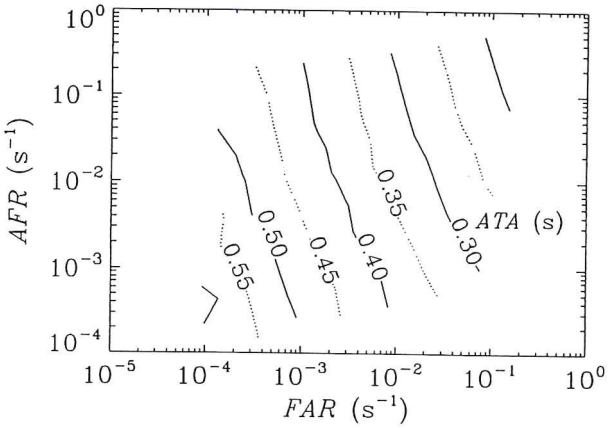

Figure 3-10. Contour plot of *ATA* for q=1.5

Table 3-3 shows the *FAR*, the *AFR* and the *ATA* for some combinations of the FAP_{des} and AFP_{des}. The FAP_{act} and the AFP_{act} are given as well. The sampling frequency is 100 Hz and q=1.5. The FAP_{act} and the *ATA* were determined by simulation as well as by theory (eq. (3-41) for the FAP_{act} and eq. (3-38) for the *ATA*).

Table 3-3. The *FAR*, the *AFR* and the *ATA* for several combinations of FAP_{des} and AFP_{des}

FAP_{des}	AFP_{des}	FAP_{act} (10^{-3})		AFP_{act} (10^{-3})	*FAR* (s^{-1})	*AFR* (s^{-1})	*ATA* (ms)	
		sim.	theory				sim.	theory
0.1	0.1	50.0	52.0	90.0	0.305	0.727	151	150
0.1	0.001	51.0	52.0	0.88	0.100	$5.8\cdot10^{-3}$	254	260
0.001	0.1	0.52	0.52	86.0	$2.7\cdot10^{-3}$	0.271	373	362
0.001	0.001	0.46	0.52	0.84	$0.83\cdot10^{-3}$	$2.33\cdot10^{-3}$	475	472

The table shows that the FAP_{act} is mainly determined by the upper threshold B and the AFP_{act} is mainly determined by the lower threshold A which is in agreement with the conclusions drawn earlier. The table also shows that lowering the FAR and AFR increases the ATA. This can also be concluded from figure 3-10. The FAP_{act} and the AFP_{act} are smaller than the FAP_{des} and the AFP_{des}, respectively. The ATA values calculated by simulation come very close to the values determined with equation (3-38). The third and fourth column show a good agreement between the values of the FAP_{act} from simulation and those from theory.

3.5 Conclusions

Three anomaly detection methods were presented in this chapter, namely the extremes, the χ^2 method and the sequential probability ratio test. Each method shows that it is not possible to minimize the three detection parameters, namely the false alarm rate (FAR), the alarm failure rate (AFR) and the average time to alarm (ATA), simultaneously.

The extremes method requires three parameters: N, m and k. By increasing N for constant m and k the AFR can be decreased but the FAR increases. The opposite is true when m is increased and N and k are kept constant. In order to achieve small values for both the FAR and the AFR, large values of m and N are needed. This, however, results in a large value of the ATA.

The χ^2 method requires two parameters: N and B or N and A if the standard deviation of the anomalous signal is smaller than the standard deviation of the signal in normal mode. By increasing N for constant B, the AFR decreases but the FAR. increases The opposite is true when B is increased and N is kept constant. The χ^2 method gives a smaller AFR than the extremes method for an equal FAR and an equal N.

The sequential probability ratio test requires two parameters: FAP_{des} and AFP_{des} or A and B. Simulation results show that the theory of the method gives proper means for selecting an upper limit for the FAP_{act} and the AFP_{act} in all practical cases where the change in standard deviation is not too small ($q \geq 1.1$). In case $1<q<1.1$ it may be possible that the FAP_{act} and AFP_{act} are slightly larger than the desired ones. This, however, can be neglected when FAP_{des} and AFP_{des} are small.

The actual probabilities decrease with increasing q and show no demonstrable dependence on each other for small values of the desired probabilities. The FAP_{act} can

be approximated using a function which mainly depends on q and on FAP_{des}. The AFP_{act} could not be fitted with a function. The ATA depends on the desired probabilities and on q. The smaller the probabilities the larger ATA. ATA decreases for increasing value of q.

A disadvantage of the SPRT method with respect to the other two methods is that σ_1 must be known or chosen before the method is applied. Only when the standard deviation of the anomaly occurring is smaller than the chosen σ_1 the AFP_{act} may be larger than the AFP_{act} expected. In practical applications it is therefore recommended to choose a lower limit for σ_1 in order to be certain that the AFP_{act} is smaller than its desired value.

Chapter 4

OPTIMIZATION AND COMPARISON OF ANOMALY DETECTION METHODS[1]

4.1 Introduction

The three anomaly detection methods, namely the extremes method, the χ^2 method and the sequential probability ratio test, that were presented in the previous chapter, will be compared in this chapter.

First, a theoretical comparison will be presented. The methods are compared on their ability to give a fast detection of a step in the standard deviation of a Gaussian distributed white noise signal for a given false alarm rate. According to the Neyman-Pearson lemma the χ^2 method is the 'best' test for detecting a change of the standard deviation of a Gaussian distributed white noise signal (Hoel, 1984). The SPRT method is, according to Wald, an optimal method for testing a hypothesis against an alternative one (Wald, 1947). In this chapter, the validity of these statements will be checked by comparing the three detection methods. In order to come to this comparison each method will be optimized first. Optimization means minimizing the *ATA* for a given value of the *FAR*. This is done for a large range of *FAR* values for each method. The best method is the method which gives on the average the smallest *ATA* for the range of *FAR* values studied.

---

[1]This chapter is an adapted version of the papers:
H. Schoonewelle, T.H.J.J. van der Hagen and J.E. Hoogenboom, "A Comparison of Three Time-Domain Anomaly Detection Methods", *Annals of Nuclear Energy*, **23-2**, 159 (1996)
H. Schoonewelle, T.H.J.J. van der Hagen and J.E. Hoogenboom, "Practical and Theoretical Aspects of the Sequential Probability Ratio Test for Anomaly Detection", *Proc. of SMORN-VII, A Symposium on Nuclear Reactor Surveillance and Diagnostics*, June 19-23, 1995, Avignon, France

Second, anomaly detection will be performed on actual thermocouple noise signals measured at the Delft Simulated Reactor (DeSiRe) at the Interfaculty Reactor Institute in Delft. Measurements with changing heating power were performed during which a transition from a non-boiling (normal situation) to a boiling state (anomalous situation) occurred. The three detection methods are applied to the thermocouple signals and to the results from signal processing (AR, wavelet and fractal analysis) of the thermocouple noise signals. For each application the same false alarm and alarm failure rate values are chosen and the results are compared on the basis of the *ATA*.

4.2 Optimization of each anomaly detection method

Before the methods can be compared they have to be optimized, meaning that the minimum *ATA* for a given *FAR* value has to be found for each method. Only the optimization for $q=\sigma_1/\sigma_0=1.5$ will be discussed in detail. The results of the optimization for other values of q will be mentioned. The minimization of *ATA* will be done for a set of *FAR* values.

4.2.1 Extremes method

The extremes method was introduced in section 3.2. For this method a record of N successive data values is considered and from this record the number of data values whose absolute value exceeds a certain predetermined threshold ($= k\cdot\sigma_0$) are counted. An anomaly is declared whenever this number exceeds m ($1 \leq m \leq N$).

The extremes method has 3 method parameters, namely k, m and N. If a certain *FAP* is required N and m ($\leq N$) can be chosen independently and k can be calculated in order to get the desired *FAP*. There are still two degrees of freedom left for minimization of the *ATA*. Thus by varying m and N and adjusting k every time to get the desired *FAP*, the values of m and N can be found for which the *ATA* has its minimum. This has to be done for several values of the *FAP*.

Figure 4-1 gives an example of the *ATA* for $FAP=10^{-4}$ and $q=1.5$ for values of N ranging from 1 to 100 and values of m ranging from 3 to $N/2+1$. The *ATA* is not shown for m and N outside this range since the *ATA* only increases for other values of m and N. The *ATA* has been determined by simulation using an artificially generated Gaussian distributed white noise signal. For every combination of m and N the *ATA* has been

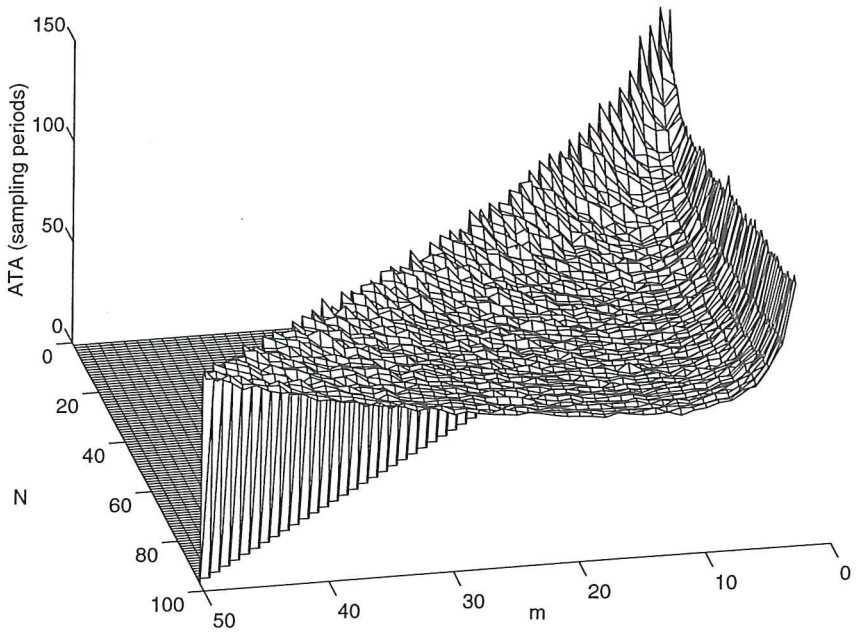

Figure 4-1. The *ATA* as a function of *m* and *N* for the extremes method

determined by averaging over 1000 simulations. The 3-dimensional graph does not have a sharp minimum. In order to determine the overall minimum, first the minimum per value of *N* has been determined after which the curve connecting the minimum values of the *ATA* for each *N* has been smoothed. This resulted in a overall minimum for the *ATA* of 64.3 sampling periods for N=54 and m=10. This calculation has been performed for 7 different values of the *FAP*. The results for q=1.5 are listed in table 4-1. Again a sampling frequency of 100 Hz was taken.

In comparing Table 4-1 with Table 3-1 it can be noticed that minimizing the *ATA* does certainly not minimize the *AFR*. In some cases the *AFP* is even close to 1. The comparison also shows that the minimum values of the *ATA* are reached for relatively small values of *N*. The smaller *N*, the fewer former data values are kept in the record, resulting in a faster response to an anomaly.

It is remarkable that the ratio of *m* to *N*, at which the *ATA* has its minimum, is constant. This gives the opportunity to predict the *m* value that will yield the smallest

Table 4-1. Minimum values of the *ATA* for several values of the *FAR* for the extremes method

FAR (s^{-1})	*AFR* (s^{-1})	*k*	*m*	*N*	*ATA* ($\cdot 10^{-2}$ s)	*m'*
10.0	72.7	1.65	1	1	3.68 (±0.03)	1
1.0	91.4	2.58	1	1	11.7 (±0.11)	1
0.10	97.2	3.29	1	1	35.2 (±0.36)	1
0.010	49.7	2.02	10	54	64.3 (±0.40)	10
$1.0 \cdot 10^{-3}$	58.1	2.04	12	63	84.6 (±0.57)	12
$1.0 \cdot 10^{-4}$	37.6	1.95	19	103	104.5 (±0.53)	19
$1.0 \cdot 10^{-5}$	29.4	1.95	24	134	124.6 (±0.54)	24

ATA for a given *FAR* and *N*. Consider column 7 showing *m'* which is equal to $0.182 \cdot N$ rounded to the nearest integer ($m' \geq 1$).

The minimum values of the *ATA* were also determined for *q* equal to 2.0, 2.5 and 3.0. For these values of *q* the difference between *m'* and *m* is 0 or 1 for all the *FAR* values considered. Thus the relation $m=0.182 \cdot N$ can be used in determining the combination of *m* and *N* which minimizes the *ATA*.

4.2.2 χ^2 method

For the χ^2 method the variable *S* is calculated using equation (3-11) and compared with the threshold *B*. When *S* passes this threshold an anomaly is declared.

This method has one parameter less than the extremes method. For each value of the *FAR*, *N* can be varied and *B* can be adjusted in order to minimize the *ATA*. The curves of the *ATA* against *N* were again smoothed. The results for 7 different values of the *FAP* and for $q=1.5$ are listed in Table 4-2. The sampling frequency is 100 Hz.

In Table 4-2 it can be seen that the minimum *ATA* is reached for high values of the *AFR*. Comparing Tables 4-1 and 4-2 it can also be seen that the χ^2 method gives smaller values for the *ATA*. In case of the extremes method only the number of data values for which equation (3-1) holds is counted, the magnitude of the data values is not taken into account. This is not the case for the χ^2 method, since this method considers the magnitude of the values. This results in a smaller value of *N* for which the *ATA* is minimized and in a smaller value of the *ATA* for the χ^2 method. Only for *FAR* equal to 0.10 s^{-1} and 0.01 s^{-1} the *ATA* is comparable to the *ATA* of the extremes

Table 4-2. Minimum values of the *ATA* for several values of the *FAR* for the χ^2 method

FAR (s^{-1})	*AFR* (s^{-1})	*N*	*B*	*ATA* (10^{-2} s)	*N'*
10.0	72.7	1	2.71	3.67 (± 0.031)	1
1.0	91.4	1	6.64	11.4 (± 0.11)	3
0.10	97.2	18	42.3	26.8 (± 0.21)	21
0.01	51.9	31	69.1	39.0 (± 0.27)	34
$1.0 \cdot 10^{-3}$	34.5	53	108.8	50.6 (± 0.27)	53
$1.0 \cdot 10^{-4}$	30.3	68	138.4	62.7 (± 0.31)	68
$1.0 \cdot 10^{-5}$	28.8	81	165.3	74.6 (± 0.35)	81

method since *N* is 1 in both cases.

Notice that the ratio of *B* to *N* is nearly constant in the last 5 rows. The last column shows *N'* which is equal to $0.49 \cdot B$.

4.2.3 Sequential probability ratio test (SPRT)

The sequential probability ratio test uses recursive equation (3-32) to calculate the parameter λ. This parameter is compared to a lower threshold *A* and an upper threshold *B* given by equation (3-22). When λ passes *A* a normal situation is declared, when it passes *B* an anomaly is declared. After a decision has been taken λ is reset to zero.

For finding the minimum *ATA* as a function of the *FAR*, the approximation of the *ATA* (eq. (3-38)), derived in section 3.4.2, can be used. This equation must be rewritten to get a relation for the *ATA* as a function of the *FAR*. For obtaining this, an equation for the *FAR* has to be derived first. This is done by making use of equation (3-41):

$$FAR = \frac{FAP_{act}}{\langle n \rangle} \cdot f_s \simeq \frac{FAP_{des}\, q^{-c_2}}{\langle n \rangle} \cdot f_s , \qquad (4\text{-}1)$$

where f_s is the sampling frequency and $\langle n \rangle$ the expectation value of the number of steps between two decisions. Using (3-22), an equation for the FAP_{des} can be derived:

$$FAP_{des} = \frac{\exp(A) - 1}{\exp(A) - \exp(B)} . \qquad (4\text{-}2)$$

$\langle n \rangle$ can be approximated by dividing A by $\langle \Delta\lambda \rangle_{norm}$ (eq. (3-34)). By substituting both the FAP_{des} and $\langle n \rangle$ into equation (4-1), the following equation is obtained:

$$FAR \approx \frac{\exp(A)-1}{\exp(A)-\exp(B)} \cdot \frac{\frac{q^2-1}{2q^2} - \ln(q)}{q^{-c_2 A}} \cdot f_s . \tag{4-3}$$

The FAR is constant for a given value of q if

$$\frac{1}{A} \frac{\exp(A)-1}{\exp(A)-\exp(B)} = c , \tag{4-4}$$

where c is equal to $-15.1 \cdot FAR/f_s$ for $q = 1.5$ and $c_2 = 1.616$ (eq. (3-42)).

Using equation (4-4), B can be written as a function of A and c and can be substituted into equation (3-38). After dividing the result by f_s, an equation for the ATA as a function of A and q is obtained:

$$ATA \approx \frac{1}{f_s} \cdot \frac{-A + 2\ln\left(\frac{1-\exp(A)}{cA} + \exp(A) \right)}{q^2 - 1 - 2\ln(q)} . \tag{4-5}$$

Figure 4-2 shows a graphical representation of equation (4-5) for several values of the FAR for a sampling frequency of 100 Hz. It can be seen that the ATA demonstrates only minor dependence on A. For FAR smaller than 10^{-3} the minimum of ATA is close to A=0. For higher values of the FAR, the minimum shifts to more negative values of A.

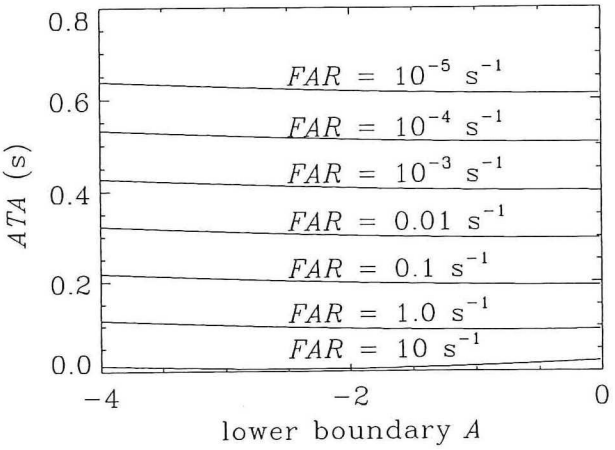

Figure 4-2. Theoretical ATA for the SPRT method (q=1.5)

Figure 4-3 gives the

theoretical result of the *ATA* for A=0 (eq. 4-5) and the results from simulation where A has been put equal to 0 and equal to -4.0. The sampling frequency is 100 Hz. An artificially generated Gaussian distributed white noise signal in which a step in standard deviation occurred, was used to determine the *ATA* by simulation. Again, it can be seen that the *ATA* depends only little on A. The theoretical predictions of the *ATA* (eq. 4-5) are in good agreement with the results from simulation, in spite of the several approximations applied.

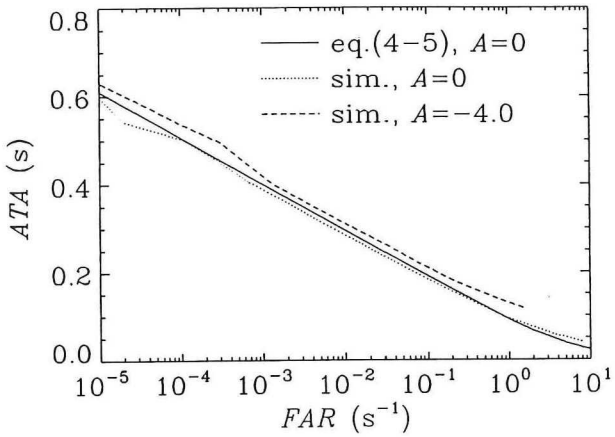

Figure 4-3. The *ATA* determined by simulation for the SPRT method

4.3 Theoretical comparison of the methods

After having determined the minimum values of the *ATA*, the three methods can be compared. Figure 4-4 shows the combined results of table 4-1 (extremes method), table 4-2 (χ^2 method) and figure 4-3 (SPRT method). From figure 4-3 the results from simulation with A=0 have been chosen. The error margins corresponding to one standard deviation of the *ATA* are given in figure 4-4, but are too small to be noticed. It is clear that the SPRT gives the fastest response to a change in standard deviation of the residual noise for a given *FAR*.

The result presented here endorses the statement of Wald that the SPRT method frequently results in a considerable saving in the number of observations over the most efficient test procedure based on a fixed number of observations (like the other two methods) (Wald, 1947).

The simulations have been performed for other values of q as well, ranging from 2.0 to 6.0. For all these values of q the SPRT method gives the smallest *ATA* for FAP_{act} values ranging from 10^{-1} to 10^{-7}. In case of the extremes and the χ^2 method the model parameters for which the *ATA* obtains its minimum depend on q. For higher values of

q the minima of the *ATA* are reached for smaller values of N and m (extremes method) and for smaller values of N and B (χ^2 method).

When q increases the *ATA* decreases. For q=2.0 the minimum *ATA* is equal to 0.2 s (*FAR*= 10^{-5} s^{-1}) and for q=2.5 it is even less than 0.1 s (*FAR*=10^{-5} s^{-1}). It must be noted here that these figures apply to a sampling frequency of 100 Hz.

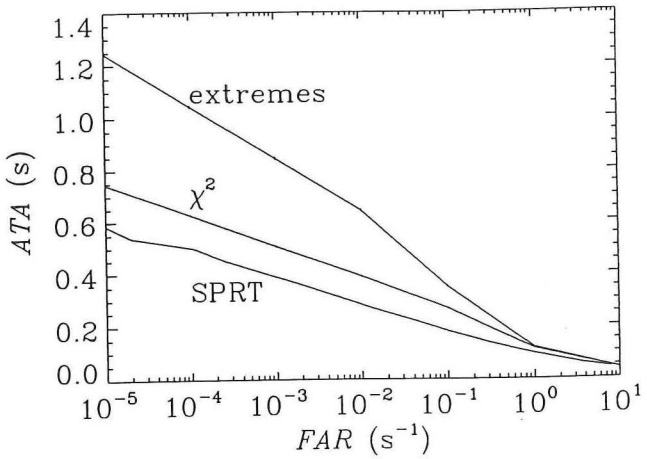

Figure 4-4. Comparison of the *ATA* for the three detection methods as a function of the *FAR* (f_s = 100 Hz, q = 1.5)

By decreasing the sampling frequency, the *ATA* is increased considerably for a given value of the *FAR*. For example, a sampling frequency of 10 Hz gives a minimum *ATA* of approximately 5 s; a sampling frequency of 1 Hz results in a minimum *ATA* of almost 40 s (*FAR*=10^{-5} s^{-1} in both cases).

Simulations for q<1 have been performed as well. Again it was found that the SPRT method is the best method, since it gives the smallest *ATA* for a given *FAR*.

4.4 Application of the signal processing and anomaly detection methods to thermocouple signals

In this section the signal processing methods presented in chapter 2 and the three anomaly detection methods are applied to noise signals from thermocouples. Results are shown of applying the anomaly detection methods directly to the thermocouple noise and of applying them to the outcomes of signal processing.

Measurements were performed on the Delft Simulated Reactor (DeSiRe) (van de Graaf, 1994) at the Interfaculty Reactor Institute. DeSiRe is an electrically heated scaled model of the Dodewaard BWR. It consists of the most important parts that govern the natural circulation: a fuel assembly, a riser and a downcomer. The assembly

consists of 35 electrically heated 'fuel' rods, which have a cosine axial power distribution, and one instrumentation rod. DeSiRe is equipped with a lot of measurement devices among which thermocouples. Inspection of the coolant is possible through viewing ports located at several axial positions in the assembly wall. Two experiments with changing heating power were performed with this facility. The temperature of the coolant was measured with a thermocouple in the instrumentation rod located at 12 cm above the inlet of the 'fuel' assembly.

When performing anomaly detection in a practical situation different steps can be distinguished. First, the signals to be measured and the measurement parameters (sampling and filter frequencies, duration of measurement etc.) have to be chosen. Second, signal processing has to be applied to the measured signals. Third, the methods for anomaly detection and their parameters must be chosen. Finally, the detection results must be interpreted. These steps will be discussed separately for the experiments that were performed with the DeSiRe facility.

4.4.1 Measurements

Two experiments were performed with DeSiRe:

1. Step in heating power from 24 kW to 45 kW at t=433 s after the beginning of the measurement. The beginning of boiling was observed at approximately 7 s after the step through a viewing port located at 7.5 cm above the inlet of the 'fuel' assembly.
2. Heating power slowly increasing from 15 kW to 47 kW (ramp). The start of the ramp is at t=311 s after the beginning of the measurement and its duration is approximately 413 s. A clear beginning of boiling could not be observed due to the slow increase of the heating power.

For every experiment the temperature of the coolant was measured with a

Table 4-3. Measurement parameters

Sampling period, sampling frequency	$\Delta T = 30$ ms, $f_s = 33\frac{1}{3}$ Hz
Filter frequencies (*HP*=high pass, *LP*=low pass)	$f_{HP} = 0.04$ Hz, $f_{LP} = 12$ Hz
Number of samples per signal	$100 \times 256 = 25600$
Duration of signal	$T = \Delta T \cdot 25600 = 768$ s

thermocouple. The parameters used in both the measurements are given in table 4-3.

4.4.2 Signal processing

AR analysis

For measurement 1, AR analysis (Burg's method) was applied to the first 5000 data points (t = 0-15 s) of the thermocouple noise signal. Using the *FPE* led to a model order of 27 (see paragraph 2.2.1).

For measurement 2, AR analysis was also applied to the first 5000 data points of the thermocouple noise signal. Using the *FPE* led to a model order of 30.

The fact that the two signals yield a different order of the AR-model is probably due to statistics.

Wavelet analysis

Wavelet analysis was applied to both thermocouple noise signals using the Gabor mother-wavelet with input order ranging from 2 until 25 (central wavelet frequency ranging from 16.667 Hz (Nyquist frequency) until 0.31 Hz). This resulted in 24 wavelet coefficient time series. The results with input order 7 (central frequency = 7 Hz) will be presented at the end of this chapter. For this input order 27 signal data points are needed to determine one wavelet coefficient.

Fractal analysis

Fractal analysis was applied to both thermocouple noise signals for $\{N,k\}$ = {(32, 1-4); (64, 1-8); (128, 1-16); (256, 1-32); (512, 1-64); (1024, 1-128)}. The results for N,k = (512, 1-64) will be presented at the end of this chapter. It can be noticed that fractal analysis requires much more data points (512) compared to AR-analysis and wavelet analysis, which require only 28/31 and 27 data points, respectively.

4.4.3 Setup of the anomaly detection

The anomaly detection methods will now be applied to the thermocouple noise signals and to the results from signal processing. This means that 12 detection results per measurement are obtained. Before starting the anomaly detection, the method parameters must be chosen. In practical applications it is usually demanded that the *FAR* must be smaller than or equal to a certain value. Here it is required that the

number of false alarm encountered is zero. In case of the first measurement the first 433 seconds of the detection result are used for counting the number of false alarms. In case of the second measurement the first 311 seconds are used.

For each application of the extremes method the minimum value of N, for achieving a false-alarm-free detection result, will be determined. Once N is known, m and k must be determined, demanding that the anomaly is detected as fast as possible. The parameters m and k are not determined by trail and error but by making use of the results obtained earlier in this chapter. For determining m and k the results from section 4.2.1 are used, namely the relation $m=0.182 \cdot N$ for m and a value of k according to table 4-1. For these values of m and k the ATA is minimized, in theory. The same is done for the χ^2 method, be it, that B must be determined from N. For this the relation of $B=N/0.49$ is taken (see section 4.2.2). For the SPRT method A is set equal to zero and the minimum value of B is determined (see section 4.2.3).

For the SPRT method the standard deviation of the data series in the anomalous situation must be chosen, since it appears in the equation with which the method parameter λ is calculated (eq. (3-32)). In this application q ($=\sigma_1/\sigma_0$) is chosen equal to 1.25. When performing anomaly detection with the SPRT method there is the problem what to decide when λ is in between the two decision boundaries A and B. Actually the method takes no decision at all. In this application the state of the process is taken to be equal to the outcome of the last decision. This means that at every step the state of the process is defined.

Table 4-4 shows the parameters of the detection methods determined in such a way as described earlier in this section. There are two exceptions, namely the parameters of the extremes and χ^2 method applied to the first fractal dimension time series. In these two cases it was not possible to eliminate every false alarm. Therefore, the demand that ATA should be minimal, in theory, was put aside in order to obtain a false-alarm-free detection result. It can be seen that the smallest parameter values are obtained when applying the detection methods to the residual noise.

The anomalies which were introduced in the measurements may not only change the standard deviation but may also change the average value of the data series. This is even rather likely in case of the wavelet coefficient and fractal dimension time series. For the sake of comparison the standard deviation test will be applied to all the data series. The average value of the first 5000 data points of the data series will be subtracted from the data series before the anomaly detection method is applied.

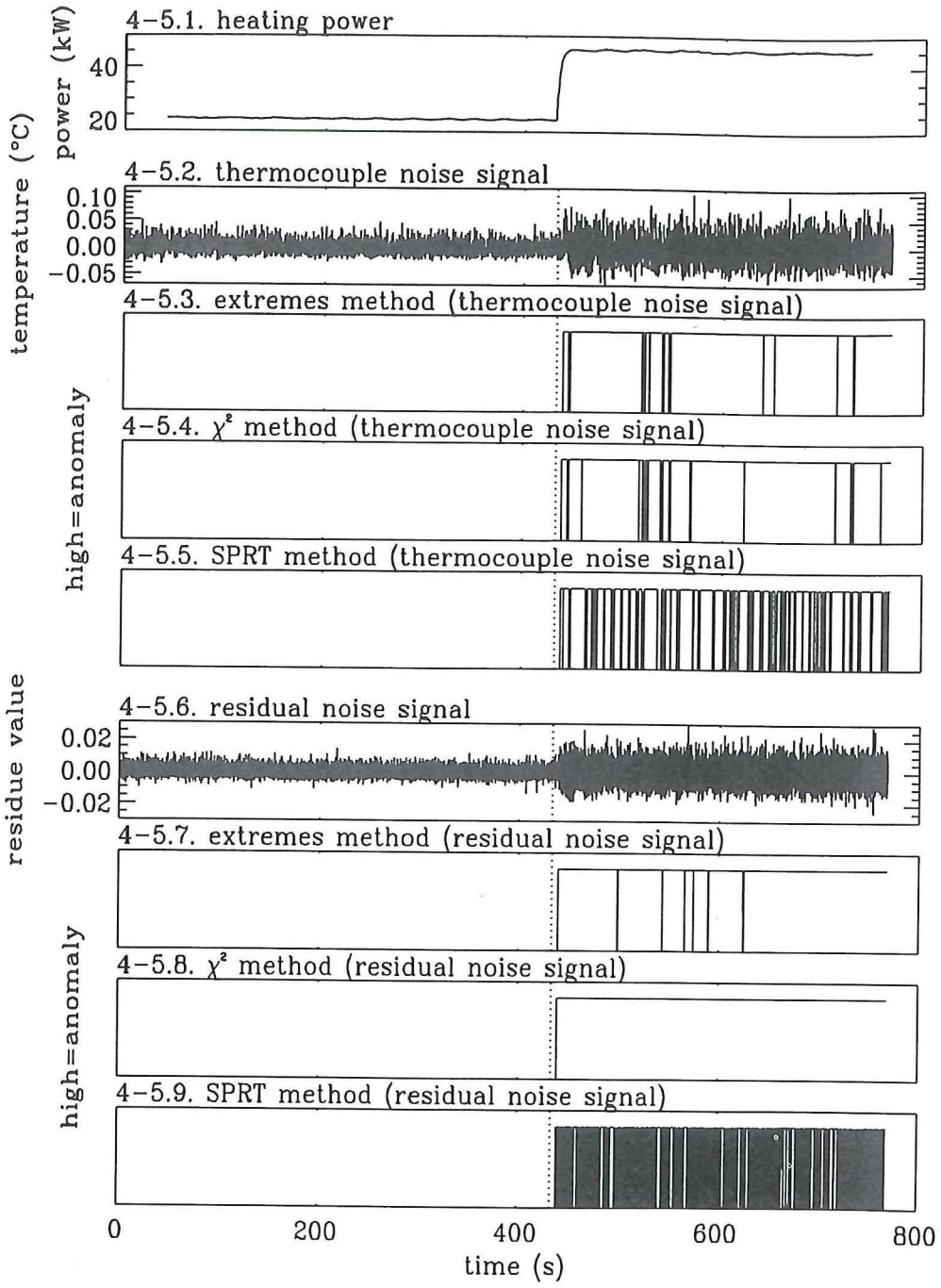

Figure 4-5. Detection of a step in heating power

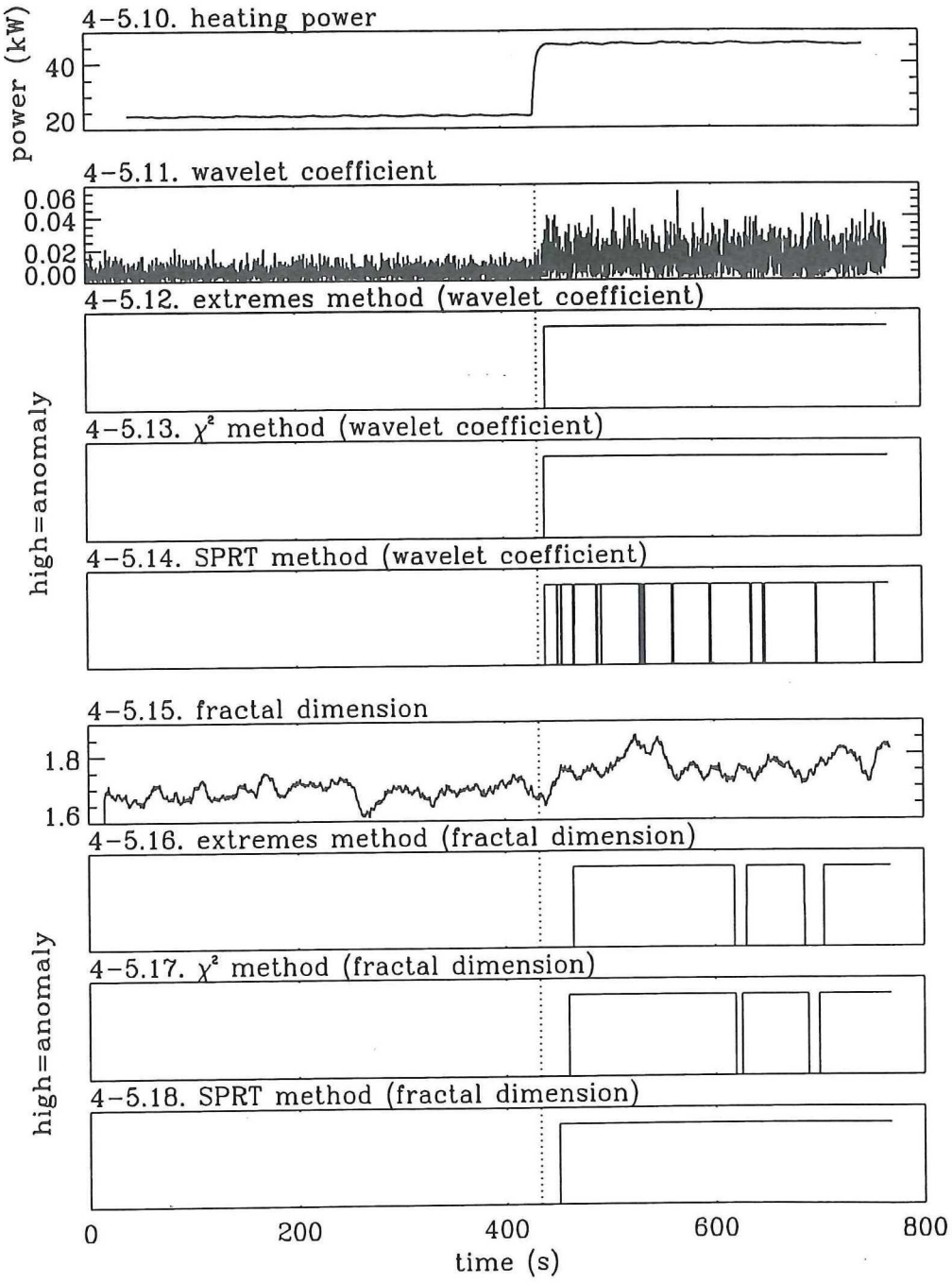

Figure 4-5. Detection of a step in heating power

Table 4-4. Parameters of anomaly detection methods

		extremes			χ^2		SPRT
		N	*m*	*k*	*N*	*B*	*B*
Step in heating power	temperature noise	125	23	1.95	97	198.0	16.5
	residual noise	47	9	2.04	50	102.0	10.5
	wavelet coefficient	196	36	1.95	194	395.9	31.7
	fractal dimension	600	540	1.95	600	5229.0	2401.0
Ramp in heating power	temperature noise	102	19	1.95	112	228.6	21.4
	residual noise	91	17	1.95	71	144.9	10.7
	wavelet coefficient	152	28	1.95	138	281.6	25.4
	fractal dimension	600	334	1.95	1247	2544.9	295.0

4.4.4 Results of the anomaly detection

Figure 4-5 and 4-6 show the results of the analysis and the anomaly detection. Figure 4-5 gives the results of the detection of boiling of the coolant due to a step in heating power. Figure 4-6 shows the results in case of a power ramp. Each figure presents the results of applying the three anomaly detection methods, using the parameters given in table 4-4, to the thermocouple noise signal and to the results from signal processing. Table 4-5 presents the times to alarm (*TA*) values obtained with the anomaly detection.

Detection of a step in heating power (figure 4-5)

- The SPRT method gives, on the average, the smallest *TA*. When applied to the thermocouple noise signal it gives the smallest *TA* overall. (table 4-5)
- The differences between the *TA* values of the χ^2 and SPRT method are small, except for the fractal dimension time series. The extremes method gives substantially higher *TA* values. (table 4-5)
- The *TA* values obtained with the thermocouple and residual noise signals differ only slightly and are somewhat smaller than the ones obtained with the wavelet

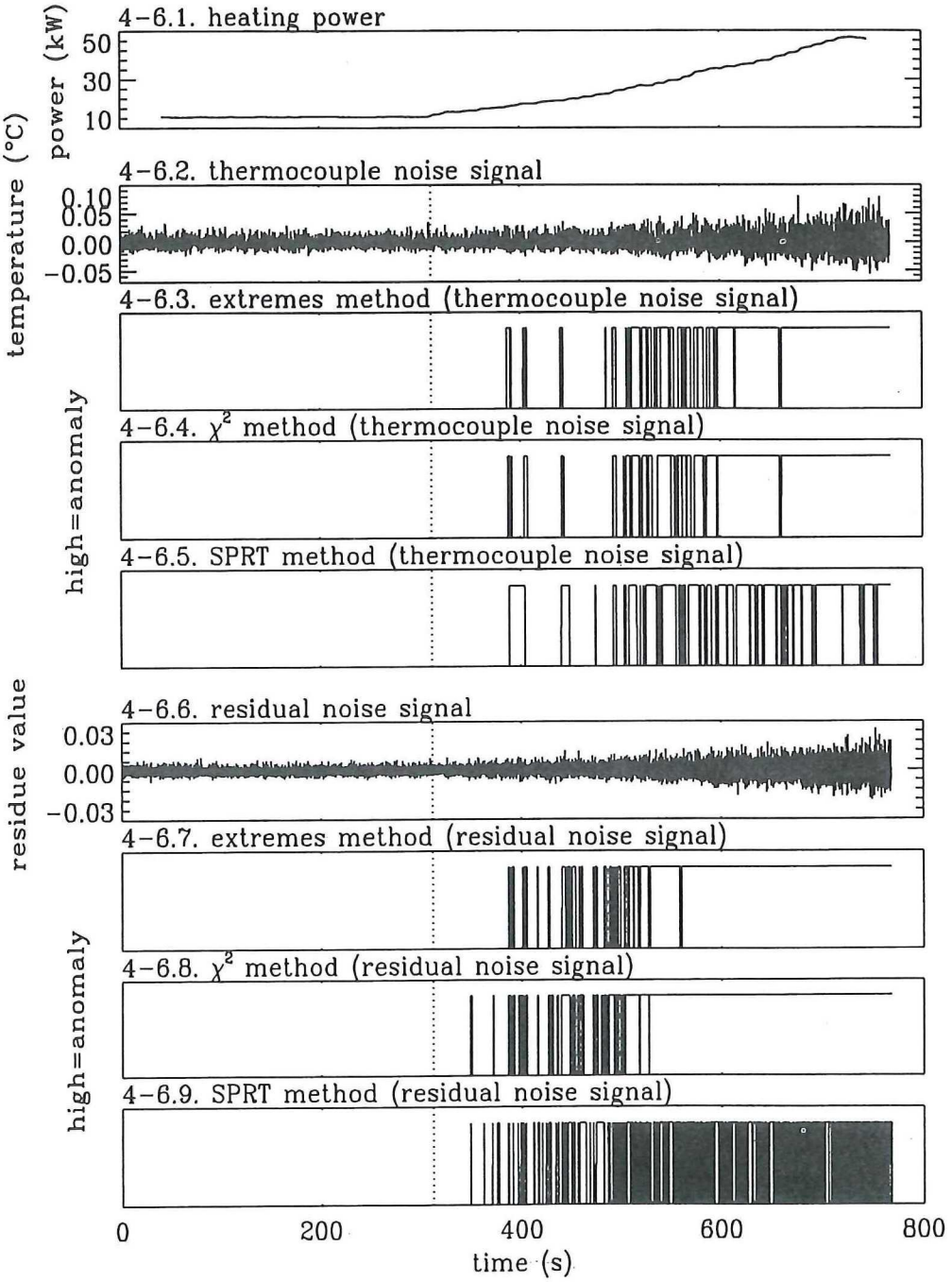

Figure 4-6. Detection of a ramp in heating power

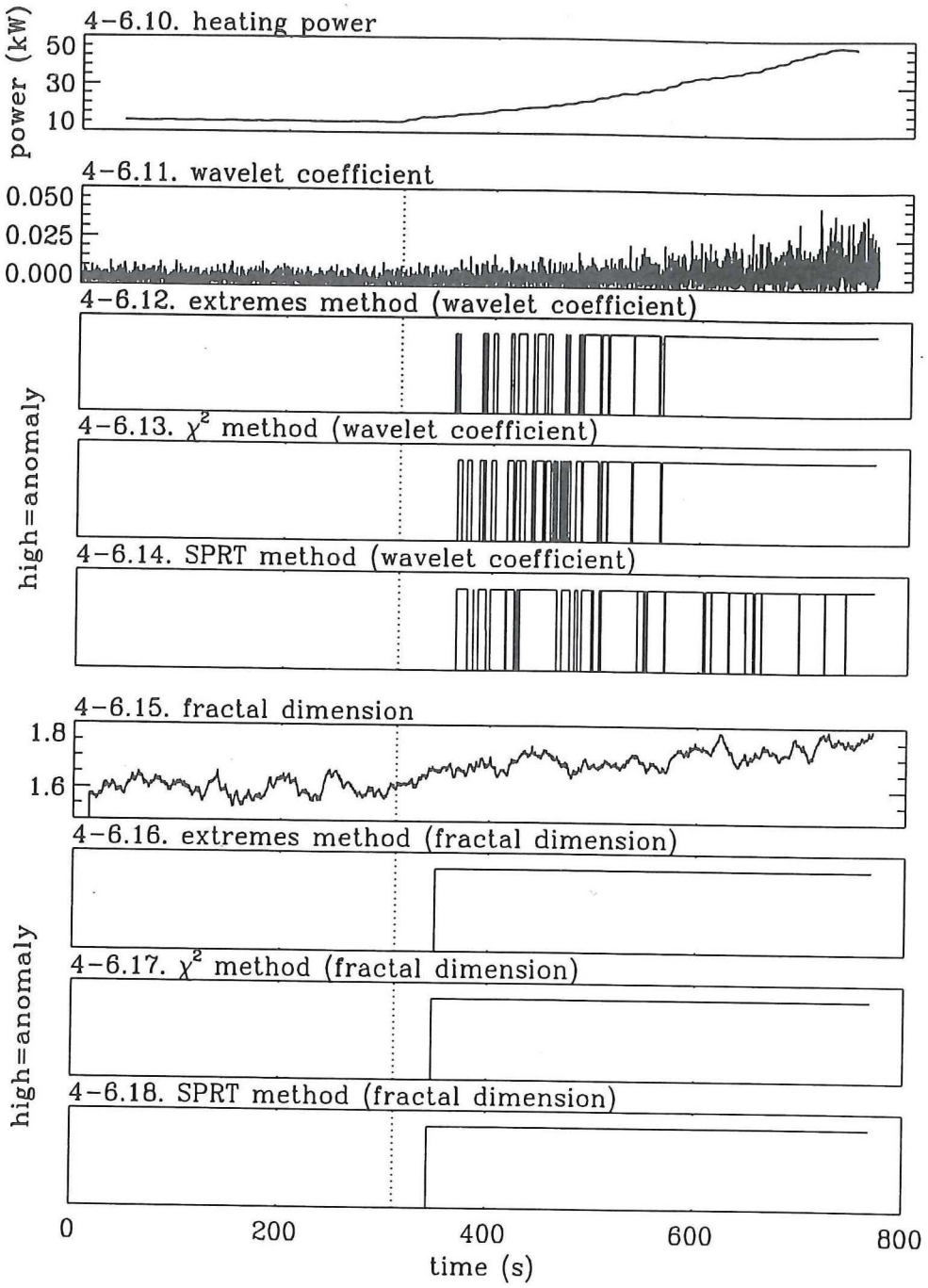

Figure 4-6. Detection of a ramp in heating power

coefficient time series. The *TA* values obtained with the fractal dimension time series are much larger. (table 4-5)

Table 4-5. Points of detection of anomaly (figure 4-5 and 4-6)

Detection method	applied to:	Points of detection step	ramp
extremes	temp. noise	6.42 s	75.99 s
χ^2	temp. noise	6.09 s	76.95 s
SPRT	temp. noise	6.03 s	77.61 s
extremes	residual noise	6.39 s	75.90 s
χ^2	residual noise	6.18 s	37.29 s
SPRT	residual noise	6.18 s	37.23 s
extremes	wavelet coef.	7.86 s	51.69 s
χ^2	wavelet coef.	6.60 s	55.62 s
SPRT	wavelet coef.	6.54 s	55.56 s
extremes	fractal dim.	32.55 s	38.10 s
χ^2	fractal dim.	27.54 s	36.45 s
SPRT	fractal dim.	17.79 s	33.09 s

- The SPRT method gives more alarm failures than the other two methods, except for the fractal dimension time series (figure 4-5). The number of alarm failures could be reduced by lowering the lower threshold A. If A is made smaller than $-\ln(q)= -0.22$ than the parameter λ cannot reach the lower threshold within one step (see section 3.4.2). Setting A equal to -0.25 in case of the thermocouple noise, the residual noise and the wavelet coefficient time series reduces the number of alarm failures but keeps the *TA*s at the same value. Again, it should, however, be said that the *AFR* is of minor importance (see chapter 1).
- Four detection results are free from alarm failures. (figures 4-5.8, 12, 13 and 18)

Detection of a ramp in heating power (figure 4-6)

- Applying the detection methods to the fractal dimension time series gives the smallest *TA* values. Only the χ^2 and the SPRT method applied to the residual noise give comparable *TA* values. This result is very much in contrast with the result obtained with the step in power.
- When the fractal dimension is used, an alarm-failure-free detection result is obtained.
- Applying the χ^2 and the SPRT method to the residual noise gives a much better result than when applying them to the thermocouple noise signal.

4.5 Conclusions

Three anomaly detection methods, namely the extremes, the χ^2 and the SPRT method were compared with each other. It was found theoretically and numerically that the SPRT method is the best method, since it gives the smallest *ATA* for all values of the *FAR* and q studied. The *AFR* is considered to be of minor importance. The χ^2 method is better than the extremes method in this respect.

The optimization of the extremes method made it clear that two method parameters can be chosen independently for a given *FAR*. There is a strong indication that the minimum *ATA* is obtained for a constant ratio of m to N for all possible values of q and the *FAR*. The larger q, the smaller N for which the *ATA* is minimized for a given *FAR*.

For the χ^2 method only one method parameter has to be chosen for a given *FAR*. The larger q, the smaller N for which the *ATA* is minimized for a given *FAR*.

The FAP_{act} and the AFP_{act} of the SPRT method are smaller than the FAP_{des} and AFP_{des} in correspondence with the theoretical result of chapter 3. The *ATA* depends only little on A.

The practical applications of the detection methods show that the SPRT method does not always give the smallest *TA* but is in some cases outstripped by the other two methods. The *TA* values of the χ^2 and the SPRT methods differ only slightly, on the average, but are mostly substantially smaller than the *TA* of the extremes method.

The performance of the detection methods applied to the wavelet coefficient and fractal dimension time series could further be improved if the methods would also account for a change in average value. The methods that were applied only focussed on a change in standard deviation.

The application of the detection methods to the fractal dimension time series gave some remarkable results. In a DeSiRe measurement with a gradually increasing heating power, this increase was detected very early, whereas an abrupt change of the heating power was detected with much delay. This could indicate that fractal analysis is very sensitive to small changes in the thermocouple noise signal but is also very slow.

When performing a continuous anomaly detection, it must be noticed that the normal state of the process under surveillance is subject to slow and small changes. This means that not only the characteristics of the anomalous data series but also the characteristics of the 'normal' data series are a variable entity. To account for this fact, the characteristics of the normal data series have to be determined again from time to time during the continuous anomaly detection.

Chapter 5

DECISION MAKING USING FUZZY LOGIC

5.1 Introduction

Fuzzy logic represents a widening of the classical binary calculation. It extends the two conditions known from binary calculation (true and false or 0 and 1) with in between conditions (for example suspect or ½, respectively). The theory stems from the desire to create a computer logic to deal with human ambiguities such as small, medium and large. Zadeh extended this theory with a mathematical description of variables with linguistic values (Zadeh, 1965). The rules for combining these variables constitute the axiomatic basis of the theory of fuzzy logic.

In this chapter fuzzy logic is used to combine the results of several signal processing techniques. Suppose a signal is analyzed with three signal processing techniques. Each technique will probably be sensitive to changes of different features of the signal. Therefore, it is desirable to combine the outcomes of the different techniques in order to arrive at one single decision about the state of the process.

A possible method for combining the outcomes could be a simple m out of n approach. In case three anomaly detection methods are used, it could simply be stated that if two out of the three methods detect an anomaly, the state of the process is anomalous, else it is normal. A m out of n approach also greatly reduces the FAP. Suppose a two out of three approach is used and each method has a known FAP denoted by FAP_i, i=1..3. The overall FAP is then equal to $FAP_1 \cdot FAP_2 + FAP_1 \cdot FAP_3 + FAP_2 \cdot FAP_3$ plus a higher order term. This is, however, only true when the three methods are independent, else the overall FAP will be higher.

A disadvantage of a m out of n approach is that a lot of information is lost due to the crisp boundaries that are used in the anomaly detection methods and in the final decision. Imagine, for example, that a certain anomaly is detected by one method but

not by the other two methods due to the fact that their decision boundaries were chosen too high. The erroneous final decision using the two out of three approach would be that the process is in a normal state. By using fuzzy logic in this case the taking of a crisp decision can be postponed as long as possible, avoiding the discarding of any valuable information.

Fuzzy logic is especially used in the field of system and process control (Kuan *et al.*, 1992; Park *et al.*, 1995) and in the field of safety analysis and management (Yu *et al.*, 1993; Park *et al.*, 1994) and has some applications in signal detection and analysis (Saade *et al.*, 1994; Chen *et al.*, 1995) although mainly outside the field of reactor science and technology.

Holbert, Heger and Alang-Rashid applied fuzzy logic to the problem of sensor validation (Holbert *et al.* 1994). In their case the important quantities are the magnitude of the deviation of the sensor signal from normal operation and the rate of occurrence of this deviation. The same quantities will be used in the approach presented in this chapter with the exception that the data value instead of the signal deviation will be used. The more general name of 'data value' instead of 'signal value' is used here, since the input data of the fuzzy-logic approach can be signals or time series. Here, time series will be used as input data for the fuzzy-logic approach. Two so-called universes of discourse (UOD) are defined, namely the UOD *data value* and the UOD *probability of occurrence*.

Per UOD a number of membership functions are defined using time series data. The purpose of the membership functions is to translate the time series data from the numeric (crisp) domain to the fuzzy domain. This is also called the fuzzification. Within the fuzzy domain, relationships between the input and the output fuzzy variables are defined. This is called the inference. The final step is the defuzzification during which the fuzzy output data are translated back to crisp data. Each of these steps will be explained in more detail in the remaining of this chapter.

The fuzzy-logic approach will be presented and explained by applying it to results from signal processing. These results are obtained through analysis of a signal generated by an AR model. The synthetic signal and its analysis results are shown in section 5.2. In section 5.3 the fuzzy-logic approach is presented. Finally, the approach will be applied to time series obtained through analysis of other synthetic signals in order to test the applicability of the approach.

5.2 The input data for the fuzzy-logic approach

In this section, a signal is generated by AR models which were estimated using a measured neutron noise signal. This means that the synthetic signal has real physical characteristics. The advantage of using a synthetic signal is that the start and the duration of the signal parts, corresponding to different process states, are exactly known. This is necessary, since a large amount of information about the input and the output required is needed for the fuzzy-logic approach. This also means that the approach is different from the anomaly detection methods that were presented in chapter 3. In case of the anomaly detection methods no information about the anomaly and the features of the anomalous part of the signal is needed. It is only necessary to know the features of the normal part of the signal.

The AR models for generating the signal are determined using a neutron noise signal from the IRI08 measurement performed with the NIOBE facility (see chapter 1) (Kozma, 1992). Figure 5-1 shows the thermocouple signal of the measurement. Three intervals, each one consisting of 4000 points, of the neutron noise signal were used for estimating three AR models with model order 50, referred to as model number 1,2 and 3, respectively. Burg's method was used for estimating the AR models (see par. 2.2.2). The first interval corresponds to a normal situation in which there is no boiling. The second and third interval represent anomalous states characterized by intermediate and

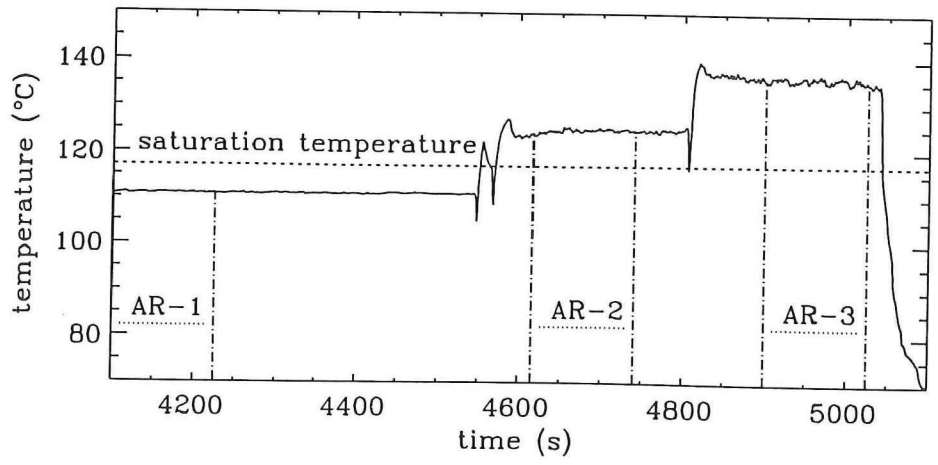

Figure 5-1. Thermocouple signal of IRI08 measurement (NIOBE facility)

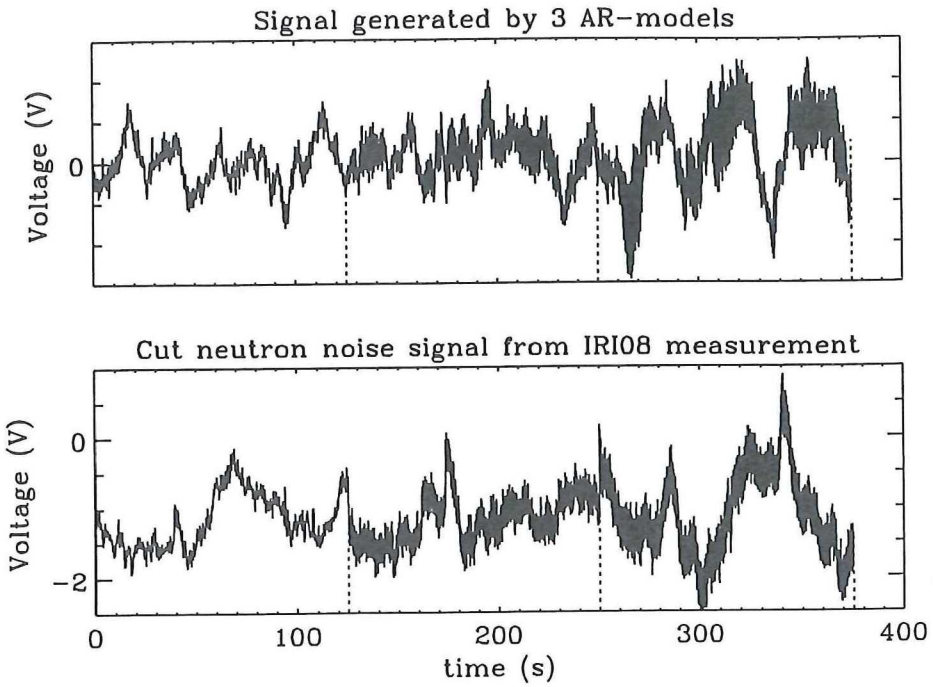

Figure 5-2. Synthetic and measured neutron noise signal

full boiling, respectively. The sampling frequency of the neutron noise signal is 32 Hz.

For generating the synthetic signal a white noise signal was used as input to the AR models. In order to introduce the first anomaly into the signal the AR coefficients of the first AR model were changed to the coefficients of the second model at data point 4001 (125.03 s). The second anomaly was introduced at data point 8001 (250.03 s) by changing the AR coefficients to the ones of the third model. A smooth transition from one part to the other is guaranteed by using data of the former part to calculate the initial signal values of the present part of the signal.

Figure 5-2 shows the synthetic signal and the neutron noise signal existing of the three time intervals connected to each other. Also shown are the intervals. By taking a closer look at the cut neutron noise signal abrupt transitions can be seen at data points 4001 and 8001. There are no abrupt transitions in the synthetic signal.

Autoregressive, wavelet and fractal analysis were applied to the synthetic signal. For AR analysis the model was used that was estimated using the first 4000 data points of the neutron noise signal. The parameters of this AR model were not changed during the

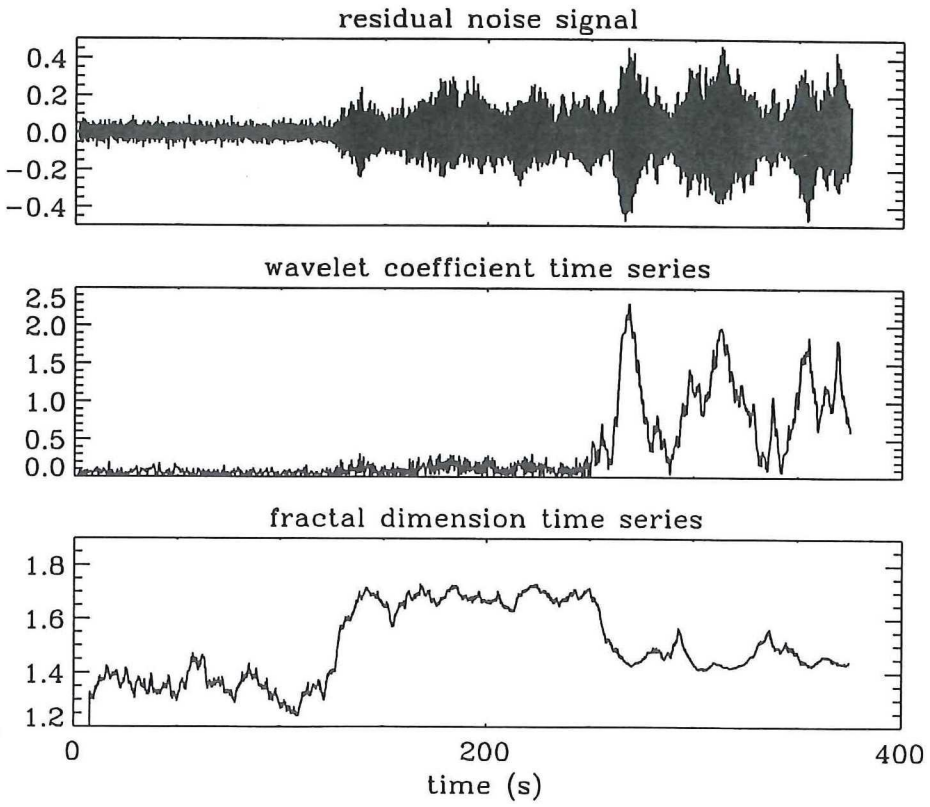

Figure 5-3. Results of analysis of synthetic signal

analysis. For the wavelet analysis many input orders were applied of which input order 12 was used here. For fractal analysis the result obtained with N=128 and k=1-8 was used. Figure 5-3 shows the results from the three analysis techniques.

As can be seen in figure 5-3 the three analysis techniques react differently to the three process states. For the residual noise there is a clear distinction between the normal part on one hand and the two anomalous parts on the other. The difference between the two anomalous parts is much less clear. The wavelet coefficient time series shows an opposite result. Here the difference between the two anomalous parts is clearly visible, whereas the difference between the normal and the first anomalous part seems only small. The fractal dimension time series has different characteristics for each of the three process states. Another feature to be noticed is the fluctuating behaviour of both the residual noise and the wavelet coefficient time series during the presence of an anomaly.

5.3 The fuzzy-logic approach

In this section all the steps of the fuzzy-logic approach are presented and explained using the three signal analysis results obtained in the previous section. The membership functions and the relationships between the input and output fuzzy variables are defined. Finally, it will be shown that the fuzzy-logic approach is able to give a fast detection of the two anomalous states without any false alarms.

The membership functions

The first step is to define the membership functions in the UODs *data value* and *probability of occurrence*. A membership function is a mathematical description of the distribution of membership values that characterize the uncertainty of input value x belonging to a subset G. The degree of association of an input data value with its respective fuzzy variable is numerically represented by the membership value μ. Common membership functions are triangular or trapezoidal or are modified versions of the Gaussian distribution (Kaufmann, 1975). Here trapezoidal membership functions will be used. The general form of the trapezoidal membership function is:

$$\mu = \mu_G(x) = \mathrm{MIN}\left(1 , \frac{x - a_1}{a_2 - a_1} , \frac{x - a_4}{a_3 - a_4} \right) \quad (\mu \geq 0) , \qquad (5\text{-}1)$$

where $a_{1..4}$ are specific points of the membership function as given in figure 5-4. It should be noted here that a_1 and a_2 can have the value zero and a_3 and a_4 can be infinite.

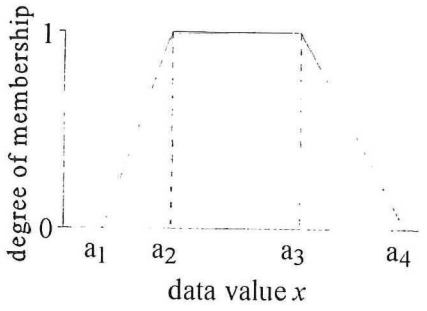

Figure 5-4. trapezoidal membership function

Within the UOD *data value* three membership functions are defined, which are called: small (*sm*), medium (*md*) and large (*lg*). The points of the membership functions are determined using the probability density function (PDF) of a time series at a certain process state. This means that per time series three PDFs are determined, namely a PDF of the normal part, a PDF of the first anomalous part and

a PDF of the second anomalous part. Figure 5-5 shows how the PDF is used in determining the points of the membership functions. It must be noted that the membership functions *medium* and *large* consist of two parts each as can be seen in figure 5-5. The sum of the membership values is equal to 1 everywhere. This is not compulsory; it is, however, not allowed to have gaps in the definitions of the membership functions within a UOD (Schulte, 1994).

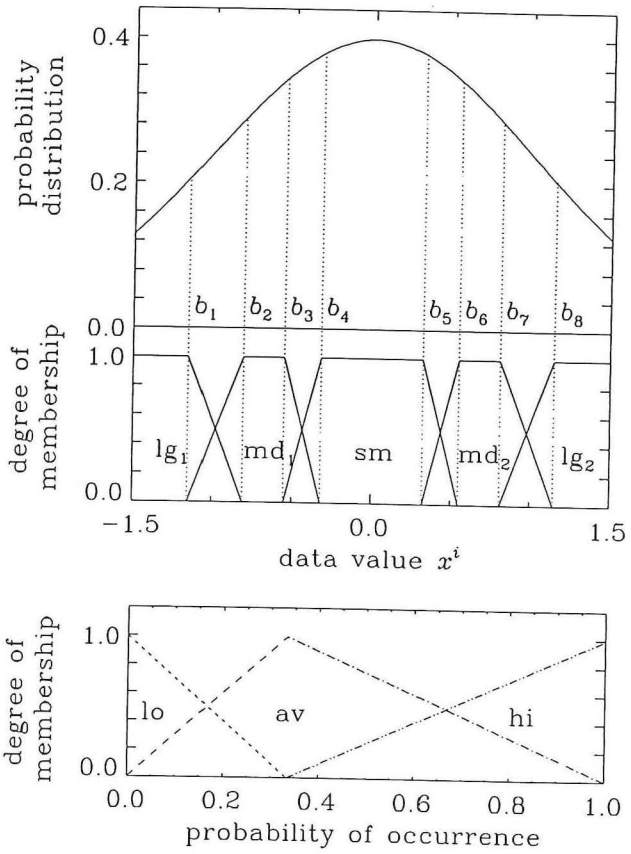

Figure 5-5. Definition of the membership functions in the two UODs

Each membership function covers one third of the PDF. Table 5-1 shows how the b_1 till b_8, given in figure 5-5, are determined. If a randomly taken time series value belongs to the same process state as the membership functions to which it is applied, then this value has an equal probability to be a member of one of the three membership functions.

When all the membership functions have been determined, the time series values are applied to the membership functions of the time series corresponding to the three process states. The degree of association of each input time series value with a membership function is numerically represented by the fuzzy membership value $\mu^{ij}{}_k$, where i denotes the time series number, j process state number and k the membership function. This means that for one time series value 9 membership values are obtained. At least three of these membership values are equal to zero.

Over the last N data points of the input time series the probability of occurrence of each data value class is determined by calculating the sum of the membership values of the N data points and dividing this by N:

$$f_k^{ij} = \frac{1}{N}\sum_{n=1}^{N} \mu_k^{ij}(x^{ij}(n)) . \qquad (5\text{-}2)$$

Table 5-1. Points of membership functions

b	Surface under PDF left of line $x=b$
b_1	1/6 - 1/24
b_2	1/6 + 1/24
b_3	1/3 - 1/24
b_4	1/3 + 1/24
b_5	2/3 - 1/24
b_6	2/3 + 1/24
b_7	5/6 - 1/24
b_8	5/6 + 1/24

Dividing N by the sampling frequency gives a value for the time interval T_d needed for calculating the f^{ij}_k. The probabilities of occurrence are then applied to the membership functions of the corresponding UOD which are also shown in figure 5-5. This UOD also contains three membership functions which are called: low (*lo*), average (*av*) and high (*hi*). As can be seen in figure 5-5 the membership function *av* has its maximum for f^{ij}_k=1/3. In this manner, 27 membership values per signal value are obtained: one for each data value class, probability of occurrence class and process state combination.

The decision rules

If the last N time series values were taken from a certain process state and were applied to the membership functions belonging to that same process state, then it would be very likely that each data value class has an average probability of occurrence. Therefore, the relationships between the input and output fuzzy variables are defined as shown in table 5-2. These relationships are also called the decision rules of the fuzzy-logic approach.

Table 5-2. Definition of decision rules for one process state

data value → / probability of occurrence ↓	small (*sm*)	medium (*md*)	large (*lg*)
low (*lo*)	anomalous	anomalous	anomalous
average (*av*)	normal	normal	normal
high (*hi*)	anomalous	anomalous	anomalous

A time series is 'normal' if each data value class has an average probability of occurrence. It should be noted that 'normal' and 'anomalous' are relative names. If, for example, the matrix belongs to the first anomalous state ('intermediate boiling' state) then 'normal' means that the time series has characteristics that are in accordance with those expected at this process state.

The fuzzy membership value of the 'normal' state is defined as:

$$\mu_{norm}^{ij} = \frac{1}{3}(\mu_{sm,av}^{ij} + \mu_{md,av}^{ij} + \mu_{lg,av}^{ij}). \qquad (5\text{-}3)$$

The fuzzy membership values of the three states are defined as:

$$\mu_{norm}^{tot} = \frac{1}{3}(\mu_{norm}^{1,1} + \mu_{norm}^{2,1} + \mu_{norm}^{3,1}), \qquad (5\text{-}4)$$

$$\mu_{anom1}^{tot} = \frac{1}{3}(\mu_{norm}^{1,2} + \mu_{norm}^{2,2} + \mu_{norm}^{3,2}), \qquad (5\text{-}5)$$

$$\mu_{anom2}^{tot} = \frac{1}{3}(\mu_{norm}^{1,3} + \mu_{norm}^{2,3} + \mu_{norm}^{3,3}). \qquad (5\text{-}6)$$

In equation (5-3) till (5-6) the average of three fuzzy membership values is taken instead of the minimum or the product (bounded, algebraic) (Kruse *et al.*, 1994) which are commonly used in case of an AND statement. Taking the minimum or a product operator, however, led to much higher values of N and to longer ATAs for the two anomalous states in the applications that will be shown later in this chapter.

Defuzzification

The final step in the fuzzy-logic approach is to leave the fuzzy environment and return to a crisp environment. This is done using the maximum membership defuzzification scheme. This scheme simply selects that fuzzy output variable having the largest value. This means that the process state with the largest membership value is chosen as the most probable state of the process.

Result of applying the fuzzy-logic approach to analysis results

The fuzzy-logic approach is applied to the three time series presented in figure 5-3. For N=45 (T_d=1.41 s) a false-alarm-free detection result is obtained for which the ATAs of the anomalous states are minimized. A false-alarm-free detection result means that the process states are not detected before they actually occur. The first three graphs of figure 5-6 show the fuzzy membership values of the three states for N=45. The fourth graph of figure 5-6 shows the result of the defuzzification for N=45. The first

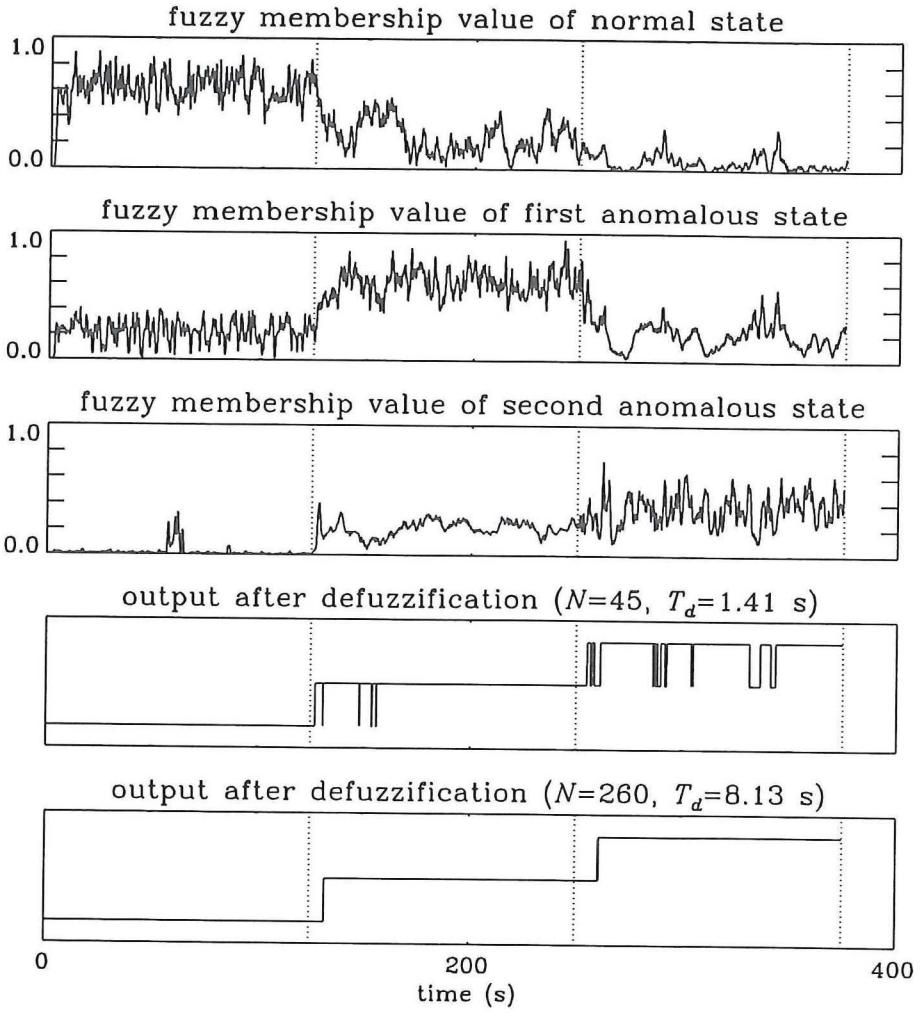

Figure 5-6. Results of applying the fuzzy-logic approach to the analysis results shown in figure 5-3

anomalous state is detected for the first time at position 4076 and the second anomalous state at position 8171. This means that the *ATA*s are equal to 2.34 s and 5.31 s, respectively.

For obtaining a detection result free from identification errors N must be at least 260 (T_d=8.13 s). The bottom graph of figure 5-6 shows that for this value of N each process state is, apart from a detection delay, identified correctly during its presence. In this case, the times to detection are equal to 7.16 s and 11.03 s, respectively.

5.4 Application of the fuzzy-logic approach

In order to check the validity of this fuzzy-logic approach it will be applied to the analysis results of a signal which was determined using the same AR models but with a white noise signal having a different seed as input to the AR models. The membership functions determined in the previous section are used here. Figure 5-7 shows the new synthetic signal. The three analysis techniques were applied to this new signal.

For N=72 (T_d=2.25 s) the *ATA*s of the two anomalous states are minimized, under the restriction that no false alarms occur. The first anomalous state is detected after

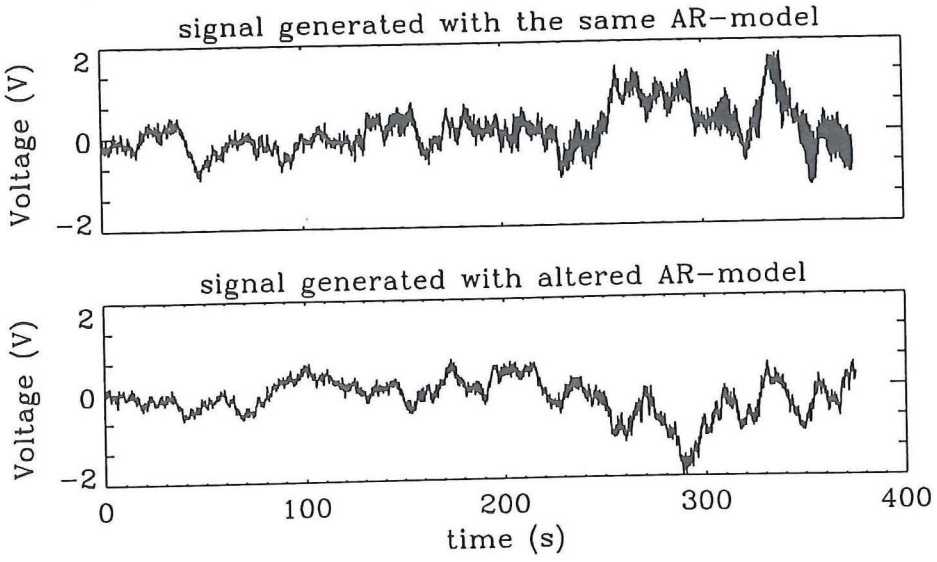

Figure 5-7. Signals generated for checking the fuzzy-logic approach

3.38 s and the second anomalous state after 3.72 s. An identification-error-free detection result requires N to be equal to 385 (T_d=12.03 s). The times to detection are 10.44 s and 8.59 s, respectively. This shows that the fuzzy-logic approach also gives good results in case of another signal having the same characteristics as the original signal.

Finally, the fuzzy-logic approach is tested using a different synthetic signal. Again, the membership functions are not changed. The spectrum of the measured neutron noise signal in case of boiling shows a dominant 3.2-Hz peak, which is not present in the spectrum in case of no boiling (see figure 5-8). For generating the new synthetic signal AR models 2 and 3 were slightly changed in order to remove the 3.2-Hz peak from the spectrum of the new signal. This was done by shifting one pair of complex conjugated poles of the two AR models.

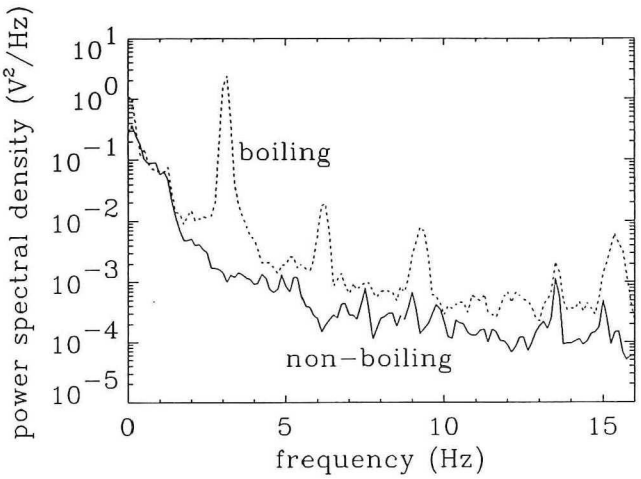

Figure 5-8. Spectrum of 'boiling' and 'non-boiling' neutron noise signal

The three signal processing techniques are applied to the new synthetic signal and their results are used as input to the fuzzy-logic approach. AR and fractal analysis still show a reasonable change due to the anomalies but wavelet analysis shows no deviating response to the two anomalous states. The response of wavelet analysis can be explained by considering the fact that for input order 12 wavelet analysis focuses on changes in the frequency content of the spectrum around 2.8 Hz.

The result of this fuzzy-logic application is that the second anomalous state is not detected at all, but is identified as the first anomalous (intermediate boiling) state. The first anomalous state is detected only after 16.25 s (N=45) or 16.38 s (N=72). The fact that this state is still detected can be explained by the fact that removing the 3.2-Hz peak does not change the 'intermediate boiling' state to such an extent that it becomes undetectable.

5.5 Conclusions

The fuzzy-logic approach presented in this chapter is a very promising approach for combining the outcomes of several signal processing techniques. It enables one to distinguish one process state from the other. The parameters of the approach are fully determined by the PDFs of the different parts of the input data series. The only parameter which has to be chosen is the number of data points used per decision (N).

In this chapter, the processing techniques were all applied to one signal (signal processing redundancy). It is, however, also possible to use signals from several redundant sensors and apply the same analysis technique(s) to all the signals (sensor redundancy). Another option is to apply the fuzzy-logic approach directly to the signals without analyzing them first. In this manner the measurement results from different redundant sensors can be combined.

Another option is to perform anomaly detection on the results of signal processing and then use adapted versions of the output of the anomaly detection methods as input for the fuzzy-logic approach. If, for example, SPRT would be applied to the residual noise the SPRT parameter λ or a variable derived from this parameter (see par. 3.4) could be used as input.

In order to apply this approach in practice, one has to know all possible process states and the characteristics of the time series at each process state.

Chapter 6

NEUTRON NOISE MEASUREMENTS WITH THE SIMBOL FACILITY

In this chapter, the experiments performed with the SIMBOL facility and their results are presented. First, the general considerations that led to the construction of SIMBOL and a description of this facility will be given. Second, the experimental conditions and the setup of the experiments will be discussed. The chapter will be concluded with the application of the signal processing techniques (chapter 2), the anomaly detection methods (chapter 3) and the fuzzy-logic approach (chapter 5) to the measurement results.

6.1 General considerations

The aim of the experiments with the SIMBOL facility is to simulate boiling of the coolant of a PWR by blowing nitrogen bubbles and to investigate the effect of the bubbles on the neutron noise. SIMBOL is positioned next to the core of the Hoger Onderwijs Reactor (HOR) of the Interfaculty Reactor Institute (IRI). The experiments are done without interrupting the normal operation schedule of the HOR.

The HOR is a pool-type research reactor of 2 MWth power with a maximum thermal neutron flux of approximately $2 \cdot 10^{13}$ $cm^{-2}s^{-1}$. The core is located at the bottom of a 8 m deep pool filled with 250,000 l of demi-water. The water streams downwards through the core with an average velocity in the fuel assemblies of 60 cm/s. The HOR is fuelled with highly enriched uranium (93 wt %) located in the fuel plates of the MTR-type assemblies. An MTR assembly consists of 19 fuel plates of 1.1 mm thickness each. The fuel assemblies have a 76×80 mm^2 rectangular cross-section and an active length of

600 mm. The main construction material of the core is aluminium. The reactor is controlled by 4 control rods. The HOR is a combined water- and Beryllium-reflected system. An example of the core configuration of the HOR is shown in figure 6-1, with 25 fuel elements and 11 Be-reflector elements.

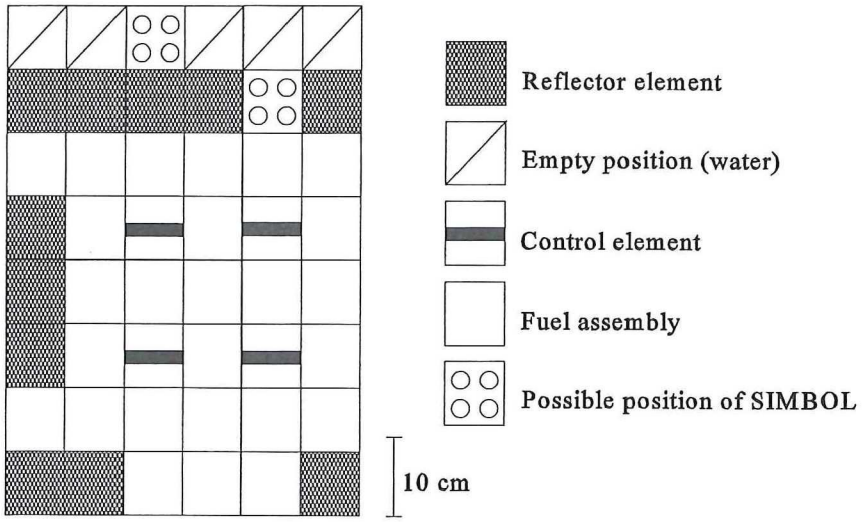

Figure 6-1. Map of the HOR core. There are two possible positions for SIMBOL.

The SIMBOL facility was developed as a result of shortcomings of the former experimental facility named NIOBE (see chapter 1). This facility was designed to evoke boiling of the coolant through electrical heating of 3 metal plates. It was equipped with neutron detectors and thermocouples of which the latter were positioned inside the plates. This meant that the thermocouples measured the temperature of the inside of the plates, which is different from the temperature of the coolant. With NIOBE it was impossible to determine the starting time and the starting position of boiling, which, however, is essential for doing research on the application of anomaly detection to reactor noise signals. Moreover, the plates were not the only heat source due to the heat production of the reactor core, thus making the decision about the presence of boiling even more difficult.

Therefore, an experimental facility was needed in which the position, starting time and intensity of boiling are exactly known. This led to the design of SIMBOL in which

boiling is simulated by blowing nitrogen bubbles into the water. No heat is added in this facility. The disadvantage of this facility is that blowing nitrogen bubbles is different from boiling in the physical sense. Investigating this difference is beyond the scope of this thesis. This is why the connection with boiling will be abandoned and the general word anomaly will be used instead from now on.

6.2 Description of SIMBOL

SIMBOL consists of a simulated 4×4 PWR assembly (the core of the facility), a closed water circuit with a circulation pump, a nitrogen supply to the core of the facility via capillaries and a number of manual valves and gas flow meters to control the nitrogen flow rate. Figure 6-2 shows the lower part of the facility consisting of the pedestal, the core and the upper chamber where the capillaries are connected to thicker tubes. The water and nitrogen are transported from the core of the facility via the upper chamber to the outlet-pipe. The outlet-pipe is connected to a cask (not shown in figure 6-2) which is located above the water surface of the reactor pool. In this cask the nitrogen is separated from the water in order to avoid that the nitrogen is transported through the core more than once. Also shown in figure 6-2 are the vertical and horizontal scale. The core and the upper chamber are shown open for visual purposes but are closed in reality. Figure 6-3 shows a section of the core of the facility. In both figures the position with respect to the core is indicated.

Unfortunately, it was not possible to use the circulation pump during the experiments that were performed with SIMBOL (see further on in this chapter), since radiation measurements during operation of SIMBOL have shown that the dose rate near the cask reaches unacceptably high values in case of operation of the pump. Natural circulation of the water was prohibited too by closing a valve in the supply-pipe. This means that the nitrogen bubbles were released in stagnant water.

The core of the facility consists of 4×4 tubes in a PWR configuration (see fig. 6-3). These 16 tubes are positioned in a square case with inner dimensions of 52×52 mm^2. Each tube has a length of 554 mm and a diameter of 10 mm; the pitch of the assembly equals 13 mm. The innermost 2×2 tubes of the assembly all have a ring of 10 equally spaced holes on 5 different axial levels, resulting in 20 levels all together. In the remaining of this chapter, a 'ring of holes' is abbreviated to 'ring'. The bottom ring is located at 30 mm from the water inlet of the case and the subsequent rings are spaced

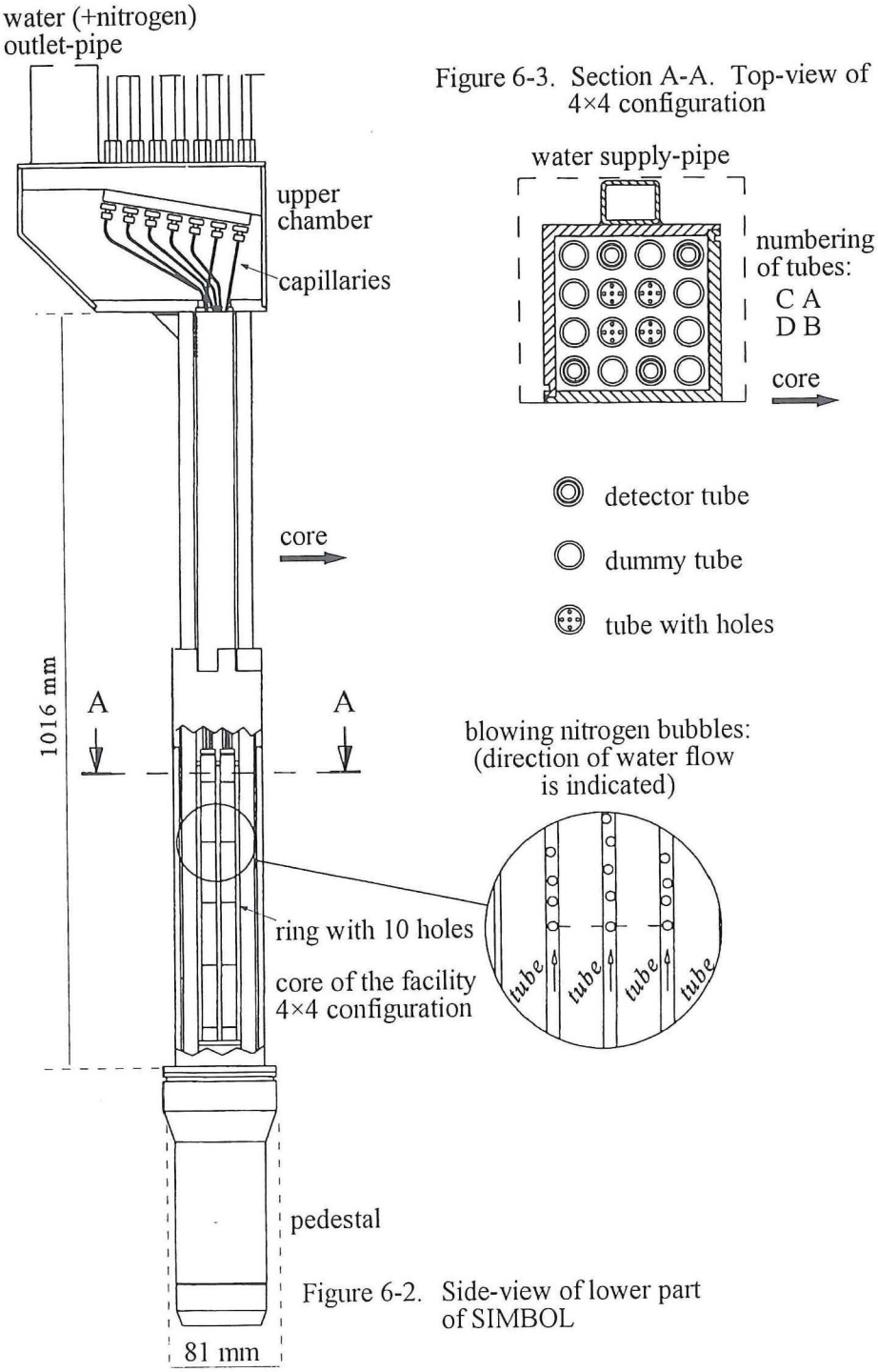

Figure 6-3. Section A-A. Top-view of 4×4 configuration

Figure 6-2. Side-view of lower part of SIMBOL

125 mm apart. The rings are numbered 1 to 5 from the top to the bottom of the tube. Each tube with holes is denoted by a capital letter from A to D as shown in figure 6-3. The holes have a diameter of 0.2 mm.

Each ring can be connected separately to the nitrogen supply through a capillary, causing nitrogen bubbles to escape from the 10 holes into the water. Since the bubbles are released inside the core of the reactor it was not possible to use air because it would become too much radioactive because of production of ^{41}Ar. A maximum of 4 rings can be connected to the nitrogen supply at one time with no restrictions with respect to the number of combinations of 4 rings. The nitrogen flow to one ring can be adjusted by manually operated valves, independently of the nitrogen flows to the other rings. The nitrogen flow rate can be measured with a flow meter of type Top-Trak 820/06. All these measures enable one to determine exactly the position of the origin of the bubbles (position of the anomaly), the time of origin of the bubbles (starting time of the anomaly) and the average amount of bubbles per time interval (magnitude of the anomaly).

The facility is equipped with 4 strings of 2 self-powered neutron detectors (SPNDs), each one located in a separate tube (see fig. 6-3). The strings are numbered from 1 to 4 as shown in figure 6-6 (section 6-4). The SPNDs consist of a Cd emitter and a stainless steel collector and have a diameter of 4.5 mm and a length of 40 mm. The SPNDs in one string are positioned at a relative axial distance of 10 cm. The strings can be shifted in a vertical direction.

6.3 Testing the facility

The facility was first tested outside the reactor pool in order to determine whether it is possible to create nitrogen bubbles at all the rings. This was done by measuring the chordal averaged void fraction between the tubes using gamma transmission technique (Hewitt, 1978). At the same time void fraction measurements were performed for several rings together and for different nitrogen flow rates. During these measurements the water level in SIMBOL was approximately 1 m above the lowest ring and there was no water circulation. This means that these measurements were performed under different conditions (approx. 20 °C and 1.1 bar) than the experiments performed later with SIMBOL positioned next to the core of the reactor (approx. 35 °C and 1.7 bar).

Figure 6-4 gives an impression of how the gamma transmission experiments were

performed. This figure shows a horizontal cross section of the core of the facility. The source and detector are positioned in one line and the beam does not cross a tube. A 300 mCi ^{241}Am source is used which emits 60 keV gammas. For collimation of the beam two circular diaphragms of 1 mm diameter are used, one positioned near the source and one positioned near the detector. The transmitted gammas are detected by a NaI scintillator. The source and detector can be moved simultaneously since they are interconnected by a U-shaped rod. This rod, together with source and detector, can also be rotated in the horizontal plane. In this manner gamma transmission measurements can be performed for six different paths denoted by a, b, c, d, e and f, as shown in figure 6-4. The source and detector are in the correct position when the transmitted beam intensity (without bubbles) is maximum, meaning that the beam does not cross any tubes.

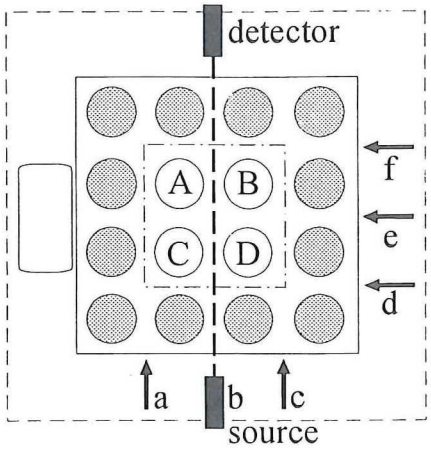

Figure 6-4. gamma transmission technique

The chordal averaged void fraction α_c can be determined using the following equation (Hewitt, 1978):

$$I(\alpha_c) = I_R \cdot \exp(\mu_l \alpha_c), \qquad (6\text{-}1)$$

where I and I_R stand for the beam intensity with and without bubbles, respectively. μ_l is the linear attenuation coefficient of water being equal to 0.204 cm^{-1} for 60 keV gammas (Blatz, 1959). The beam intensity is determined by counting the number of gammas that are detected by the NaI scintillator during a specified period T and by dividing this number by T. By rewriting equation (6-1), an equation for α_c as a function of I and I_R is obtained:

$$\alpha_c = \frac{1}{\mu_l} \cdot \ln\left(\frac{I}{I_R}\right). \qquad (6\text{-}2)$$

Thus by measuring the beam intensity with and without bubbles, the chordal averaged void fraction can be determined. The standard deviation of α_c can be derived from equation (6-2) and from the standard deviation of I. Since I has a Poisson distribution, σ_I is equal to:

$$\sigma_I = \sqrt{I/T}\,. \tag{6-3}$$

The standard deviation of α_c is then given by:

$$\sigma_\alpha = \frac{1}{\mu_l}\left(\frac{1}{\sqrt{I \cdot T}} + \frac{1}{\sqrt{I_R \cdot T}}\right). \tag{6-4}$$

First, each ring was tested separately by placing detector and source at 5 cm above the ring. It appeared that 3 rings were plugged due to construction faults with unknown cause. These rings are: D1, D2 and D5. These rings cannot be used during the experiments.

Second, void fraction measurements were performed at several horizontal and vertical positions for ring B5, rings {B2, B3, B4, B5} and rings {A3, B3, C3, D3}. The notation {..} indicates that all the rings, given between brackets, are used simultaneously. For ring B5 these measurements were also performed for different nitrogen flow rates. Figure 6-5 shows the void fraction as a function of the flow rate for path b at 5 cm above ring B5. Also shown are the error margins of one standard deviation of the void fraction.

The volumetric averaged void fraction α_l, can be estimated by the relation:

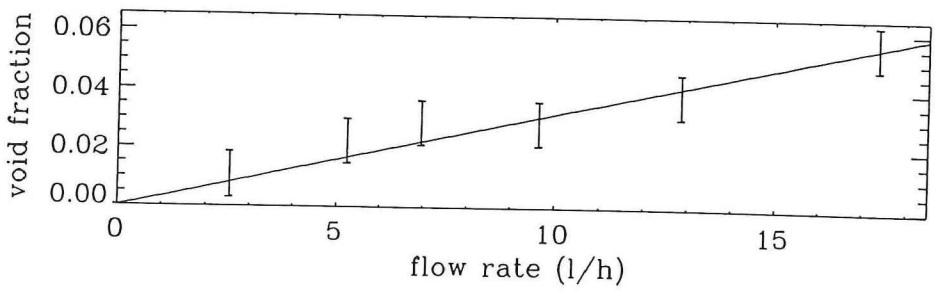

Figure 6-5. Chordal averaged void fraction as a function of the nitrogen flow rate from ring B5. The source is located at position b (see figure 6-4) and at 5 cm above ring B5.

$$\alpha_{l'} = \frac{Q_g}{v_b A_b}, \qquad (6\text{-}5)$$

where v_b is the terminal velocity of a swarm of bubbles in a medium of restricted extent (see section 6.5.2). A_b is the cross-sectional area through which the bubbles flow and Q_g the volumetric nitrogen flow rate. If v_b and A_b are independent of Q_g then $\alpha_{l'}$ is linearly related to Q_g. Assuming that $\alpha_{l'}$ and α_c are linearly related too, then α_c is proportional to the volumetric flow rate. This is shown in figure 6-5 by a straight line fitted through the points. The fitting was done using a least-squares fitting procedure. Later, it will be shown that v_b is, in fact, almost independent of Q_g for small void fractions (see section 6.5.2).

The chordal averaged void fractions obtained when the source is in positions b, c, e and f are higher than in the other positions in case ring B5 or rings {B2, B3, B4, B5} are used. This datum is independent of the vertical position of the source and detector, as long as they are positioned above the lowest ring B5. When rings {A3, B3, C3, D3} are used, the void fraction along path b and e is higher than along the other paths. This is independent of the vertical position of the source and detector. Paths a, c, d and f give comparable void fractions. These results indicate that the bubbles stay close to the tube from which they originate meaning that there is almost no void drift.

6.4 Experiments performed with SIMBOL

Experiments with different combinations of rings and various nitrogen flow rates have been performed with SIMBOL. During all the experiments the facility was positioned between the reflector elements (see figure 6-1). As mentioned in section 6.2 the water circulation pump could not be used.

Nitrogen bubble injection experiments have also been performed with the NIOBE facility (Kozma, 1992). Kozma studied the connection between the intensity of the neutron noise and the void fraction. This topic will not be treated here. Interested readers are referred to the work of Kozma or others (Bernard *et al.*, 1982; Miteff *et al.*, 1982; Kozma, 1992). Here the main attention is focused on applying signal processing techniques and anomaly detection methods to the neutron noise signals obtained through the measurements with SIMBOL.

For neutron flux measurements four SPNDs were used, namely the upper one from string 1, the lower one from string 2 and two from string 3. They are denoted by ND1H, ND2L, ND3L and ND3H, respectively, where ND stands for "neutron detector", L for "low" and H for "high". String 4 could not be used due to the fact that the tube was stuck at a high position meaning that the detectors were located far above the core. Figure 6-6 gives a 3-dimensional view of the core of the facility showing the positions of the four SPNDs. The dark-grey tubes are the detector tubes and the light-grey ones are the tubes with holes. The position of the reactor core is also indicated in the figure. Table 6-1 gives the vertical distance between the SPNDs and the bottom ring (ring 5). Since subsequent rings of one tube are spaced 12.5 cm apart, ND1H is located 10.5 cm above ring 4, ND2L is located 2.5 cm above ring 4, ND3L is located 8 cm above ring 3 and ND3H is located 5.5 cm above ring 2.

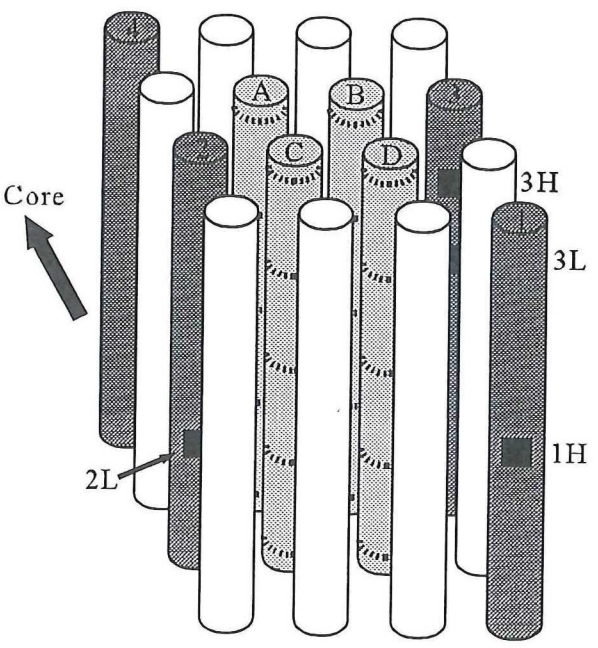

Figure 6-6. Schematic 3-d view of the core of SIMBOL (not to scale)

Six measurements were performed with SIMBOL. Table 6-2 gives a short description of each measurement. The abbreviation Ms stands for measurement. The neutron detector signals are first filtered using 8th order low-pass filters with a cut-off frequency of 20 Hz. After filtering they are amplified using differential amplifiers. AC-coupling of the amplifiers, with a cut-off frequency of 0.04 Hz, is used. The DC value of the neutron detector signal is recorded every 5 s. The nitrogen flow rate is measured using mass flow meters which return an output voltage proportional to

Table 6-1. Vertical distance between centre of detector and ring 5

SPND	position
ND1H	+23 cm
ND2L	+15 cm
ND3H	+43 cm
ND3L	+33 cm

Table 6-2. Measurements performed with SIMBOL

Ms	Rings	Duration	Nitrogen flow rate
1	B2, B3, B4, B5	3840 s (1:04 h)	Stepwise increase (4 steps) of nitrogen flow rate from 0 l/h to approx. 6.5 l/h per ring. (Total flow rate: 0 - 26.1 l/h)
2	B5	900 s (15 min.)	Gradual increase of nitrogen flow rate from 0 l/h to approx. 22 l/h.
3	B5	2000 s (33:20 min.)	Stepwise increase (2 steps) of nitrogen flow rate from 0 l/h to approx. 10.6 l/h. (Flow rate signals were recorded incorrectly.)
4	B5	1500 s (25 min.)	Stepwise increase (3 steps) of nitrogen flow rate from 0 l/h to approx. 10 l/h.
5	A3, B3, C3, D3	1650 s (27:30 min.)	Stepwise increase (2 steps) of nitrogen flow rate from 0 l/h to approx. 6.5 l/h per ring. (Total flow rate: 0 - 26.1 l/h)
6	A3	1500 s (25 min.)	Stepwise increase (4 steps) of nitrogen flow rate from 0 l/h to approx. 3.3 l/h

the mass flow rate. The flow meters have a maximum range of 37.5 g/h corresponding to 30 l/h (at 0 °C and 1.0 bar) and an accuracy of 2 % full scale. The nitrogen is released under different conditions, namely at approximately 35 °C and 1.7 bar (conditions in the reactor core). The actual volumetric flow rate can be determined using the ideal gas law:

$$Q_2 = \frac{P_1}{P_2} \cdot \frac{T_2}{T_1} \cdot Q_1 , \qquad (6\text{-}6)$$

where P_1, T_1 and Q_1 are the pressure, temperature (in K) and volumetric flow rate under reference conditions (0 °C, 1.0 bar). Index "2" refers to the actual conditions. Using equation (6-6) it can be determined that the actual volumetric flow rate is 0.664 times the flow rate indicated by the flow meter. The voltage signals from the flow meters are also low-pass filtered using the same filter settings as with the neutron detectors. No AC-coupling is used in case of the flow signals. Both the filtered and amplified neutron

detector signals and the flow signals are recorded on magnetic tape.

In order to analyse the signals with a computer they are read from magnetic tape, filtered and amplified, if necessary, and are sampled with a sampling period of 30 ms. The flow rate and neutron detector signals are filtered, this time using a low-pass frequency of 5 Hz and 12 Hz, respectively.

6.5 General analysis of neutron noise signals

Before the signal processing techniques and anomaly detection methods are applied to the neutron noise signals it is important to have a proper picture of the anomaly that is introduced by blowing bubbles. In this section, results of spectral and statistical analysis of neutron noise signals, obtained with the SIMBOL measurements, are given. At the same time the bubble transit time will be calculated for several flow rates.

6.5.1 Spectral and statistical analysis

Figure 6-7 shows the normalized auto power spectral densities (NAPSDs) of ND3H

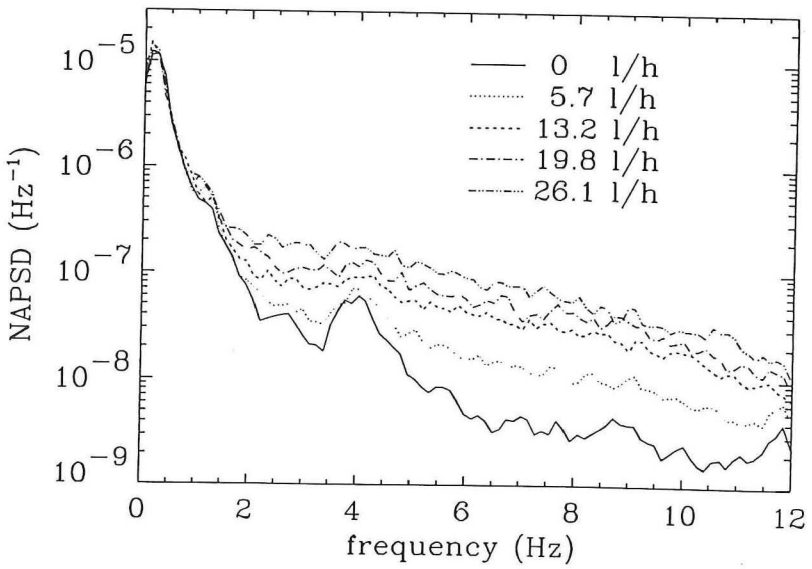

Figure 6-7. Spectrum of ND3H for five different total flow rates (measurement 1)

of the first measurement for the five flow rate steps. The flow rate values given in the legend of figure 6-7 are the average values of the sum of the flow rates from the four rings determined over a period during which the flow rate is almost constant. The total flow rate of measurement 1 as a function of time is shown in figure 6-13a (section 6.6).

For determining the spectrum, the signal was first normalized using the DC-value of the detector. It can be seen that the amplitude of the spectrum for frequencies higher than 1.5 Hz increases due to the blowing of nitrogen. The amplitude of the noise added by the bubbles increases with the nitrogen flow rate. The spectrum below 1.5 Hz does not change because the amplitude of the noise added by the bubbles is much smaller than the amplitude of the global noise. The global noise is caused by reactivity fluctuations during normal reactor operation.

Figure 6-8 shows the probability density functions (PDFs) of the same neutron noise signal. The neutron noise signal was first filtered using a low-pass filter with a cut-off frequency of 1.5 Hz. It is clear that the standard deviation of the filtered neutron noise signal changes due to blowing of nitrogen bubbles. Without pre-filtering the neutron noise signal no change of the standard deviation occurs. The explanation for this was already given in the previous paragraph, namely, that the spectra of the neutron noise signal for different nitrogen flow rates were uniform for the frequency range from 0 to approximately 1.5 Hz. When studying the same (unfiltered) neutron noise signal in time domain (see figure 6-13b, next section) there is, as expected, no visible change either.

Figure 6-9 shows the NAPSDs of the four detectors used in measurement 1 in case of maximum nitrogen flow rate. The spectra of ND3L and ND3H are different from the spectra of ND1H and ND2L. If these spectra are compared with the corresponding spectra for a nitrogen flow rate of 0 l/h (not shown in figure 6-9) it becomes clear that

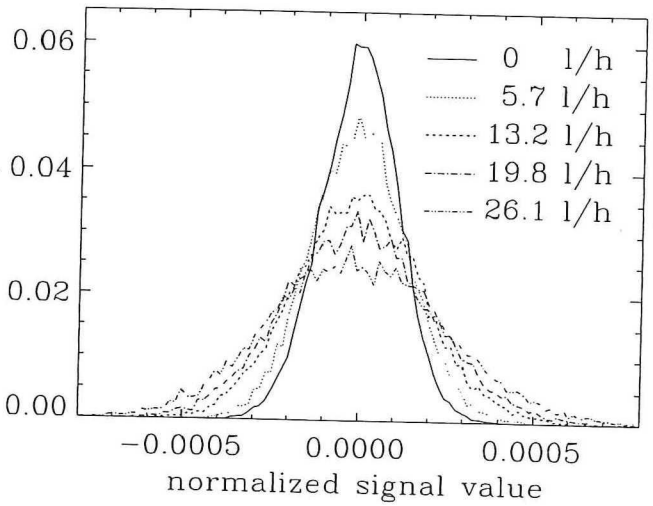

Figure 6-8. PDFs of ND3H for five different total flow rates (measurement 1)

the spectra of ND1H and ND2L do not change visibly due to the bubbles, whereas the spectra of the detectors in string 3 do change. This can be explained by looking at the positions of the detectors relative to the origin of the bubbles. In figure 6-6 it can be seen that the bubbles which originate at the four rings of tube B pass along the detectors in string 3 at very small distance (except the bubbles from ring B2 which do not pass ND3L). This is however not the case for ND1H and ND2L. This shows that, in principle, it is possible to localize the bubbles.

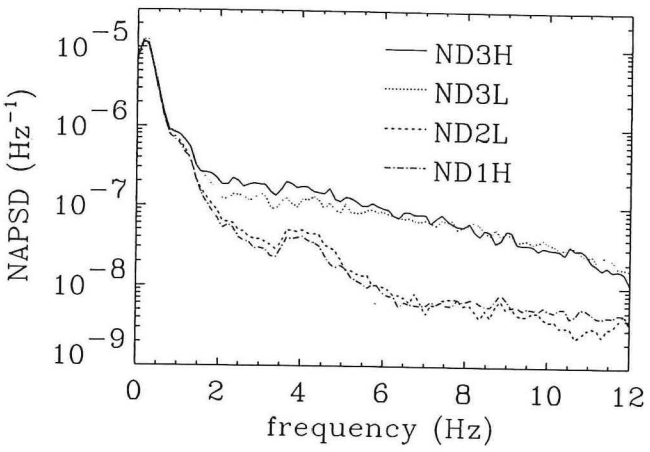

Figure 6-9. Spectra of neutron noise signals from four detectors (measurement 1, maximum flow rate)

The effect on the reactivity of the blowing of nitrogen bubbles was too small to be detectable by control rod position. The DC-values of the SPND signals remained constant during the experiments.

6.5.2 Transit-time calculations

Since the two detectors in string 3 are axially displaced and bubbles pass along both detectors it is possible to determine the transit time and thus the velocity of the bubbles using signals from both detectors. Transit-time calculations have been done for measurements 3 and 4.

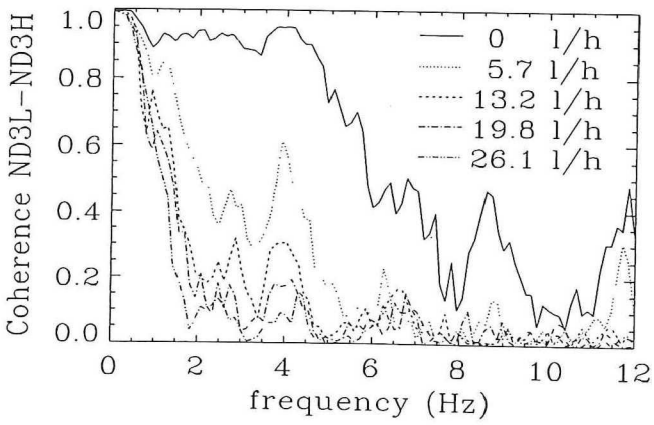

Figure 6-10. Coherence between ND3L and ND3H for five different flow rates (measurement 1)

Figure 6-10 shows the coherence between ND3L and ND3H for several nitrogen flow rates. It can be seen that the coherence diminishes when the flow rate is increased and becomes very small for high frequencies. The bubbles themselves and the distribution of the bubbles can easily change shape on their way from the 3L to the 3H detector. The effect of this deformation will most probably be found in the range of relatively high frequencies. This could explain the decrease of the coherence between the two detector signals.

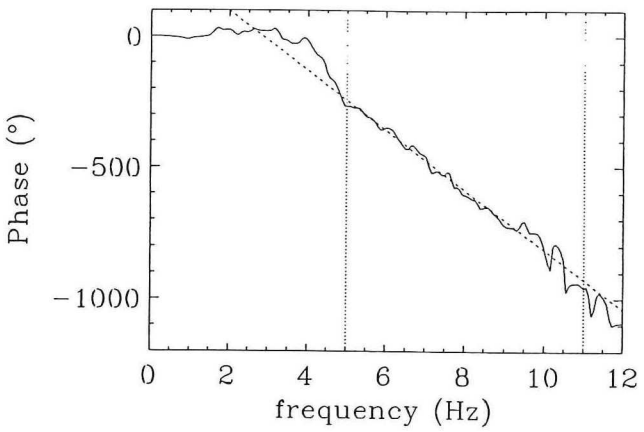

Figure 6-11. Phase of CPSD of ND3L and ND3H for maximum flow rate (measurement 3)

First, the phase of the cross power spectral density (CPSD) is used for transit-time determination. The variance of the phase φ of the CPSD increases with decreasing coherence ξ: $\sigma_\varphi \propto 1/\xi^2 - 1$. In order to obtain an accurate transit-time value the coherence should be high. Figure 6-11 shows how the transit time of the bubbles between the two detectors is determined by a least-squares fit of a straight line to the phase of the CPSD of measurement 3 (flow rate: 10.6 l/h). The slope of the line determines the transit time. The figure also shows that a transit time becomes apparent above approximately 4 Hz. For lower frequencies the intensity of the noise caused by the bubbles is apparently too small compared to the global noise component present in both signals. The fitting in the figure was done for the range from 5 to 11 Hz. The transit time was only calculated when the average coherence over the interval from 5 to 11 Hz was higher than 0.05 in order to have sufficient accuracy.

Second, the bubble velocity can be determined using the cross correlation function (CCF) of ND3L and ND3H. The signals from the two detectors were first high-pass filtered using a fifth-order Butterworth filter with a cut-off frequency of 4 Hz before the CCF was calculated. The pre-filtering was done in order to remove the global noise component. Figure 6-12 shows the CCF of measurement 3 (flow rate: 10.6 l/h). The CCF shows a fluctuation with a frequency of 5.1 Hz corresponding to the maximum

of the spectra of ND3L and ND3H after filtering. The spectrum of ND3L or ND3H from 2 Hz till 12 Hz can be approximated by a straight line (1/*f*-spectrum) (see for example figure 6-9). Filtering the spectrum with a fifth-order Butterworth filter can thus be approximated by multiplying this line with the transfer function of the filter. The result of this multiplication has its maximum at 4.9 Hz which is close to the 5.1 Hz determined here. Beyond this frequency the spectra fall off very quickly explaining the fluctuating behaviour of the CCF. The position of the maximum of the CCF gives the transit time. The maximum shown in figure 6-12 is not the real maximum of the CCF, since the points of the CCF are only known at multiples of the sampling period. The exact position of the maximum of the CCF is very difficult to determine due to the fluctuating behaviour of the CCF. Therefore, the CCF will not be used here for transit-time determination.

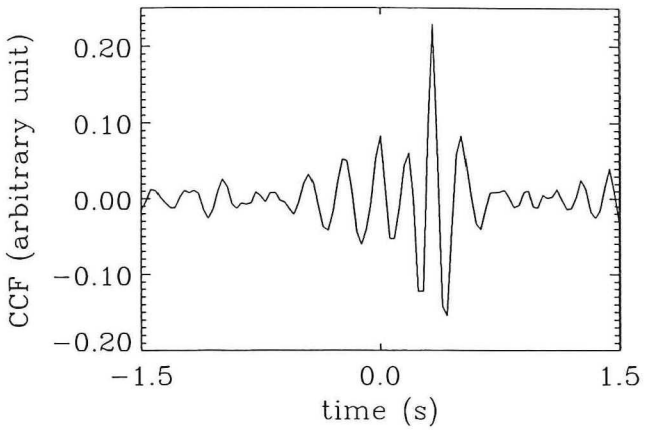

Figure 6-12. CCF of ND3L and ND3H for maximum flow rate (measurement 3)

Table 6-3 gives the results of the bubble velocities determined with the phase of the CPSD for several nitrogen flow rates. When studying table 6-3 one can see that the velocities are seemingly independent of the nitrogen flow rate.

From theory it is possible to determine the terminal velocity of bubbles in a medium of restricted extent. The holes in the tubes have a radius r_h of 0.1 mm which means that the bubbles reach a diameter:

$$d_b = \left(\frac{12 r_h \sigma_l}{\Delta \rho g} \right)^{1/3} \qquad (6\text{-}7)$$

before they detach (Chesters, 1978). σ_l is the surface tension of water ($7.27 \cdot 10^{-2}$ \ $7.04 \cdot 10^{-2}$ N/m). The values between brackets apply to the conditions: ({20 °C, 1.1 bar} \ {35 °C, 1.7 bar}) corresponding to: (SIMBOL outside the pool \ SIMBOL next to the

core of the HOR reactor), respectively. $\Delta\rho$ is the difference between the density of water and the density of nitrogen which can be approximated by the density of water (ρ_l) ($10.0 \cdot 10^2 \setminus 9.9 \cdot 10^2$ kgm^{-3}). g is the gravitational acceleration (= 9.8 ms^{-2}). The diameter of a bubble thus becomes: ($2.07 \cdot 10^{-3} \setminus 2.06 \cdot 10^{-3}$ m).

The correct equation to be used for determining the bubble velocity depends on the Reynolds number Re_b (742 \ 968) of the bubble (Govier *et al.*, 1972). Since in both cases, the Re_b is found in the beginning of the range ([740, 1370] \ [960, 1870]), the following equation must be used to calculate the velocity of a single bubble in an infinite medium ($v_{b0\infty}$) (Govier *et al.*, 1972):

$$v_{b0\infty} = 1.35\left(\frac{2\sigma_l}{\rho_l d_b}\right)^{0.5}. \qquad (6\text{-}8)$$

This equation is independent of the dynamical viscosity. The bubbles are deformed, flattened horizontally and ellipsoidal in cross section and move in spiraling, zigzag paths. The effect of wall proximity reduces the bubble velocity by a factor of (0.917 \ 0.915) (Harmathy, 1960) thus obtaining a terminal bubble velocity v_{b0} in the core of the facility of (32.8 \ 32.5 cms^{-1}).

In case of a swarm of bubbles the average velocity of the bubbles v_b can be calculated by (Govier *et al.*, 1972):

$$v_b = v_{b0}(1-\alpha_V)^K, \qquad (6\text{-}9)$$

where α_V is the volumetric void fraction. The exponent K depends on the bubble size. For $0.05 < d_b < 2.0$ cm K must be taken equal to 1.5 (Govier *et al.*, 1972). If the bubbles stay close to the tube from which they originate, A_b can be estimated to $3.6 \cdot 10^{-4}$ m^2. If the flow rate is 10 l/h and the velocity of the bubbles is approximated by the velocity of a single one, then the volumetric void fraction according to equation (6-5) becomes 2.4 %. After substituting this value of α_V into equation (6-10) it becomes clear that the velocity of a swarm of bubbles differs only slightly from the velocity of a single bubble ($v_b = 0.965 \cdot v_{b0}$).

Table 6-3. Bubble velocities

Ms	Total flow rate (l/h)	bubble velocity (cm/s)	
		phase CPSD	theory
3	6	31.1 (0.3)	31.8
	10.6	31.6 (0.2)	31.2
4	6.6	31.5 (0.5)	31.7
	10	31.5 (0.4)	31.3

Table 6-3 shows the theoretical values of the bubble velocities for the two measurements. The experimentally obtained bubble velocities come very close to the ones obtained from theory. It can be concluded that for the flow rates applied, the bubble velocity is almost independent of the flow rate. If A_b is also independent of the flow rate and if α_V is small (< 10 %) then the void fraction is proportional to the flow rate. This is in accordance with what was found in section 6.3.

Knowing the diameter of the bubbles it is also possible to determine the number of bubbles that are released per second for a specific flow rate. If the flow rate from one ring is 1 l/h then from each hole 6.63 bubbles per second are released.

6.6 Applying process-monitoring techniques to neutron noise signals

The three signal processing techniques and the three anomaly detection methods are applied to the neutron noise signals in the same way as was done in section 4.4. This is done for all the detectors from all the measurements except measurement 3. This measurement was not used because the nitrogen flow rate was recorded incorrectly meaning that it was not possible to determine exactly the starting time of a step in flow rate.

6.6.1 Signal processing

First of all, the signal processing techniques were applied to the neutron noise signals. Figure 6-13 shows the result of applying the three techniques to ND3H from measurement 1. Figure 6-13a presents the total nitrogen flow rate and figure 6-13b the neutron noise signal. Graph a shows fluctuations at the start of the second, third and fourth step in nitrogen flow rate. These fluctuations are caused by the fact that the nitrogen flow rate is adjusted manually. Finding the right opening of the valves takes some time and effort. The first step does not show any fluctuations since the valves were already adjusted before the start of the measurement. In order to introduce the first step, nitrogen pressure was simply applied to the valves by opening a fifth valve located in the conduit-pipe connecting the nitrogen bottle to the four valves.

The neutron noise signal shows no visible change due to the presence of nitrogen bubbles. Figures 6-13c till e present the time series from the three signal processing techniques.

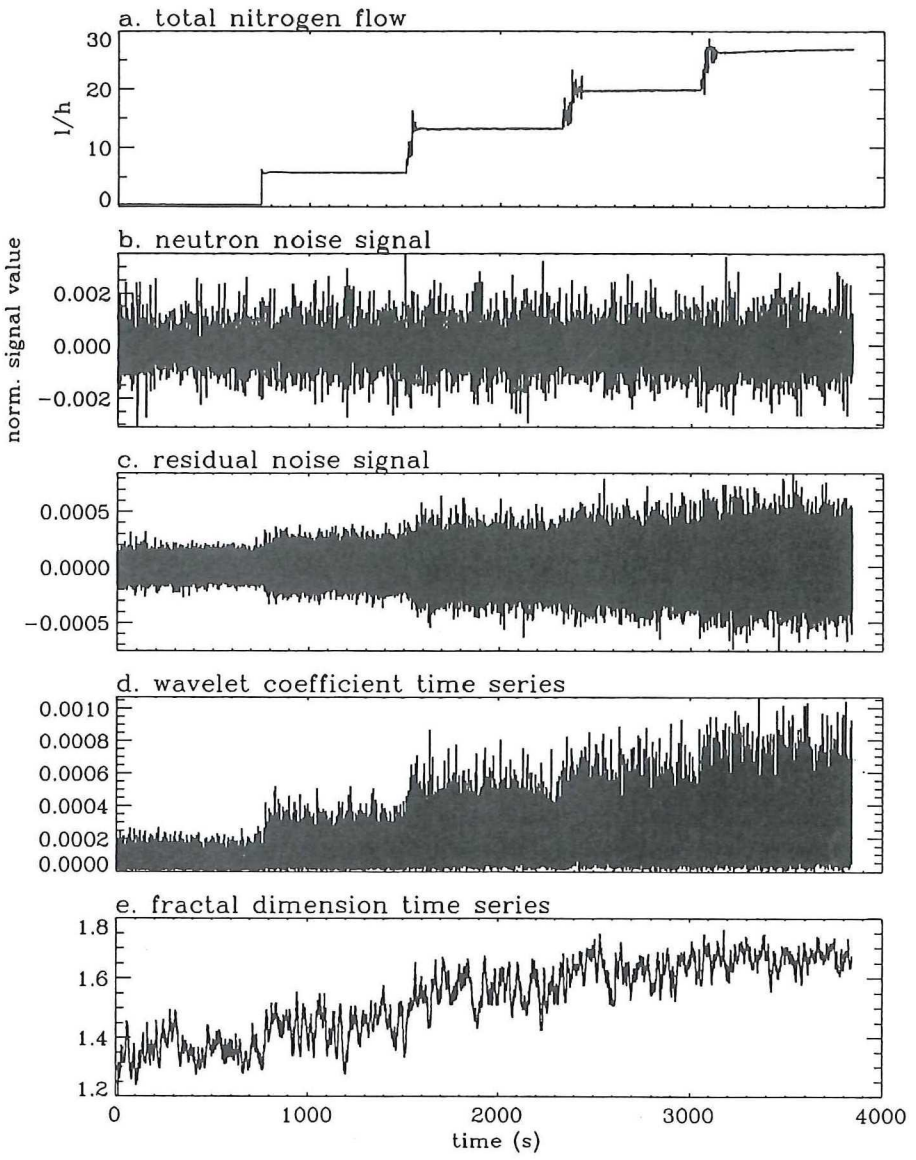

Figure 6-13. Results of applying signal processing techniques to ND3H signal from measurement 1

AR analysis was applied to the first 5000 data points of the ND3H signal from measurement 1. Using the *FPE* led to an optimum model order of 40 (see section

2.2.1). When applying AR analysis to the signals from the other detectors the same model order was found. The standard deviation of the residual noise increases 2.86 times when the total nitrogen flow rate is increased from 0 l/h to 26.1 l/h.

Wavelet analysis was applied to the ND3H signal for input orders 4 until 15. Input order 7 (central frequency = 7 Hz) showed the largest change due to the noise introduced by the blowing of bubbles. This is understandable considering the changes of the spectra of the SPNDs (see figure 6-7). The result with input order 7 is shown in graph 6-13d. This wavelet coefficient time series will be used for further applications. Other neutron noise signals were also analysed using the same input order. Also here a clear change of the wavelet coefficient is visible due to the blowing of nitrogen bubbles. The average value and the standard deviation of the wavelet coefficient increase 4.10 and 4.09 times, respectively, when the total nitrogen flow rate is increased from 0 l/h to 26.1 l/h.

Fractal analysis was applied to the ND3H signal for many different combinations of N and k-ranges. Graph 6-13e shows the result for N=512 and k=1-16. Fractal analysis was also applied to the other neutron noise signals using this $\{N,k\}$-combination. The fractal dimension increases from an average of 1.36 to 1.67 when the total nitrogen flow rate is increased from 0 to 26.1 l/h.

These analysis results show that each of the three signal processing techniques is sensitive to the noise added by the blowing of nitrogen bubbles. All the time series will therefore be used as input for the anomaly detection methods.

6.6.2 Anomaly detection

The next step is to apply anomaly detection methods to the results from signal processing. Similar to section 4.4.3 it is demanded that the detection results have no false alarms and that the times to alarm (TAs) are as small as possible. The method parameters are determined using the numerical results obtained through optimization of each method (see section 4.2). The only difference with the approach presented in section 4.4.3 is that for the SPRT method q is chosen equal to 1.1 here.

As was done in section 4.4.3 it is also possible to apply the anomaly detection methods directly to the neutron noise signals. Figures 6-14 and 6-15 show the detection results with minimum TA obtained with the ND3L signal from measurement 2 and 4, respectively. When the detection result in figures 6-14b and 6-15b is high, an anomaly is detected. From both figures it can be concluded that the anomaly is not detected.

There is merely an isolated spike detected in both cases. Therefore, a criterium is required, which determines whether there is really an anomaly detected or not. Here, the following method is introduced:

- The surface under the graphical representation of the detection result is determined.
- This surface is divided by the maximum obtainable surface.
- If this quotient κ is higher than a certain threshold value then an anomaly has been detected. κ is called the detection result decision parameter.

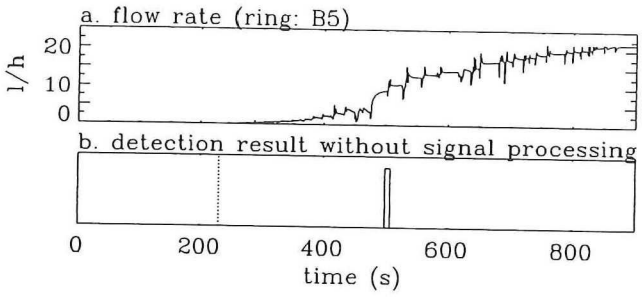

Figure 6-14. Result of applying extremes method directly to ND3L signal of measurement 2

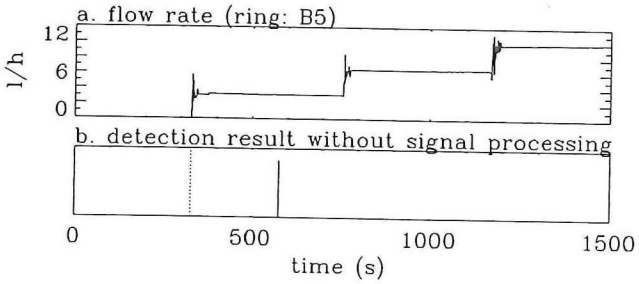

Figure 6-15. Result of applying SPRT directly to ND3L signal of measurement 4

Table 6-4 shows the κ values for the ND3L signal from measurement 2 and 4. The values in the second column of this table were determined from figures 6-17d and 6-18c, respectively. For the values in the third column figures 6-14b and 6-15b were used. It is clear that first applying signal processing techniques leads to much better detection results than the first mentioned approach. What is shown for these two signals also accounts for the other signals. Therefore, from here on signals are always first processed before anomaly detection methods are applied.

Table 6-4. κ values with and without signal processing.

Ms	κ (with signal processing)	κ (without signal processing)
2	0.465	0.013
4	0.490	0.0007

In every application the goal is to detect the first step or the ramp (gradual increase) in case of measurement 2. Per

detector 9 (3 signal processing techniques × 3 anomaly detection methods) detection results are obtained. Thus in total 5×4×9 = 180 detection results are obtained. The threshold value for κ is chosen equal to 0.333 here. This means that whenever a

Table 6-5. Smallest *TA*s obtained per measurement and per detector

Ms	anomaly	neutron detector	*TA* (s)	method combination	κ
1	Step from 0 to 6.6 l/h total N_2-flow rate (rings: B2, B3, B4, B5)	1H	43.29	frc-sprt	0.986
		2L	41.82	frc-sprt	0.843
		3L	34.44	frc-sprt	0.989
		3H	27.90	wav-sprt	0.960
2	Gradual increase of N_2- flow rate (ring: B5)	1H	247.23	wav-sprt	0.351
		2L	248.70	AR-χ^2	0.446
		3L	247.59	AR-sprt / AR-χ^2	0.465
		3H	246.87	frc-sprt	0.632
4	Step from 0 to 3.3 l/h N_2- flow rate (ring: B5)	1H	38.10	frc-sprt	0.968
		2L		AR-χ^2	0.088
		3L	4.83	AR-sprt	0.490
		3H	11.85	wav-ext	0.830
5	Step from 0 to 13.3 l/h N_2- flow rate (rings: A3, B3, C3, D3)	1H	4.65	AR-ext	0.598
		2L		AR-sprt	0.184
		3L		AR-sprt	0.285
		3H	4.59	wav-χ^2	0.694
6	Step from 0 to 0.66 l/h N_2- flow rate (ring: A3)	1H		AR-sprt	0.070
		2L		frc-sprt	0.232
		3L		AR-χ^2 / wav-sprt	0.015
		3H		AR-sprt	0.050

AR=autoregressive analysis, wav=wavelet analysis, frc=fractal analysis, ext=extremes method

detection result has a κ smaller than 0.333, there is, by definition, no anomaly detected. Table 6-5 shows the smallest *TA*s obtained per detector and per measurement and it shows which combination of a signal processing technique and an anomaly detection method gave the fastest detection. Only when κ is larger than 0.333 the *TA* is given in table 6-5.

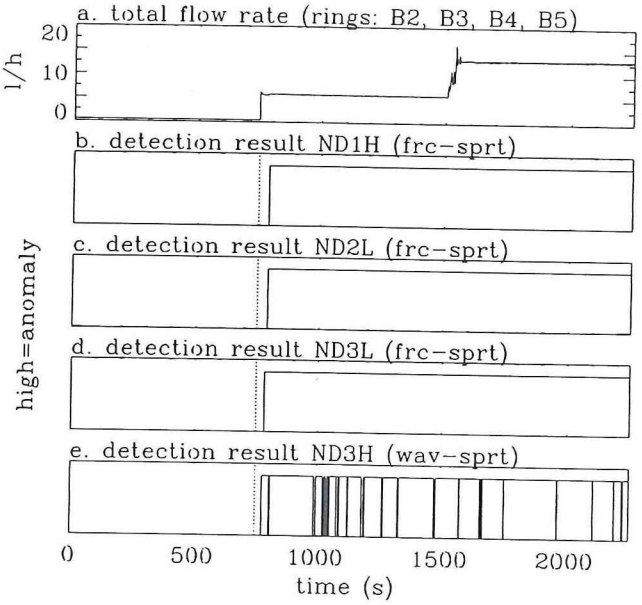

Figure 6-16. Detection results with four detector signals from measurement 1

The detection results obtained with measurement 1 show that for all detectors the step is detected with high κ values. This is surprising, since only the spectra of the detector signals from string 3 showed a change due to the blowing of bubbles (see figure 6-9). This demonstrates the strength of the process monitoring techniques in detecting small anomalies. The *TA*s obtained with ND1H and ND2L are, however, larger than the *TA*s obtained with ND3L and ND3H. It is remarkable that the step is detected much earlier for ND3H than for ND3L. By taking a look at figure 6-16 one can see, however, that with ND3L a result without any alarm failures is obtained which is not the case for ND3H. It should also be noted that only approximately 3/4 of the total flow passes ND3L because this detector is positioned above ring 3 but below ring 2.

In case of measurement 2, the anomaly is also detected by all four detectors. Again, for ND3H the anomaly is detected first. The κ values are not as high as for measurement 1, because the anomaly is detected much later. Figure 6-17 shows the detection results. The *TA* obtained with ND1H is rather questionable since after the first detection of the anomaly there is a long period during which nothing is detected (figure 6-17b). The nitrogen flow rate shows a rather capricious behaviour owing to the non-linearity of the manually operated valves and the difficulty of adjusting the flow

rate with these valves. At that point in time where the ramp is detected for the first time, the nitrogen flow rate equals 2.9 l/h (≈19 bubbles per second per hole).

The detection results obtained with measurement 4 are shown in figure 6-18. Here, the opposite occurs, namely that ND3L detects the anomaly earlier than ND3H. It can also be seen that ND3H gives an alarm-failure-free detection of the second and third step. ND1H gives a alarm-failure-free detection result but the *TA* is rather high.

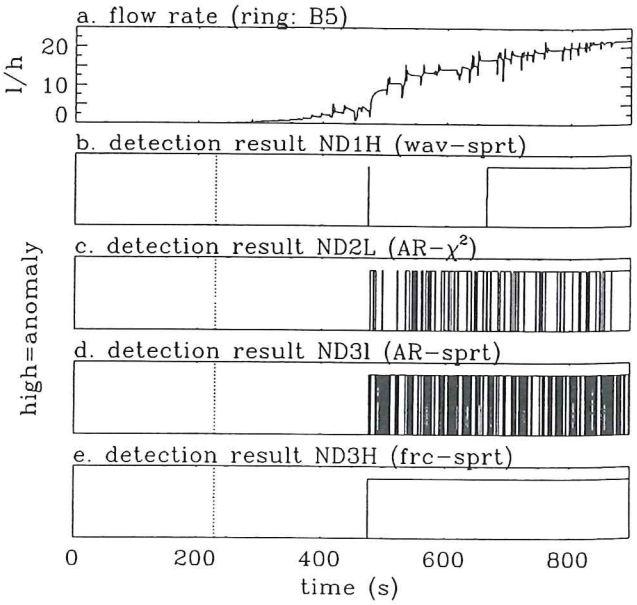

Figure 6-17. Detection results with four detector signals from measurement 2

In case of measurement 5 the anomaly is detected for only two detectors with a sufficiently high κ value. There is in fact only minor difference between the *TA*s. Figure 6-19 shows the detection results. It is surprising that with ND3L the anomaly is not detected, although this detector is located nearer to the origin of the bubbles (rings A3, B3, C3

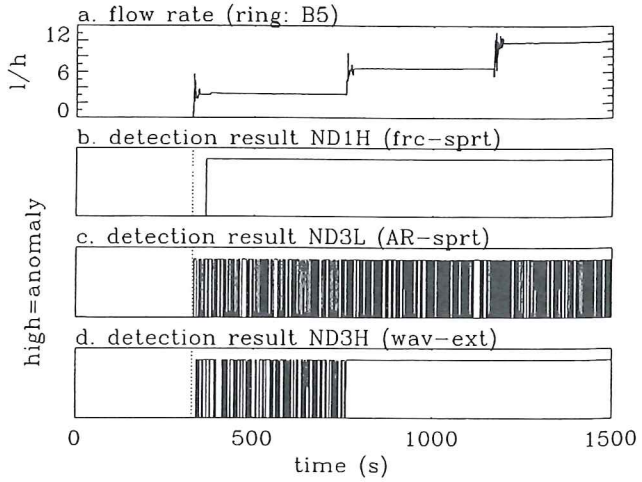

Figure 6-18. Detection results with three detector signals from measurement 4

and D3) than ND3H. ND1H gives a strong detection of the anomaly which could be explained by the fact that ND1H is positioned only 2 cm below the origin of the bubbles. ND2L is located 10 cm below the origin.

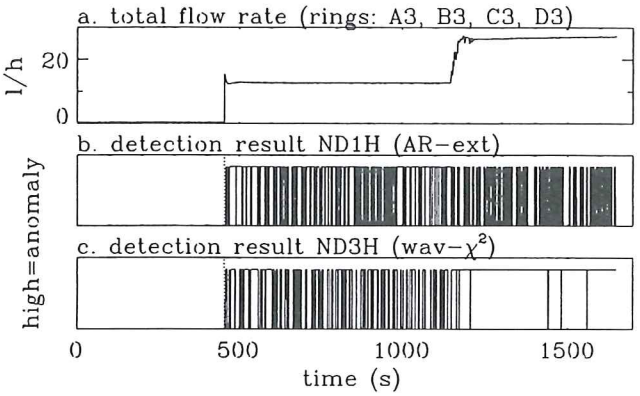

Figure 6-19. Detection results with two detector signals from measurement 5

The very small step in nitrogen flow rate introduced in measurement 6 is not detected at all. There is only a small and short disturbance detected which occurs at around 45 s after the step. It should be noted that the bubbles appear at ring A3 which is located relatively far from all the detectors and that the nitrogen flow rate is only 0.66 l/h. Considering the result obtained with measurement 2 (detection of the ramp at a flow rate of 2.9 l/h) it is not surprising that this small step is not detected.

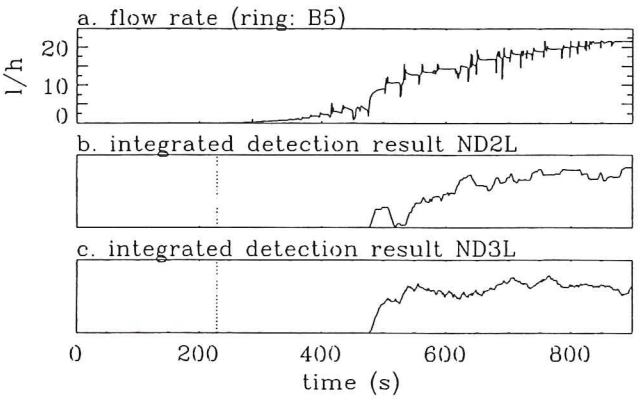

Figure 6-20. Integrated detection results with two detector signals from measurement 2

Some detection results show strongly fluctuating behaviour making it very difficult to determine if and when the anomaly is detected. This can be made easier by integrating the detection result $x(t)$:

$$\kappa(t) = \frac{1}{\Delta T} \int_{t-\Delta T}^{t} x(t)\,dt\,, \qquad (6\text{-}10)$$

where ΔT is the integration interval. The same variable name κ as for the previously defined criterium (page 98) is used here since this criterium is simply a special case of (6-10) namely with ΔT equal to the entire duration of the anomaly. An anomaly is detected when $\kappa(t)$ exceeds a certain value and remains above this value for the duration of the anomaly. Figure 6-20 shows the result of applying equation (6-10) to two detection results from measurement 2. ΔT has been taken equal to 30 s here (=1000 sampling periods). It is clear that the fluctuating behaviour is eliminated by using the integrator given by equation (6-10).

When studying the entire table 6-5 it can be seen that the method combination for which the smallest *TA* is achieved, changes from application to application. In order to get an overall ranking of the method combinations the following was done. For each application (20 in total: 5 measurements × 4 detectors) the *TA* obtained with a certain method combination was divided (weighed) by the smallest *TA* obtained for this application (shown in table 6-5). Next, all the 20 weighed *TA*s for each method combination were summed and the 9 sums (one for each method combination) were arranged in order to get the overall ranking as shown in table 6-6. A similar approach was used to get a ranking of the anomaly detection methods and the signal processing techniques. This is shown in the same table.

The detection results obtained with autoregressive and wavelet analysis are in many cases very close but autoregressive is on the average slightly better than wavelet

Table 6-6. Ranking of anomaly detection methods, signal processing techniques and combinations of them

Overall ranking of methods:	Ranking of anomaly detection methods:
1. AR-SPRT	1. SPRT
2. Wavelet-SPRT	2. $\chi 2$
3. Wavelet-$\chi 2$	3. Extremes
4. AR-extremes	
5. AR-χ^2	Ranking of signal processing techniques:
6. Wavelet-extremes	1. AR
7. Fractal-SPRT	2. Wavelet
8. Fractal-χ^2	3. Fractal
9. Fractal-extremes	

analysis with respect to achieving a fast detection. Fractal analysis can sometimes give a fast detection (see table 6-5) but is on the average worse than AR and wavelet analysis. The ranking of the anomaly detection methods underlines the theoretical result obtained earlier (section 4.3) and the results obtained from the practical applications in section 4.4.4. It is remarkable that AR-extremes is rated higher than AR-χ^2 in the overall ranking because the ranking of the anomaly detection methods shows the opposite. This is not the case for the other two signal processing techniques. It should, however, be noted that these conclusions are drawn from a limited set of detection results.

Table 6-7. Comparison of *TA*s obtained with test for detection of change of average value and test for detection of change of standard deviation

Ms	method	*TA* (s) (avg.)	*TA* (s) (std.)
2	wav-dist	247.74	247.65
	wav-sprt	247.74	247.80
	frc-dist	251.25	255.30
	frc-sprt	250.86	248.49
4	wav-dist	5.31	5.13
	wav-sprt	5.16	5.13
	frc-dist	15.30	15.45
	frc-sprt	15.39	15.21

dist=distribution method

The *TA*s in table 6-5 were all obtained assuming the standard deviation of the time series to change. In case of the wavelet coefficient and fractal dimension time series not only the standard deviation but also the average value changes due to the blowing of nitrogen bubbles (see figure 6-13). Table 6-7 shows the *TA*s obtained after applying a test for the detection of a change in average value to both time series. Only the results for the ND3L signal of measurements 2 and 4 are shown. For the distribution method inequality (3-10) and for the SPRT method equation (3-31) were used. Before they could be used the average value of the time series in the normal situation had to be subtracted first from the time series. Table 6-7 also gives the *TA*s obtained when applying a test for the detection of a change of the standard deviation. These values were taken from table 6-5. The results obtained with the two tests are comparable. This means that in this case it is not necessary to account for a possible change in average value since a test for the detection of a change in standard deviation suffices.

6.7 Applying the fuzzy-logic approach to results from signal processing

The fuzzy-logic approach as presented in chapter 5 has been applied to the case of signal processing redundancy and to the case of signal redundancy. Measurements 1 and 5 were chosen because for each measurement a completely different set of four rings was used. In case of measurement 1 only the first two steps are considered (until t= 2250 s) and the results from applying the three signal processing techniques to the ND3H signal are taken as input for the fuzzy-logic approach. From measurement 5 three different signals were taken (from ND1H, ND2L and ND3H, respectively) and for each signal the wavelet coefficient time series was determined. This time series was chosen because it shows the largest change in standard deviation due to the anomaly. The resulting three time series were used as input for the fuzzy-logic approach.

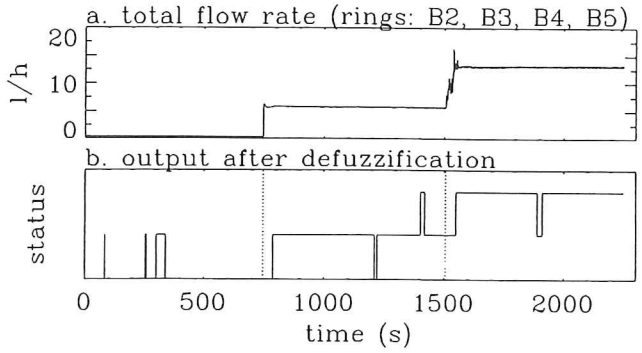

Figure 6-21. Result of applying fuzzy-logic approach to case of signal processing redundancy

Concerning the theory, the reader is referred to chapter 5. Here only the results are presented. Figure 6-18 shows the result of the first application (measurement 1) and figure 6-19 the result of the second one (measurement 5). In both cases it was not possible to obtain a detection result free from false alarms or even

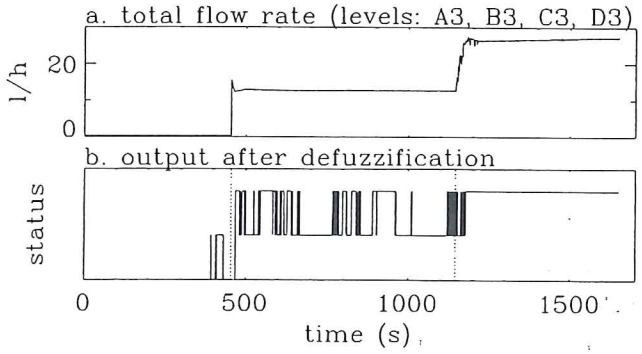

Figure 6-22. Result of applying fuzzy-logic approach to case of signal redundancy

identification errors (see section 5.3 for definitions). The results shown, were obtained for N=1000 and N=1500, respectively.

6.8 Conclusions and discussion

Experiments were performed with the SIMBOL facility which was placed next to the core of the IRI research reactor. In this facility the anomaly is created by blowing nitrogen bubbles.

Gamma transmission experiments and transit-time calculations show that the void fraction in the core of the facility is by approximation proportional to the applied nitrogen flow rate. The bubbles that are released from the holes in a tube stay close to this tube. The bubble velocity was estimated using the phase of the cross power spectral density. Estimated bubble velocities are in good agreement with the values determined by theory.

The spectra of the neutron noise signals measured with self-powered neutron detectors show a clear change due to the blowing of nitrogen bubbles. The amplitude of the noise added by the bubbles increases with increasing nitrogen flow rate. In time-domain no change of the neutron noise signal is visible without first pre-filtering the signal.

The three signal processing techniques are all sensitive to the noise introduced by the blowing of bubbles. The residual noise shows an increase of the standard deviation whereas the fractal dimension time series shows an increase of the average value. For the wavelet coefficient time series both the average value and the standard deviation increase.

It was not possible to detect the anomaly without first processing the neutron noise signals. After an extensive comparison of all the results obtained with anomaly detection it was concluded that AR-SPRT is in fact the best method. Fractal analysis in combination with the extremes method turned out to be the worst. A comparison of the signal processing techniques resulted in a first rank for AR analysis and a good second rank for wavelet analysis. As expected, SPRT is the best anomaly detection method. A nitrogen flow rate as small as 2.9 l/h, corresponding to approximately 19 bubbles per second per hole, is detectable. Unfortunately, no 'global' effect on the reactivity of the blowing of nitrogen bubbles was observed.

Localization of the anomaly is also possible as was shown by spectral analysis and

results from anomaly detection. No conclusive explanation could be given for the fact that sometimes a far-off detector detected the anomaly earlier than a nearby detector. More research into this field is therefore required.

The fuzzy-logic approach was applied to the results from three different signal processing techniques which were all applied to one neutron noise signal (signal processing redundancy) The approach was also applied to the result from wavelet analysis on three different neutron noise signals (sensor redundancy). It was however not possible to achieve a detection result free from false alarms. More research into the applicability of this fuzzy-logic approach to real neutron noise signals is therefore needed.

In order to learn more about the detection of actual boiling more research should be done to understand the connection between blowing nitrogen bubbles and actual boiling.

Chapter 7

TOWARDS AN APPLICATION OF PROCESS MONITORING

7.1 Process monitoring at the Dodewaard nuclear power plant

The Dodewaard nuclear power plant is a natural circulation cooled boiling water reactor with a nominal thermal power of 183 MW (60 MWe). For safety and economical reasons it is necessary to monitor the operation of the reactor continuously. For this purpose, a number of reactor-physics and thermohydraulic parameters are determined at the Dodewaard NPP using specific measurement devices like, for example, neutron detectors, gamma detectors and thermocouples. Important quantities which are determined, are: neutron flux, pressure, temperature, feedwater flow and water level (GKN, 1994).

At the Dodewaard NPP a process monitoring software package is installed on a VAX-computer. The package was written in VMS and FORTRAN code. It was developed in order to reduce the number of measurement data that was stored and to give a graphical presentation of signals in case an anomalous situation was detected. Before its installation it was customary to store all the measurement data, irrespective of whether they contained specific information or not. At present, only the data of those measurements are stored that show some kind of deviating behaviour. The installation of the package greatly reduced the backup frequency.

The package samples a number of analogue signals and tests the signals for anomalies. This is achieved by first starting a learning period during which the reference characteristics of the signals are determined. Next, the actual process monitoring is started during which the characteristics of the measured signals are compared with the reference characteristics. In case there is too much difference

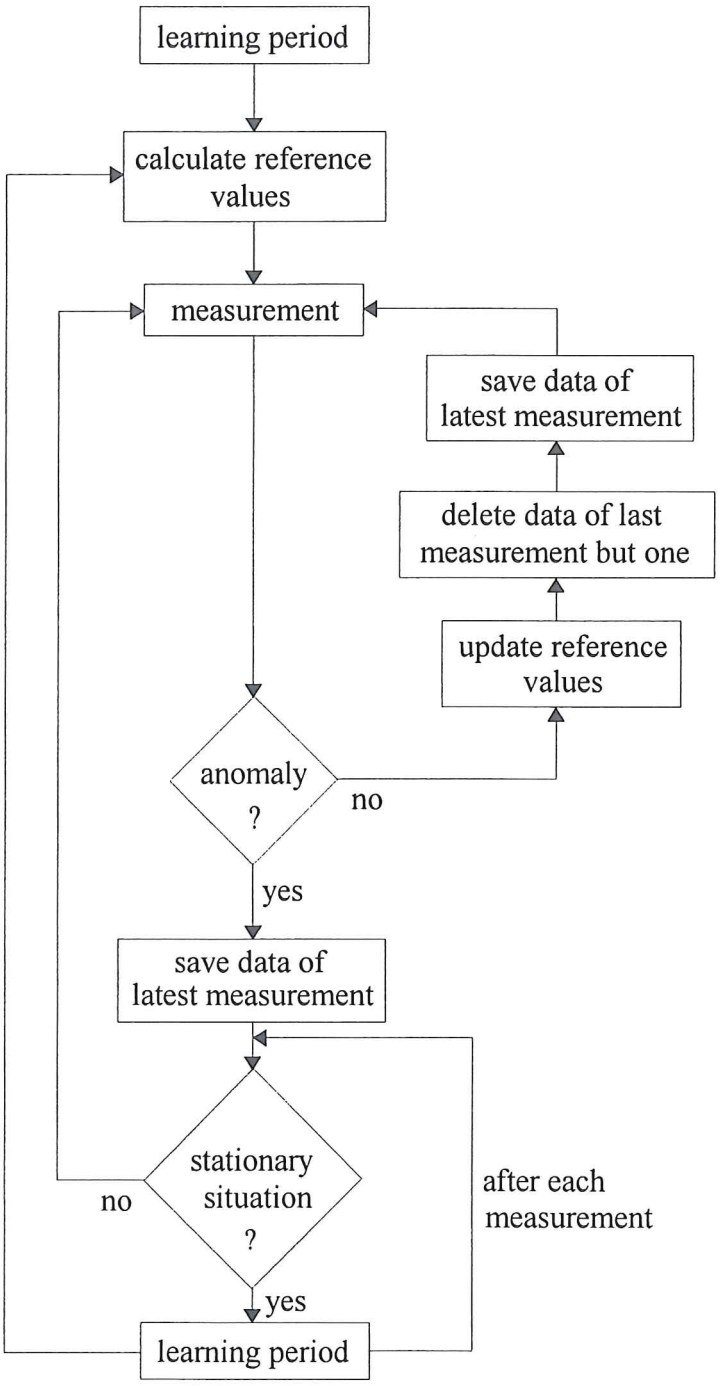

Fig 7-1. Flow diagram of the process monitoring software package

between the two characteristics an anomaly is declared. Another possibility is that one or more sensors are defective (see chapter 1). In this application the process and the sensors is regarded as one and denoted by 'process'. The program accounts for the fact that the process can return to a stationary state after the occurrence of an anomaly, by restarting the learning period.

For the anomaly detection two statistical variables per signal are calculated, namely the average value and the standard deviation. The more sophisticated methods presented in chapter 2 and 3 are not used in the package since the purpose of the package is to focus on relatively large changes of the process characteristics. There are plans to install the methods described in chapter 2 and 3 in the future.

The software package was installed in December 1993 and has been running successfully since. It was regularly tested, revised and updated. The package has been extended with a plot package which automatically plots signals which show anomalous characteristics.

In this chapter, a description of the process monitoring software package will be given and some results of its operation at the Dodewaard NPP will be presented. Finally, a concept for a surveillance and diagnosis expert system will be described.

7.2 Description of the process monitoring software package

The process monitoring software package performs continuous data acquisition with anomaly detection. The package will be described on the basis of the flow diagram shown in figure 7-1. This description is a summary of two IRI-reports (Schoonewelle, 1994; Schoonewelle, 1995).

The package starts with a learning period during which a previously specified number of measurements is done in order to determine the reference data for the anomaly detection. A measurement is the sampling of a number of analogue signals during a specified period. The reference data will later on be used for comparison purposes in order to determine whether the process is anomalous or not. The measurement data of the learning period are stored for later inspection. It must be noted here that these data can only be checked using expert knowledge since there are no reference data available.

For each signal of a learning measurement two variables are calculated, namely the average value and the standard deviation. At the end of the learning period, the

following four values are determined:

1. The average of the average values:

$$\bar{y}_R = \frac{1}{P}\sum_{i=1}^{P} \bar{y}_i , \tag{7-1}$$

where $\bar{y}_i$ is the average value of a signal from measurement i and P is the number of learning measurements.

2. The average of the standard deviation values:

$$s_R = \frac{1}{P}\sum_{i=1}^{P} s_i , \tag{7-2}$$

where s_i is the standard deviation of a signal from measurement i.

3. The standard deviation of the average values:

$$\sigma_{\bar{y}} = \sqrt{\frac{1}{P-1}\sum_{i=1}^{P} (\bar{y}_i - \bar{y}_R)^2} . \tag{7-3}$$

4. The standard deviation of the standard deviation values:

$$\sigma_s = \sqrt{\frac{1}{P-1}\sum_{i=1}^{P} (s_i - s_R)^2} \tag{7-4}$$

Together with the two reference values certain acceptance intervals around these values are defined. Such an interval is a multiple of the standard deviation of the reference values. When a future calculated value (average value or standard deviation) lies outside its acceptance interval, the corresponding signal is said to have anomalous characteristics.

After the learning period, the actual process monitoring is started. During a certain time, signals are measured and after each measurement the anomaly detection is performed. First, the average value and standard deviation of the signals are calculated, whereafter they are compared with the reference values mentioned earlier. If

$$\bar{y}_i \notin [\bar{y}_R - \theta_1 \cdot \sigma_{\bar{y}} , \bar{y}_R + \theta_1 \cdot \sigma_{\bar{y}}] \quad \vee \quad s_i \notin [s_R - \theta_2 \cdot \sigma_s , s_R + \theta_2 \cdot \sigma_s] \quad (7\text{-}5)$$

then the corresponding signal has anomalous characteristics. The variables θ_1 and θ_2 define the width of the intervals. If the width of an interval is enlarged, the *FAP* is reduced. For the process to be defined as anomalous, a minimum number (M) of monitored process variables (average value or standard deviation) must lie outside their interval. M must be chosen between 1 and twice the number of signals (= the number of process variables) in one measurement. If M is increased, the *FAP* is reduced.

Table 7-1 gives some values of the *FAP* for the average value $\bar{y}_i$. Table 7-2 gives some values of the *FAP* for the standard deviation. For both tables it is assumed that M=1 and the signal is Gaussian distributed. For the standard deviation the *FAP* values are different due to the fact that the standard deviation is χ^2-distributed. In this case the *FAP* depends not only on θ_2 but also on the number of learning measurements P.

When M has a value different from unity, the separate false alarm probabilities must be multiplied in order to get the overall false alarm probability. This is, however, only correct if the separate signal variables are independent.

In order to calculate the *FAR* the duration of one measurement must be known. If one measurement takes 24 minutes and θ_1 is equal to 4, the *FAR*, due to the testing of the average value, will be $6.3 \cdot 10^{-5} \times 1/24 \text{ min}^{-1} = 1.38 \text{ yr}^{-1}$.

When the process state is normal the measurement data are used to update the reference values as is shown in the flow diagram. The data of the previous

Table 7-1. *FAP* for average value

θ_1	*FAP*
2	$4.6 \cdot 10^{-2}$
3	$2.7 \cdot 10^{-3}$
4	$6.3 \cdot 10^{-5}$
5	$5.7 \cdot 10^{-7}$
6	$2.0 \cdot 10^{-9}$
7	$2.6 \cdot 10^{-12}$

Table 7-2. *FAP* for standard deviation

θ_2	*FAP* (P=10)	*FAP* (P=20)
2	$4.1 \cdot 10^{-2}$	$4.2 \cdot 10^{-2}$
4	$1.9 \cdot 10^{-3}$	$1.0 \cdot 10^{-3}$
6	$6.1 \cdot 10^{-5}$	$1.5 \cdot 10^{-5}$
8	$1.6 \cdot 10^{-6}$	$1.5 \cdot 10^{-7}$
10	$3.6 \cdot 10^{-8}$	$1.1 \cdot 10^{-9}$
12	$7.3 \cdot 10^{-10}$	$6.8 \cdot 10^{-12}$
14	$1.4 \cdot 10^{-11}$	$3.6 \cdot 10^{-14}$

measurement is deleted. In this manner the package adapts itself to slowly changing process characteristics which are not regarded as anomaly.

When an anomalous situation is detected the data of the present and previous measurement are stored. In this way, one can have at one's disposal the measurement data previous to an anomaly in order to be able to study the preamble of the anomaly.

As soon as a stationary situation is established, after the detection of an anomaly, a new learning period is started. This happens, for example, when the power level of the reactor is changed to a new stable level. In order to determine whether a stationary situation is present, the difference between the calculated statistical values (average value and standard deviation) of the signals from the last and last measurement but one is calculated for every signal. A stationary situation is present if

$$|\bar{y}_i - \bar{y}_{i-1}| < \theta_1 \cdot \sigma_{\bar{y}} \tag{7-6}$$

and/or

$$|s_i - s_{i-1}| < \theta_1 \cdot \sigma_s \tag{7-7}$$

is true for at least $P-M+1$ differences, by definition. This means that the package allows for only two process states, namely the normal/stationary state and the anomalous state. There is no transition state.

After each measurement, during the new learning period, it is checked whether the stationary situation is still present. When this is not the case the learning period is stopped and the old reference values are restored. When the learning period is completed successfully, new reference values are calculated and the process monitoring starts again.

7.3 Some results of the process monitoring

Since the implementation of the first version in December 1993 the process monitoring has been running almost without any interruption, apart from the times it was revised and updated. In this paragraph two results of the process monitoring will be presented. The first one is the detection of a reduction of power to 80 % of its nominal value. The second one is the detection of a reduction of power necessary to repair a steam leakage in the turbine drainage system. Both deviations from normal operation were in fact known beforehand because they were scheduled. Examples of

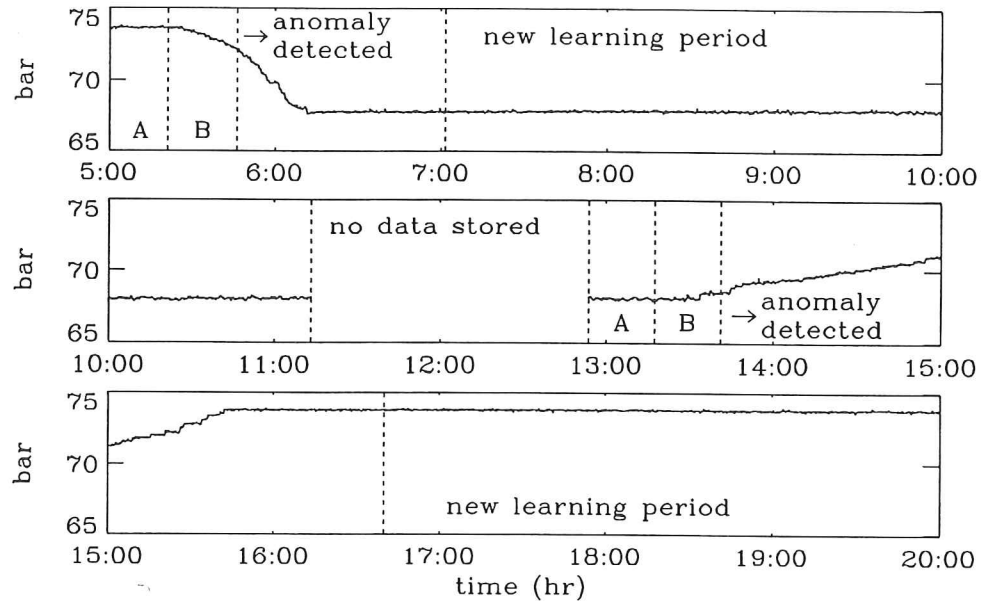

Figure 7-2. Response of pressure sensor 48PT07 to a reduction of power

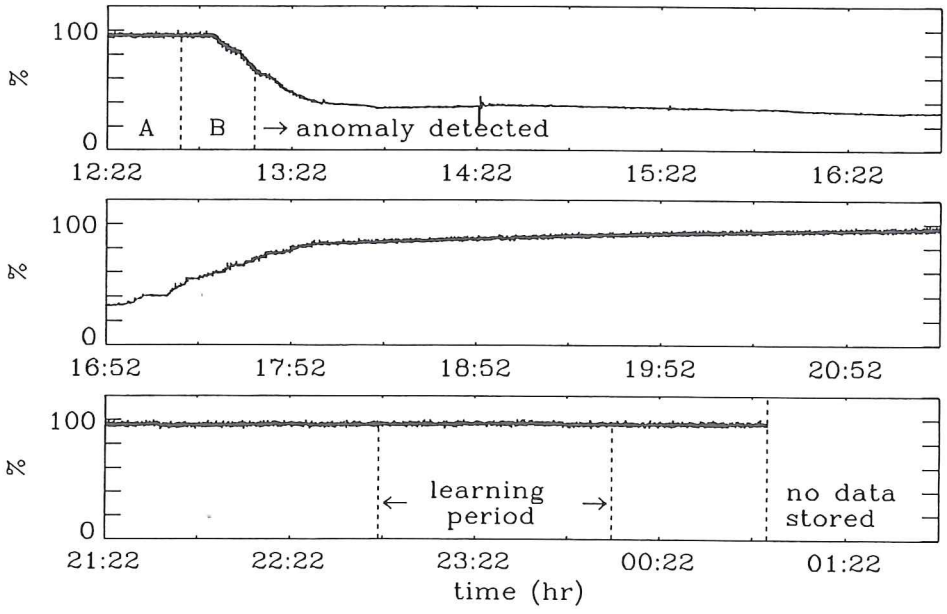

Figure 7-3. Output of neutron detector N6

unforeseen events that were detected by the process monitoring software package are scrams and turbine trips.

In both cases the following parameters were used:

$$\theta_1 = 5.0; \quad \theta_2 = 5.0; \quad M = 3$$

This means that an anomaly is declared when at least 3 signal parameters (average value or standard deviation) exceed their uncertainty intervals. The duration of one measurement equals 23 minutes and 54 seconds.

In each example 12 signals were measured among which neutron flux, reactor pressure, primary coolant flow, temperature, steam pressure and reactor water level signals. The response of only one sensor is shown per example.

Figure 7.2 shows the response of the pressure sensor 48PT07 to a reduction of power to 80 % of its nominal value starting at 5:00 h on April 23th, 1994. The three graphs follow each other in time. Apart from this sensor, nine other sensors responded to the anomaly. Only the average value of the signals changed. The uncertainty interval around the reference average value is only 0.084 bar wide which shows that the monitoring is very sensitive. The letter "B" denotes the first 'anomalous' measurement and the letter "A" the measurement preceding it. Measurement A is not 'anomalous'.

After the power has been reduced, the process becomes stationary again and a new learning period is started at 7:02 h. This learning period is completed successfully and at approximately 11:13 h new reference values are determined. From 11:13 h until 12:53 h no anomalies are detected, meaning that the measurement data are not stored during this time interval. After some time, the power is restored to its initial value leading to a new learning period which is started at 16:39 h and lasts until 20:51 h (not shown in the graph). Finally, new reference values are determined.

Figure 7-3 shows the output of the neutron detector N6. Here, the power is reduced to 32 MWe in order to repair a steam leakage of the turbine drainage system. The three graphs follow each other in time and each one covers 4.5 hours. The unit of the y-axis is a percentage of the output of the detector at nominal power. The uncertainty interval around the reference average value is 0.686 % wide in absolute sense. The neutron detector did not show a significant change in standard deviation. Five monitored signals showed a change in average value. These signals are: neutron flux, reactor

pressure, feedwater flow and two downcomer thermocouple signals. One signal showed a change in both statistical variables (average value and standard deviation) being the reactor water level.

After the power decrease, the turbine is decoupled from the reactor and the grid at around 14:21 h on July 6th, 1995 . At 14:46 h the turbine is reconnected and at 16:00 h the generator is synchronized again. No new learning period is started yet since there is still a small trend present in the signals. In the third graph it can be seen that a stationary situation is recognized and a new learning period is started at 22:50 h. After three measurements the stationary situation ceases to exist and the learning period is stopped. After two more measurements the reactor is back to the state it had before the power was reduced. This means that from this point on the measurement data are not stored anymore since the process is back to normal. It must be noted here that no new reference values are calculated.

Both examples show that the process monitoring software package performs well and is able to deal with changing process characteristics.

7.4 General architecture of an expert surveillance and diagnosis system

The process monitoring software package installed at the Dodewaard nuclear power plant is the first step towards an expert system that encompasses everything from the measurement part to the diagnosis and operator support part. The purpose of such an expert system is to digest a large amount of measurement data, perform the interpretation of it, reach a consensus about the state of the process and in case of an abnormal state, advise the operators on what abnormality exists and which actions need to be taken. In other words, the expert system must monitor the operation and ensure the safety of the nuclear power plant by supporting and facilitating the operators decision making process (Chang *et al.*, 1995; Kitamura *et al.*, 1995). In this section a concept of a general architecture of an expert system will be discussed.

In order to design an expert system more techniques are needed than just the analytical ones used in the implemented monitoring system. One could think of a combination of analytical methods, like the methods and techniques presented in this thesis, system models and artificial intelligent techniques like, for example, neural networks or fuzzy logic (Chang *et al.*, 1995).

Figure 7-4 presents a possible architecture of an expert system which is derived from an architecture suggested by Wach (Wach, 1995). The first step is to measure all kinds of process parameters and physical quantities resulting in a large amount of measurement data. The next step is to perform some kind of signal processing like, for example, the methods used in the implemented monitoring system or more sophisticated ones like the signal processing techniques presented in chapter 2. It is also possible to apply spectral analysis or to determine the PDF of signals. The latter techniques may, however, require on the average more data points than the time-domain based techniques. Therefore, one could perform a long-term monitoring using slow and more sensitive techniques in order to detect anomalies which develop gradually. Short-term monitoring using relatively fast techniques can then be used to detect quickly evolving anomalies (Kitamura *et al.*, 1995).

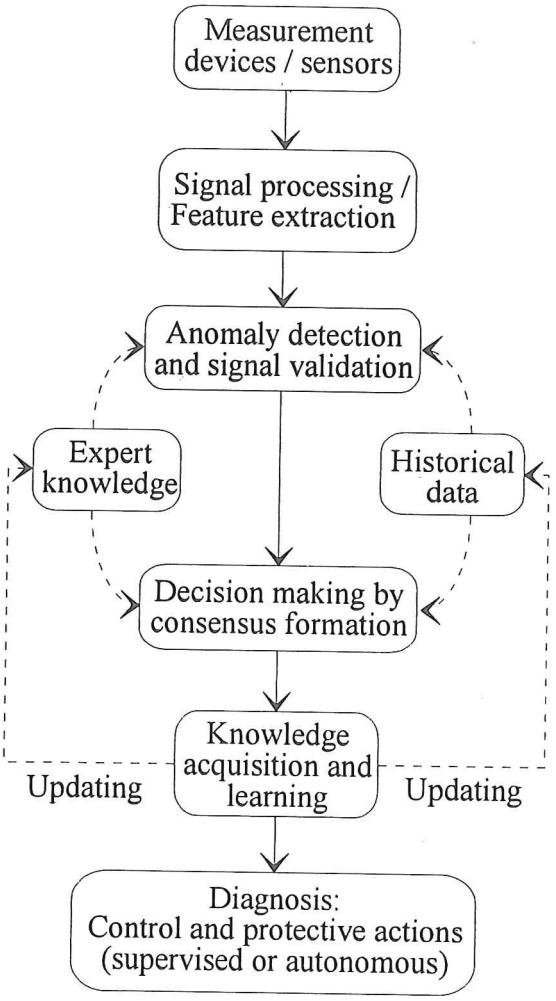

Figure 7-4. Architecture of surveillance and diagnosis expert system

The processed signals can then be checked for anomalies by employing the techniques used in the implemented monitoring system or by applying the anomaly methods that were presented in chapter 3 and 4. It is also possible that an anomaly is detected because of malfunctioning of a sensor. For example, a sensor can be

defective, stuck at some constant value, saturated or showing some kind of unnatural drift. Therefore, it is also necessary to perform signal validation and to identify faulty sensors using absolute measures or redundancy (Upadhyaya, 1985).

At the end of the anomaly detection and signal validation stage a number of anomalies may have been detected which could have been caused by one or only a few abnormalities. Thus the next step is to combine the outcomes of all the anomaly detection methods in order to come to an identification of the state of the process. This is the decision making part of the expert system, where by means of alarm filtering a clearer picture of the cause of the alarms can be presented to the operators (Chang *et al.*, 1995).

Both the anomaly detection and the decision making part make use of historical data and expert knowledge (Wach, 1995). An example of historical data is the reference data used in the implemented monitoring system. Examples of expert knowledge are the choice of the decision boundaries of the anomaly detection methods and the points of the membership functions of the fuzzy-logic approach used in the decision making part. Both the historical data and expert knowledge have to be updated, which is done during the knowledge acquisition and learning part. It may happen, for example, that the process is in a state which has not yet been defined. By means of learning under the supervision of an expert (supervised learning), the characteristics of the state can be added to the database of the expert system.

Finally, the diagnosis part is entered which is actually the interface between the expert system and the operators. At this stage, the information about the state of the process and the causes of the alarms must be presented to the operators in such a way that they are able to gain a clear picture of the state of the process and are able to employ the correct operating procedures without having to deal with an overload of information. The expert system can perform certain actions autonomous or can support the operators in taking the right decisions and measures for handling abnormalities and restoring the normal operation of the nuclear power plant.

Summary

In this thesis, nuclear reactor process-monitoring techniques are studied. These techniques are very important for the safety of a nuclear power plant. By applying these techniques to signals from a nuclear power plant it is possible to detect changing signal characteristics. Assuming that these changes are caused by process changes, like boiling of the coolant, it is possible to detect anomalous process behaviour of a nuclear power plant. These techniques are studied by applying them to simulated and measured signals..

Part of the thesis is devoted to theoretical investigations and part of it deals with experimental work. Numerical simulations were performed with the process-monitoring techniques in order to get a better theoretical understanding of their performance. Most of the experimental work was performed with the SIMBOL facility, which was positioned next to the core of the Hoger Onderwijs Reactor (HOR) of the Interfaculty Reactor Institute of the Delft University of Technology. This facility was especially designed and built for this research. SIMBOL stands for SIMulation of BOiLing. As the name suggests, boiling of the coolant of a pressurized water reactor is simulated by blowing nitrogen bubbles. This facility allows one to study the influence of the nitrogen bubbles on the neutron flux of the HOR using self-powered neutron detectors which are located in the facility itself. Experiments were also performed with two other facilities. Measured signals from the Dodewaard nuclear power plant were used as well.

The process-monitoring techniques proposed here, consist of three phases, namely:

(1) Signal analysis (or signal processing) (chapter 2)
(2) Anomaly detection (chapter 3 and 4)
(3) Expert-system approach using fuzzy logic (chapter 5)

Signal-analysis techniques extract certain features from signals and should make the detection of changes of signal characteristics more easier. Three signal-analysis techniques are introduced here: autoregressive, wavelet and fractal analysis. In order to detect these changes anomaly detection methods are used. These methods determine

whether the process is in a normal or an anomalous state. Three methods are presented here: the extremes method, the distribution method and the sequential probability ratio test (SPRT).

Three parameters are used for quantifying the performance of the anomaly detection methods. These parameters are: the false alarm probability, the alarm failure probability and the average time to alarm. Using these parameters, the performance of the methods are compared. The SPRT turns out to be the best method.

The presence of bubbles can be detected using any combination of a signal-analysis technique and an anomaly detection method. Some combinations perform, however, better than other combinations. Results from practical applications show that the combination autoregressive analysis-SPRT is the best combination. For a fast detection of an anomaly it turns out to be indeed useful to first apply signal analysis before applying anomaly detection.

In order to distinguish several process states an approach based on fuzzy logic can be used. This approach combines the outcomes of several signal-analysis techniques to come to one single decision about the state of the process.

Ideas are discussed for developing a comprehensive process monitoring system which encompasses all the beforementioned techniques and more. The process monitoring system already installed at the Dodewaard nuclear power plant could be the basis of this comprehensive system.

Samenvatting

In dit proefschrift worden procesbewakingstechnieken voor een kernreactor bestudeerd. Deze technieken zijn zeer belangrijk voor de bedrijfsveiligheid van een kernreactor. Door deze technieken toe te passen op signalen afkomstig van een kernreactor is het mogelijk om veranderende signaalkarakteristieken te detecteren. Indien wordt aangenomen dat deze veranderingen veroorzaakt worden door procesveranderingen, zoals het koken van het koelwater, dan is het dus mogelijk om afwijkend procesgedrag van de kernreactor te detecteren. De technieken worden bestudeerd door ze toe te passen op gesimuleerde en gemeten signalen.

Een gedeelte van dit proefschrift is gewijd aan theoretisch onderzoek en een gedeelte behandelt experimenteel werk. Er zijn numerieke simulaties uitgevoerd met de procesbewakingstechnieken ten einde een beter theoretisch beeld te krijgen van hun prestaties. Het grootste gedeelte van het experimentele werk is verricht met de SIMBOL opstelling welke was geplaatst naast de kern van de Hoger Onderwijs Reactor (HOR) van het Interfacultair Reactor Instituut (TU Delft). Deze opstelling is speciaal ontworpen en gebouwd voor dit onderzoek. SIMBOL is een acroniem voor: SIMulation of BOiLing. Zoals de naam aangeeft, wordt koken van het koelwater in een drukwaterreactor nagebootst door het blazen van stikstofbellen. Deze opstelling maakt het mogelijk om de invloed van stikstofbellen op de neutronenflux van de HOR te bestuderen. Hierbij kan gebruik worden gemaakt van 'self-powered' neutronen detectoren die zich in de opstelling bevinden. Er zijn ook experimenten uitgevoerd met twee andere opstellingen. Tevens zijn er gemeten signalen van de kerncentrale in Dodewaard gebruikt.

De procesbewakingstechnieken die hier worden voorgesteld, bestaan uit drie onderdelen, t.w.:

(1) Signaalanalyse (of signaalbehandeling) (hoofdstuk 2)

(2) Anomaliedetectie (hoofdstuk 3)

(3) Expert-systeem aanpak gebruikmakend van vage logica (hoofdstuk 5)

Signaalanalysetechnieken halen bepaalde kenmerken van signalen naar voren en

zouden het detecteren van veranderingen in signaalkarakteristieken moeten vergemakkelijken. Drie signaalanalysetechnieken worden geïntroduceerd: autoregressieve, wavelet en fractale analyse. Ten einde deze veranderingen te detecteren, worden anomaliedetectiemethoden gebruikt. Deze methoden bepalen of het proces zich in een normale of in een abnormale toestand bevindt. Drie methoden worden gepresenteerd: de extremen methode, de kansverdelingsmethode en de sequential probability ratio test (SPRT).

Drie parameters worden gebruikt voor het kwantificeren van de prestaties van de anomaliedetectiemethoden. Deze parameters zijn: de kans op een loos alarm, de kans op een gemist alarm en de gemiddelde tijd tot een alarm. Met behulp van deze parameters worden de methoden vergeleken. Het blijkt dat SPRT de beste methode is.

De aanwezigheid van bellen kan gedetecteerd worden met elke willekeurige combinatie van een signaalanalysetechniek met een anomaliedetectiemethode. Bepaalde combinaties presteren echter beter dan andere. Resultaten van praktische toepassingen laten zien dat de combinatie autoregressieve analyse met SPRT de beste is. Voor het snel detecteren van een anomalie blijkt het zeer zinvol om eerst signaalanalyse en daarna pas anomaliedetectie toe te passen.

Voor het onderscheiden van verschillende procestoestanden kan een aanpak gebaseerd op vage logica worden gebruikt. Deze aanpak combineert de resultaten van verschillende signaalanalysetechnieken ten einde tot één beslissing over de toestand van het proces te komen.

Er worden ideeën besproken voor het ontwikkelen van een uitgebreid procesbewakingssysteem dat alle genoemde technieken en meer moet omvatten. Het procesbewakingssysteem dat geïnstalleerd is in de Dodewaard kerncentrale zou de basis kunnen vormen van dit systeem.

Nomenclature

Symbols

A	lower threshold (χ^2 and SPRT method)	
A_b	cross-sectional area through which the nitrogen bubbles flow	m^2
A_i	coefficient of autoregressive model	
a	dilation scale	
$a_{1..4}$	points of trapezoidal membership function	
B	upper threshold (χ^2 and SPRT method)	
$b_{1..8}$	points of membership functions	
c, c_1, c_2	constants	
D	fractal dimension	
d_b	diameter of nitrogen bubble	m
e, e_i	residual noise, residual noise value	
F	distribution function	
$F(x_i\|0)$	distribution function of normal (noise) signal or time series	
$F(x_i\|a)$	distribution function of anomalous (noise) signal or time series	
$F_i(X\|H)$	distribution function of data sample set X in case hypothesis H is true	
f_c	central frequency of wavelet	Hz
f^j_k	probability of occurrence values	
f_s	sampling frequency	Hz
g	general function	
	gravitational acceleration	ms^{-2}
G	fuzzy subset	
H_0, H_1	hypothesis	
I	beam intensity	s^{-1}
i	integer value	
	imaginary unit (=$\sqrt{(-1)}$)	
j	integer value	
	input order of discrete wavelet transform	
$L(k)$	partial length of a data series (fractal dimension calculation)	
K	parameter in inequality belonging to Neyman-Pearson lemma	

k	time interval (fractal dimension calculation)	
	parameter in extremes method	
M	minimum number of monitored process variables that must lie outside their interval	
m	parameter in extremes method	
N	number of data points per record	
	parameter in extremes and χ^2 method	
	number of data points used per decision	
n	integer value	
	number of steps between two decisions (SPRT method)	
P	pressure	$kgm^{-1}s^{-2}$
	number of learning measurements	
p	order of autoregressive model	
p_0	false alarm probability for a single data value	
p_1	alarm failure probability for a single data value	
Q, Q_g	volumetric flow rate	l/h
q	quotient of standard deviation of (noise) signal / time series under anomalous and standard deviation of (noise) signal / time series under normal conditions ($=\sigma_1/\sigma_0$)	
r_h	radius of hole in tube	m
S	squared sum of noise values divided by σ_0^2	
s	standard deviation of a (noise) signal	
T	duration of signal or measurement	s
	temperature	K
T_d	time interval for calculating frequency of occurrence values (fuzzy logic approach)	
t	time	s
v_b	terminal velocity of a swarm of bubbles	cm/s
v_{b0}	terminal velocity of a single bubble	cm/s
$v_{b0\infty}$	terminal velocity of a single bubble in an infinite medium	cm/s
X	sample data set	
x, x_i	data series, data value	
	noise signal, noise signal value	
	general variable	
$\bar{x}$	average value of x	

y, y_i	signal, signal value
$\tilde{y}_i$	prediction of signal value
$\overline{y}$	average value of y

Subscripts

act	actual
anom	anomalous situation
anom1	first anomalous situation
anom2	second anomalous situation
av	average
b	bubble
des	desired
hi	high
i	integer value, counter
k	membership function number (fuzzy logic approach)
l	liquid (water)
lg	large
lo	low
md	medium
min	minimum
n	integer value, counter
norm	normal situation
R	reference
sm	small

Superscripts

i	time series number (fuzzy logic approach)
j	system state number (fuzzy logic approach)
tot	total

Greek symbols

α_c	chordal averaged void fraction
α_V	volumetric averaged void fraction
Γ	gamma function
γ	constant used in Gabor function (=5.336)

$\Delta\rho$	density difference	kgm^{-3}
$\Delta\omega$	range in angular frequency domain	Hz
ΔT	sampling period	s
Δt	range in time domain	s
η	slope of straight line fitted to the points in the double-logarithmic $L(k)$-k graph	
θ_1,θ_2	width of interval around average value, standard deviation	
κ	detection result decision parameter	
λ	decision parameter of SPRT method	
μ,μ^{ij}_{k}	membership value of variable	
μ_l	linear attenuation coefficient of water	cm^{-1}
ξ	coherence	
ρ_l	density of water	kgm^{-3}
σ	standard deviation	
σ_0	standard deviation of (noise) signal or time series under normal conditions	
σ_α	standard deviation of the void fraction	
σ_1	standard deviation of (noise) signal or time series under anomalous conditions	
σ_I	standard deviation of the beam intensity	s^{-1}
σ_l	surface tension of water	Nm^{-1}
σ_s	standard deviation of standard deviation values	
$\sigma_{\bar{y}}$	standard deviation of average values	
τ	time delay or shift	s
φ	phase of the CPSD	° or rad
Ψ	Fourier transform of wavelet function	
ψ	wavelet function	
$\psi_{(a,\tau)}$	dilated and translated wavelet function	
ω	angular frequency	Hz
ω_p	central angular frequency of Gabor function	Hz

Abbreviations

AFP	alarm failure probability	
AFR	alarm failure rate	s^{-1}
AIC	Akaike's information criterion	

AR	autoregressive	
ATA	average time to alarm	s
BWR	boiling water reactor	
CCF	cross correlation function	
CPSD	(normalized) cross power spectral density	Hz^{-1}
CWT	continuous wavelet transform	
DeSiRe	Delft Simulated Reactor (experimental facility)	
dist	distribution method	
DWT	discrete wavelet transform	
erf	error function	
ext	extremes method	
FAP	false alarm probability	
FAR	false alarm rate	s^{-1}
FPE	Akaike's final prediction error	
frc	fractal analysis	
FT	Fourier transform	
GKN	Gemeenschappelijke kerncentrales Nederland	
HOR	Hoger Onderwijs Reactor	
HP	high pass	
IAEA	International Atomic Energy Agency	
IMORN	Informal Meeting on Reactor Noise	
IRI	Interfaculty Reactor Institute	
LP	low pass	
Ms	measurement	
NAPSD	normalized auto power spectral density	Hz^{-1}
NDxy	neutron detector (x:string number {1..4}, y: position of detector {L: low, H: high})	
NIOBE	Noise Investigations on Boiling Effects (experimental facility)	
NPP	nuclear power plant	
PDF	probability density function	
PWR	pressurized water reactor	
Re	Reynolds number	
SIMBOL	Simulation of boiling by blowing nitrogen bubbles (experimental facility)	
SMORN	Specialists' Meeting on Reactor Noise	

SPND	self-powered neutron detector	
SPRT	sequential probability ratio test	
STFT	short time Fourier transform	
TA	time to alarm	s
UOD	universe of discourse	
wav	wavelet analysis	
WT	wavelet transform	

References

Bentley, P.M., and J.T.E. McDonnell, "Wavelet Transforms: an Introduction", *Electronics & Communication Engineering Journal*, **6**, 175 (1994)

Bernard, P., J. Cloue and C. Messainguiral, "Detection and Monitoring of Boiling in PWRs by Incore Neutron Noise Analysis", *Progress in Nuclear Energy*, **9**, 581 (1982)

Bernard, P., D. Fry, D. Stegemann and H. van Dam, "State of the Art on Reactor Noise Analysis", OECD Nuclear Energy Agency, Paris, France (1986)

Box, G.E.P., and G.M. Jenkins, "Time Series Analysis, Forecasting and Control", Holden-Day, San Francisco, USA (1970)

Black, J.L., and S.E.F. Rofe, "Multiple Feature Analysis of Sodium Boiling Noise Data", *Annals of Nuclear Energy*, **20**, 553 (1993)

Blatz, H., "Radiation Hygiene Handbook", McGraw-Hill Book Company, New York, USA (1959)

Chang, S.H., K.S. Kang, S.S. Choi, H.G. Kim, H.K. Jeong, C.U. Yi, "Development of the On-line Operator Aid System OASYS Using a Rule-Based Expert System and Fuzzy Logic for Nuclear Power Plants", *Nuclear Technology*, **112**, 266 (1995)

Chen, T., and M.J. Wang, "Applying Fuzzy Set Approach to Signal Detection Theory", *Fuzzy Sets and Systems*, **72**, 39 (1995)

Chesters, A.K., "Modes of Bubble Growth in the Slow-Formation Regime of Nucleate Pool Boiling", *Multiphase Flow*, **4**, 279 (1978)

Chien, T., and M.B. Adams, "A Sequential Failure Detection Technique and its Application", *IEEE Transactions on Automatic Control*, **21**, 750 (1976)

Çiftçioglu, Ö., J.E. Hoogenboom and H. van Dam, "Studies on Multivariate Auto-regressive Analysis Using Synthesized Reactor Noise-like Data for Optimal Modelling", *Progress in Nuclear Energy*, 21, 687 (1988)

Daubechies, I., "Orthogonal Bases of Compactly Supported Wavelets", *Communications on Pure and Applied Mathematics*, **41**, 909 (1988)

Djainal, D.D., M. Sakuma, R. Kozma and M. Kitamura, "Characterization of Two-Phase Flow Patterns Using Fractal Techniques", *Proc. of 2nd Int. Conf. on Multiphase Flow*, April 3-7, 1995, Kyoto, Japan

Dzwinel, W., Y. Pepyolyshev, P. Jirsa and J. Rejchrt, "Comparison of Noise Diagnostic Systems Based on Pattern Recognition and Discriminant Methods", *Annals of Nuclear Energy*, **22**, 543 (1995)

Gabor, D., "Theory of Communication", *J. Inst. Elec. Eng.* (London), **93-III**, 429 (1946)

GKN Dodewaard, N.V., "Veiligheidsrapport Kerncentrale Dodewaard", CIP-Gegevens Koninklijke Bibliotheek, Den Haag, The Netherlands (1994)

Glöckler, O., "Fault Detection via Sequential Probability Ratio Test of Multivariate Autoregressive Modeling-Based Residual Time Series", *Proc. of SMORN-VI, A Symposium on Nuclear Reactor Surveillance and Diagnostics*, May 19-24, 1991, Gatlinburg, Tennessee, USA

Govier, G.W., and K. Aziz, "The Flow of Complex Mixtures in Pipes", Van Nostrand Reinhold Company, New York, USA (1972)

Graaf, R. van de, T.H.J.J. van der Hagen and R.F. Mudde, "Scaling Laws and Design Aspects of a Natural-Circulation-Cooled simulated Boiling Water Reactor Fuel Assembly", *Nuclear Technology*, **105(2)**, 190 (1994)

Grossmann, A., and J. Morlet, "Decomposition of Hardy Functions into Square Integrable Wavelets of Constant Shape", *SIAM Journal on Mathematical Analysis*, **15**, 723 (1984)

Goupillaud, P., A. Grossmann and J. Morlet, "Cycle-Octave and Related Transforms in Seismic Signal Analysis", *Geoexploration*, **23**, 85 (1984)

Harmathy, T.Z., "Velocity of Large Drops and Bubbles in Media of Infinite of Restricted Extent", *A.I.Ch.E. Journal*, **6-2**, 281 (1960)

Hewitt, G.F., "Measurement of Two Phase Flow Parameters", Academic Press, London, UK (1978)

Higuchi, T., "Approach to an Irregular Time Series on the Basis of the Fractal Theory", *Physica D*, **31**, 277 (1988)

Hoel, P.G., "Introduction to Mathematical Statistics", 5th edition, John Wiley & Sons, New York, USA (1984)

Holbert, K.E., A.S. Heger and N.K. Alang-Rashid, "Redundant Sensor Validation by Using Fuzzy Logic", *Nuclear Science and Engineering*, **118**, 54 (1994)

Hoogenboom, J.E., T.H.J.J. van der Hagen and Ö. Çiftçioglu, "Fast and Sensitive Methods for On-line Anomaly Detection", *Specialists' Meeting on In-core Instrumentation and Reactor Core Assessment*, June 7-10, 1988, Cadarache, France

Hoogenboom, J.E., and H. Schoonewelle, "IRI contribution to the 1994 benchmark test on leak detection in a fast breeder reactor", *internal report IRI 131-94-020*, Interfaculty Reactor Institute, Delft, The Netherlands (1994)

Hoogenboom, J.E., and H. Schoonewelle, "IRI contribution to the 1994 benchmark test on leak detection in a fast breeder reactor", *internal report IRI 131-94-020/1*, Interfaculty Reactor Institute, Delft, The Netherlands (1994)

Hoon, M.J.L. de, T.H.J.J. van der Hagen, H. Schoonewelle and H. van Dam, "Why Yule-Walker should not be used for Autoregressive Modelling", *Annals of Nuclear Energy*, **23**, 1219 (1996)

Hunt, J.C.R., N.K.-R. Kevlahan, J.C. Vassilicos and M. Farge, "Wavelets, Fractals and Fourier Transforms: Detection and Analysis of Structure", *Proc. of Conference on Wavelets, Fractals and Fourier Transforms: New Developments and Applications*, December 1990, Cambridge, UK

Journeau, C., "IAEA IWGFR Extended Coordinated Research Program on Acoustic Signal Processing for the Detection of Sodium Boiling or Sodium/Water Reaction in LMFBR - Data for 1994 Benchmark Test", C.E.A., Cadarache, France (1994)

Kaufmann, A., "Introduction to the Theory of Fuzzy Subsets, Vol. 1, Fundamental Theoretical Elements", Academic Press, New York, USA (1975)

Kim, H.K., S.H. Lee and S.H. Chang, "Neural Network Model for Estimating Departure from Nucleate Boiling Performance of a Pressurized Water Reactor Core", *Nuclear Technology*, **101**, 111 (1993)

Kiss, J., J. Bokor, A. Edelmeyer and A. Soumelidis, "An Open System Approach to Change Detection and Failure Monitoring of Complex Plants: The NPP Experience", *Proc. of SMORN-VII, A Symposium on Nuclear Reactor Surveillance and Diagnostics*, June 19-23, 1995, Avignon, France

Kitamura, M., H. Furukawa, R. Kozma and T. Washio, "Guiding Rules for Development of Intelligent Monitoring System of Nuclear Power Plants", *Proc. of SMORN-VII, A Symposium on Nuclear Reactor Surveillance and Diagnostics*, June 19-23, 1995, Avignon, France

Kozma, R., "Nuclear Reactor Noise Investigations on Boiling Effects in a Simulated MTR-Type Fuel Assembly", *PHD-thesis*, Delft University of Technology, Delft, The Netherlands (1992)

Kozma, R., and K. Nabeshima, "Studies on the Detection of Incipient Coolant Boiling in Nuclear Reactors Using Artificial Neural Networks", *Annals of Nuclear Energy*, **22**, 483 (1995)

Kruse, R., J. Gebhardt and F. Klawonn, "Foundations of Fuzzy Systems", Wiley, Chichester, UK (1994)

Kuan, C.C., C. Lin and C.C. Hsu, "Fuzzy Logic Control of Steam Generator Water Level in Pressurized Water Reactors", *Nuclear Technology*, **100**, 125 (1992)

Ljung, L., "System Identification: Theory for the User", Prentice Hall, Englewood Cliffs, New Jersey, USA (1987)

Ljung, L., "System Identification Toolbox - For Use with MATLAB User's Guide", The Mathworks, Inc., Natick, Mass., USA (1991)

Mandelbrot, B.B., "Fractals, Form, Chance and Dimension", Freeman, San Francisco, USA (1977)

Mandelbrot, B.B., "The Fractal Geometry of Nature", Freeman, New York, USA (1982)

Meyer, Y., "Orthonormal Wavelets", *Proc. of International Conference on Wavelets, Time-Frequency Methods and Phase Space*, December 14-18, 1987, Marseille, France

Miteff, L., and K. Behringer, "Investigation of the Relation between the RMS-Neutron Noise and Local Void Fraction in the Bubbly Flow Region", *Progress in Nuclear Energy*, **9**, 649 (1982)

Morlet, J., G. Arens, E. Fourgeau and D. Giard, "Wave Propagation and Sampling Theory", *Advances in Geophysics*, **47**, 203 (1982)

NAG-Library, The Numerical Algorithms Group Limited, Oxford, UK (1991)

Park, G.Y., and P.H. Seong, "Nuclear Power Plant Pressurizer Fault Diagnosis Using Fuzzy Signed-Digraph and Spurious Faults Elimination Methods", *Annals of Nuclear Energy*, 21, 357 (1994)

Park, G.Y., and P.H. Seong, "Application of a Fuzzy Learning Algorithm to Nuclear Steam Generator Level Control", *Annals of Nuclear Energy*, **22**, 135 (1995)

Priestley, M.B., "Spectral Analysis and Time Series", Academic Press, London (1994)

Ruskai, M.B., "Wavelets and their Applications", Jones and Bartlett Publishers, Boston, USA (1992)

Saade, J.J., and H. Schwarzlander, "Application of Fuzzy Hypothesis Testing to Signal Detection under Uncertainty", *Fuzzy Sets and Systems*, **62**, 9 (1994)

Sakuma, M., R. Kozma, M. Kitamura, H. Schoonewelle and J.E. Hoogenboom, "Boiling Anomaly Detection by Various Signal Characterization Methods", *Proc. of SMORN-VII, A Symposium on Nuclear Reactor Surveillance and Diagnostics*, June 19-23, 1995, Avignon, France

Schoonewelle, H., "Measure/Anomtest - Anomaly Detection Software Package for the Dodewaard Power Plant Facility", internal report IRI 131-94-001, Interfaculty Reactor Institute, Delft, The Netherlands (1994)

Schoonewelle, H., "Measure/Anomtest - Anomaly Detection Software Package for the Dodewaard Power Plant Facility (Supplement 1)", internal report IRI 131-95-001, Interfaculty Reactor Institute, Delft, The Netherlands (1995)

Schulte, U., "Fuzzy Logic, een Introductie", Kluwer, Deventer, The Netherlands (1994)

Singh, O.P., G.S. Srinivasan, R. Prabhakar and R.K. Vyjayanthi, "New Approaches in Signal Processing Technique for Sodium Boiling Noise Detection", *Progress in Nuclear Energy*, **21**, 613 (1988)

"SMORN-1, Reactor Noise: from Critical Assemblies to Power Reactors", *Proc. of Specialists' Meeting on Reactor Noise* held in Rome, October 1974, Pergamon Press, Oxford, UK (1975)

Srinivasan, G.S., and O.P. Singh, "New Statistical Features Sensitive to Sodium Boiling Noise", *Annals of Nuclear Energy*, **17**, 135 (1990)

Thie, J.A., "Reactor Noise", Rownan and Littlefield, Inc., New York, USA (1963)

Uhrig, R.E., "Noise Analysis in Nuclear Systems", USAEC Division of technical Information Extension, Oak Ridge, Tennessee, USA (1964)

Upadhyaya, B.R., "Sensor Failure Detection and Estimation", *Nuclear Safety*, **26**, 32 (1985)

Upadhyaya, B.R., and E. Eryurek, "Application of Neural Networks for Sensor Validation and Plant Monitoring", *Nuclear Technology*, **97(2)**, 170 (1992)

Wach, D., "Surveillance and Diagnostics in NNPs - Progress Made, Operational Needs, and Perspective for Future Developments", *Proc. of SMORN-VII, A Symposium on Nuclear Reactor Surveillance and Diagnostics*, June 19-23, 1995, Avignon, France

Wald, A., "Sequential Analysis", Wiley, New York, USA (1947)

Yu, D., W.E. Kastenberg and D. Okrent, "Use of an Influence Diagram and Fuzzy Probability for Evaluating Accident Management in a Boiling Water Reactor", *Nuclear Technology*, **106**, 315 (1994)

Zadeh, L.A., "Fuzzy Sets", *J. Information Control*, **8**, 338 (1965)

Dankwoord

Ik wil graag iedereen bedanken die me heeft geholpen en gesteund bij mijn werk en het voltooien van mijn proefschrift. In het bijzonder noem ik:

- Prof. dr. ir. H. van Dam, voor het creëren van de mogelijkheid om mijn werk te verrichten;
- Dr. ir. Tim van der Hagen, voor alle aandacht, geduld, ondersteuning, aanmoedigingen en waardevolle discussies;
- Jelle Schut en Dick de Haas, voor al het werk dat ze hebben gedaan voor de SIMBOL opstelling en de hulp die ze me hebben gegeven tijdens het experimenteren;
- Dr. ir. Eduard Hoogenboom, voor de zinvolle ideeën en discussies;
- Dr. Robert Kozma, voor de hulp tijdens de beginfase van mijn promotiewerk en de steun en aandacht tijdens de periode dat ik onderzoek verrichtte aan de Tohoku universiteit in Sendai, Japan;
- Prof. dr. M. Kitamura, for making it possible to perform research work at his group at Tohoku University;
- Ing. Wim Nissen, voor de prettige samenwerking in Dodewaard;
- Ir. Piet de Leege and Ing. Addy Hersman, voor het oplossen van kleine probleempjes en het verrichten van rekenwerk;
- Prof. dr. Özer Çiftçioglu, for his cooperation during the experiments with SIMBOL;
- De mensen van de centrale werkplaats van de TU Delft en in het bijzonder Jos Knoester, voor het tekenen en het maken van de SIMBOL opstelling;
- De mensen van de HOR bedrijfsgroep en de reactoroperators voor de hulp bij het verrichten van de experimenten met SIMBOL;
- Sonja Jobse en Riny Purmer voor alle ondersteuning en het regelen van kleine zaken.

Curriculum Vitae

July 12, 1968	born at Zwijndrecht, The Netherlands
1980 - 1981	Gymnasium at Stade, Germany
1982 - 1986	Secondary school (VWO) at Terneuzen
1986 - 1991	University of Twente, Enschede: study of applied physics. Graduation project performed at subfaculty of Instrumentation and Measurement Technology Subject of graduation work: Development of discrete models of the heat distribution in a building using model-identification methods Masters degree with computer-science specialization obtained on December 10, 1991
1992 - 1996	Interfaculty Reactor Institute of the Delft University of Technology: PhD-work as described in this thesis.
1996 -	KPN Research, Groningen: Technical Scientific Researcher